Master's thesis

Feasibility of Ocean Heat Extraction in Icelandic Coastal Waters; Case Study of Önundarfjörður

Majid Eskafi

Advisors:
Ragnar K. Ásmundsson, Ph.D.
Steingrímur Jónsson, Prof.

University of Akureyri
Faculty of Business and Science
University Centre of the Westfjords
Master of Resource Management: Coastal and Marine Management
Ísafjörður, September 2016

Supervisory Committee

Advisors:

Ragnar K. Ásmundsson, Ph.D., Heat Research and Development, Akureyri

Steingrímur Jónsson, Prof., University of Akureyri and Marine Research Institute

Reader:

Guðni A. Jóhannesson, Prof., Director General of Orkustofnun

Program Director:

Dagný Arnarsdóttir, MSc.

Majid Eskafi

Feasibility of Ocean Heat Extraction in Icelandic coastal waters; Case Study of Önundarfjörður

45 ECTS thesis submitted in partial fulfilment of a Master of Resource Management degree in Coastal and Marine Management at the University Centre of the Westfjords, Suðurgata 12, 400 Ísafjörður, Iceland

Degree accredited by the University of Akureyri, Faculty of Business and Science, Borgir, 600 Akureyri, Iceland

Printing: Háskólaprent, Reykjavík, September 2016

Declaration

I hereby confirm that I am the sole author of this thesis and it is a product of my own academic research.

_____

Majid Eskafi

Abstract

The oceans are teeming with heat as an immense source of renewable energy. Seawater source heat pump system is a proven technology for resurrecting heat from the seawater as a source of heat. The system has attracted attention as a renewable energy solution technique for the countries where heating is essential throughout the year. As the most efficient form of technology, the system is able to extract heat from cold seawater for energy utilization and space heating. However, extracting large amounts of heat from the cold seawater is a challenge, and hardly feasible if the seawater temperature is only a few degrees above the freezing point. Iceland, as a cold country with a high demand for space heating, is surrounded by the cold seawater with the Arctic and the Atlantic Ocean sources. This thesis assesses the feasibility of ocean heat extraction in Icelandic coastal waters through a case study of Önundarfjörður, a fjord located in Westfjords region of Iceland. In order to acquire better insight about the heat source, this research collected one year field measurements and carried out numerical simulations of oceanographic parameters. The results show that the seawater temperature in the research area is generally higher than 1 °C and rarely exceeds 10 °C. The simulations indicate that the fjord is tidal dominated with higher current velocity which prominently flanks alongshore during ebb. The outcome reveals that extraction of the heat via seawater source heat pump system is theoretically feasible from Önundarfjörður. This research also presents suitable locations for extracting heat from the fjord.

Keywords: Seawater source heat pump, seawater temperature, current velocity, Önundarfjörður, Iceland

I dedicate this work to the "coastal management communities" all around the world and especially in Iceland

Table of Contents

List of Figures

List of Tables

Acronyms

2 Dimensional (2D)

3 Dimensional (3D)

Baltic Sea Region Energy Cooperation (BASREC)

Carbon Dioxide (CO_2)

Coefficient Of Performance (COP)

Courant- Friedrich-Levy (CFL)

Danish Hydraulic Institute (DHI)

East Greenland Current (EGC)

East Icelandic Current (EIC)

Energy Performance of Buildings (EPBD)

Environmental Impact Assessment (EIA)

European Union (EU)

Global Positioning System (GPS)

Global System for Mobile Communications (GSM)

Icelandic Met Office (IMO)

Integrated Coastal Zone Management (ICZM)

Irminger Current (IC)

Marine Renewable Energy (MRE)

Marine Spatial Planning (MSP)

Microbiological Influenced Corrosion (MIC)

National Oceanic and Atmospheric Administration (NOAA)

North Icelandic Irminger Current (NIIC)

North Icelandic Jet (NIJ)

Return On Investment (ROI)

Sea Surface Temperature (SST)

Strategic Environmental assessment (SEA)

Water Source Heat Pump (WSHP)

Acknowledgements

I would like to express my sincere gratitude to my advisors, Dr. Ragnar K. Ásmundsson and Prof. Steingrímur Jónsson, for the valuable discussions and guidance throughout this research.
This research was carried out under the auspices of Orkubú Vestfjarða. I gratefully acknowledge the company for its generous support. I also wish to thank the staff of the Marine Research Institute in Ísafjörður, in particular Hjalti Karlsson and Einar Hreinsson for all of their field works.
Thanks also to Gísli Halldór Halldórsson, Mayor of Ísafjarðarbær, and Guðmundur M. Kristjánsson, Harbor Master of Ísafjörður, for their encouragement and guidance.
I would like to thank all the following institutions and individuals for their helpful provision of information and interest in this work:

- Orkubú Vestfjarða, in particular Sölvi Sólbergsson
- POLS Engineering, in particular Örn Ingólfsson
- The hydrographic department of the Icelandic Coast Guard, in particular Árni Vésteinsson head of chart division
- The Icelandic Meteorological Office (IMO), in particular Björn Erlingsson, specialist in marine flooding, and Trausti Jónsson, senior meteorologist and specialist in historical climatology
- Náttúrustofa Vestfjarða, in particular Böðvar Þórisson
- Teiknistofan Eik, in particular Gunnar Páll Eydal

My thanks also go to the staff of The University Centre of The Westfjords for their assistance and advice during my work.
I also thank Gísli Jón Kristjánsson for providing his boat, Aldan ÍS 47, and seawater temperature data at one location in the field. I would also like to acknowledge the Icelandic Regional Development Institute, Byggðastofnun, for its financial support in the form of a research grant.
I wish to thank the Danish Hydraulic Institute (DHI) for providing the software MIKE21 and MIKE3 for this research. My thanks also goes to GoldenSoftware for providing the software Surfer13 in this research.
Finally, I wish to express my special appreciation to my family for their never-ending dedication and support.

1 Introduction

Growing industries and rising energy demands, combined with the scarcity of fossil fuel, are making the use of renewable energy sources increasingly worthwhile. The use of renewable energy leads to enhanced energy independence, security, sustainability, and economic benefits and carries few if any negative environmental impacts. About half of the energy used in the building sector is used for the purposes of space heating/cooling and supplying hot water. It is estimated that around 5-20% of the amount of renewable energy targeted by 2020 in the European Union (EU) will be generated by heat pump systems (International Renewable Energy Agency, 2013).

In Iceland, unique geological conditions provide a bountiful source of energy. Iceland's major sources of energy are hydropower and geothermal energy. Around 86% of primary energy in the country is provided from local sustainable sources of renewable energy (Ketilsson, Petursdottir, Thoroddsen, Oddsdottir, Bragadottir, Gudmundsdottir & Johannesson, 2015). More than 90% of the heat demand is supplied by geothermal energy for residential and service purposes (Icelandic Ministry of Industries and Innovation, 2009). Iceland's targets for renewable energy use are proportional with respect to the EU's energy policy as laid out in the Renewable Energy Directive (Baltic Sea Region Energy Cooperation [BASREC], 2014). Iceland's energy policy states the following goals: 1) "Utilization of new renewable energy resources will be supported and at the same time new and smaller energy possibilities will be supported to suit domestic industry"; and 2) "Power generation shall at all times use the best available technology to maximize efficiency and minimize pollution" (BASREC, 2014, p. 38). Based on Act No. 78/2002 and Regulation No. 284/2005, using electricity or oil for the space heating is granted in Iceland. In addition, the utilization of district heating systems for heating applications and the installation of heat pumps for space heating have been subsidized (Icelandic Ministry of Industries and Innovation, 2009). Research conducted by the National Energy Authority on the feasibility of heat pump systems in Iceland has demonstrated that these systems can play a significant role in space heating in regions where geothermal waters are not economically obtainable (Ásmundsson, 2005).

This research was conducted through observation and measurements in the field, along with scientific numerical modeling of oceanographic parameters, in order to gain a better understanding of the source of heat in the area of interest. This research reviews the national and international literature as well as previous research with respect to seawater source heat pump systems. Furthermore, measured data by other authorities were collected and analyzed.

This thesis aims to answer the following research questions:

1) What are the oceanographic conditions in Önundarfjörður with regard to the feasibility of the implementation of heat pumping system?

2) Where is the best location for heat extraction with respect to key oceanographic parameters, and port and fishing activities in the fjord?

3) If implementation of the system is feasible, what equipment for heat extraction should be taken into account?

This thesis is divided into nine chapters.

Chapter 2 contains a broad overview of the literature on seawater source heat pump systems. The chapter explores the oceanographic conditions around Iceland, mostly focused on the west and northwest coasts of the country, including the sources of water masses, seawater temperatures, and main ocean currents. Case studies and previous international experiences about seawater source heat pump systems are also described in this chapter. Chapter 3 reviews the definition of renewable energy, concentrating on ocean energy and seawater source heat pump systems. In this chapter, the operational principles and the system components of heat pumps are detailed. Also, the principle components of a heat exchanger are described with respect to the purpose of this research. Chapter 4 describes the area of study. This chapter provides readers with both general and detailed information about the location, weather conditions, maritime activities, and heat demand of the area. Chapter 5 outlines the research methodology. This chapter describes the tools and equipment used in the research and the locations where the measurements took place, as well as the theory of numerical modeling, governing equations and the creation of input data for the simulations. Chapter 6 presents the results of the field measurements and numerical simulations. This chapter includes a nuanced

analysis of the raw data as well as a delineation of the output of the models. Chapter 7 compares the results of the measurements and also the simulationes. The chapter discusses different potential sites throughout the area of interest based on the measurements and simulations and identifies the most suitable site location for the research. The chapter also draws attention to the port, fishing, and aquaculture activities taking place in Önundarfjörður.
Finally, chapter 8 discusses the results, and chapter 9 make recommendations for further study.

1.1 Motivations and objectives

The present research assesses the feasibility of seawater heat extraction from Önundarfjörður. The fjord is located in the Westfjords region of Iceland, where there are few easily accessible geothermal fields as shown in Figure 1. Also, there is a limited potential of improving the hydropower in the Westfjords as well as land and water ownership's rights in the region. Supplying energy by Marine Renewable Energy (MRE) adjacent to the inhabitant, increase the security of delivery for the users. The system reduces the cost of energy distributions and reliance on other sources of energy from the national grid for the area (Jónsson, 2010).

This research presents prominent locations for extracting heat from in the fjord. Collecting comprehensive and informative information about the oceanographic parameters in this reaserch, allows better understanding about the heat source throughout the area. Also, this work can be designated to contribute to potential utilization of seawater source heat pump system in Westfjords region. Furthermore, this research is a pilot project; if it proves feasible, seawater heat pumps offer a promising alternative for the energy utilization in other regions in Iceland. With the feasibility study the reliability, business opportunities and positive and negative aspects of the project will be determined (Jónsson, 2010).

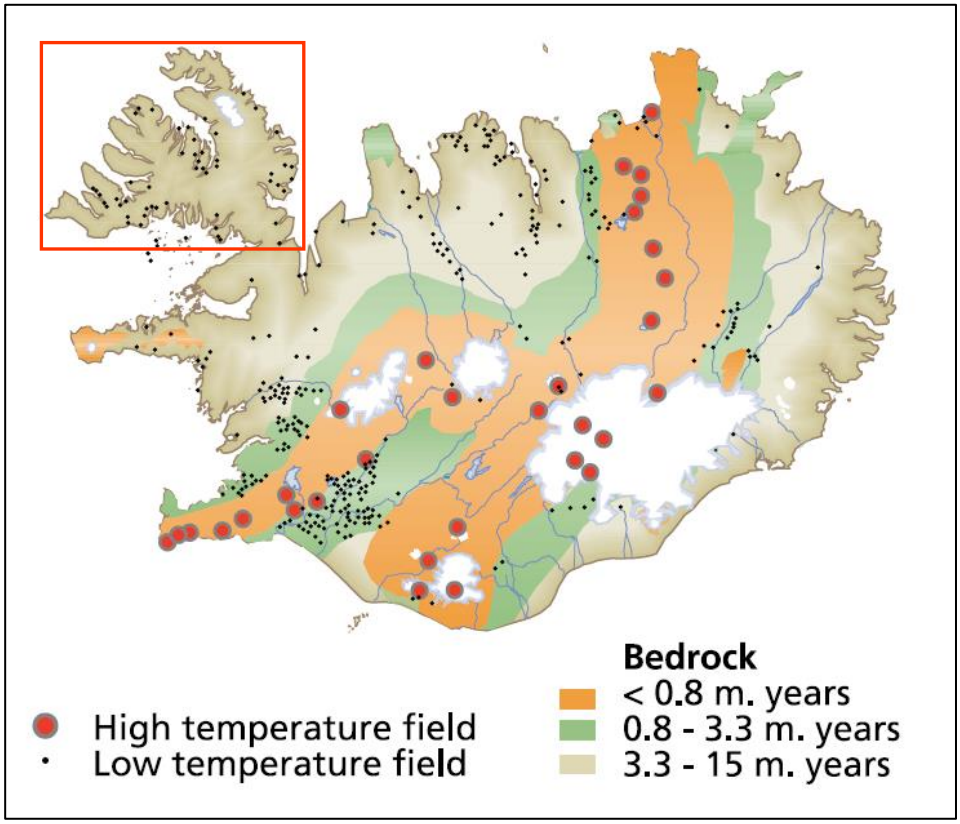

Figure 1. Distribution of geothermal fields in Iceland, red box shows Westfjords region (Loftsdottir & Thorarinsdottir, 2006)

The feasibility of seawater source heat pump system has not yet been studied in the Westfjords. This is the first time that the subject has been considered scientifically in this region of Iceland. This research concludes the first such considerations, and focuses on the heat source. This study provide a good basis for heat extraction methods to the local inhabitant and addresses recommendations based on the findings and the results.

2 Literature review

2.1 The oceanographic conditions around Iceland

Iceland is an island located in the North Atlantic Ocean at the confluence of waters from the Atlantic and Arctic Oceans from the south and north, respectively. However, waters to the south and west coasts are sourced from the Atlantic Ocean, while the north and east coasts of Iceland are also influenced by the Arctic sources. (Malmberg & Valdimarsson, 2003). Table 1 shows the bodies of water surrounding Iceland with their temperatures and origins.

Table 1. Water masses around Iceland, their temperatures and origins (Malmberg & Valdimarsson, 2003)

Water mass	Temperature °C	Origin of water mass
Atlantic Water	3-8	North Atlantic and Irminger Currents
Polar Water	< 0	East Greenland Current
Arctic/Polar Water	< 0-2	East Icelandic Current
North Icelandic Winter Water	2-3	North Icelandic Shelf
Bottom/Deep Water	<0	Deeper layers north and east of Iceland
Arctic Intermediate	0-2	Below the Polar Water in the East Greenland Current
Coastal Water	Variable	Shelves around Iceland

The country is located on the intersection between the Reykjanes Ridge (which is part of the Mid-Atlantic Ridge) in the southwest, the Kolbeinsey Ridge in the north, the Greenland-Iceland Ridge in the northwest and the Iceland-Faroe Ridge in the southeast, as depicted in Figure 2 (Valdimarsson & Malmberg, 1999). The shelves, which are narrow along the south coast and broad along the west, north, and east coasts, mostly extend to the depths of around 400–500 m

(Astthorsson et al., 2007). The shape and direction of the ridges have significant effects on the distribution of water masses and the direction of the major currents around Iceland.

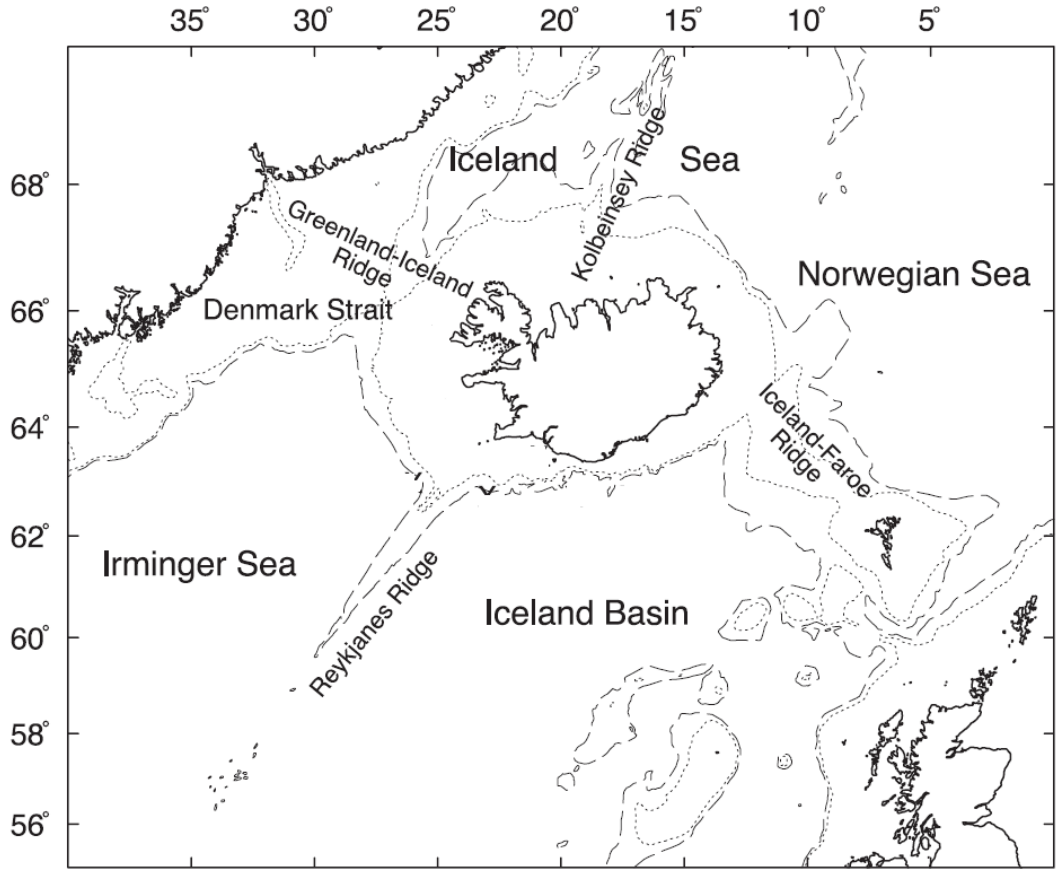

Figure 2. Bottom conditions around Iceland (Valdimarsson & Malmberg, 1999)

The confluence of several water masses and specific features of the seabed combine to create a complicated hydrographical situation around Iceland (Logemann, Ólafsson, Snorrason, Valdimarsson & Marteinsdóttir, 2013). Generally, there is a clockwise circulation of coastal water around Iceland (Jónsson, 1999). Figure 3 shows a schematic view of the main surface circulation around the country. The warm and saline Irminger Current (IC), along with water from the North Atlantic Ocean, flows from the south along the western side of the Reykjanes Ridge toward Iceland. This water mass prevails along the south and west coasts (Valdimarsson & Malmberg, 1999).

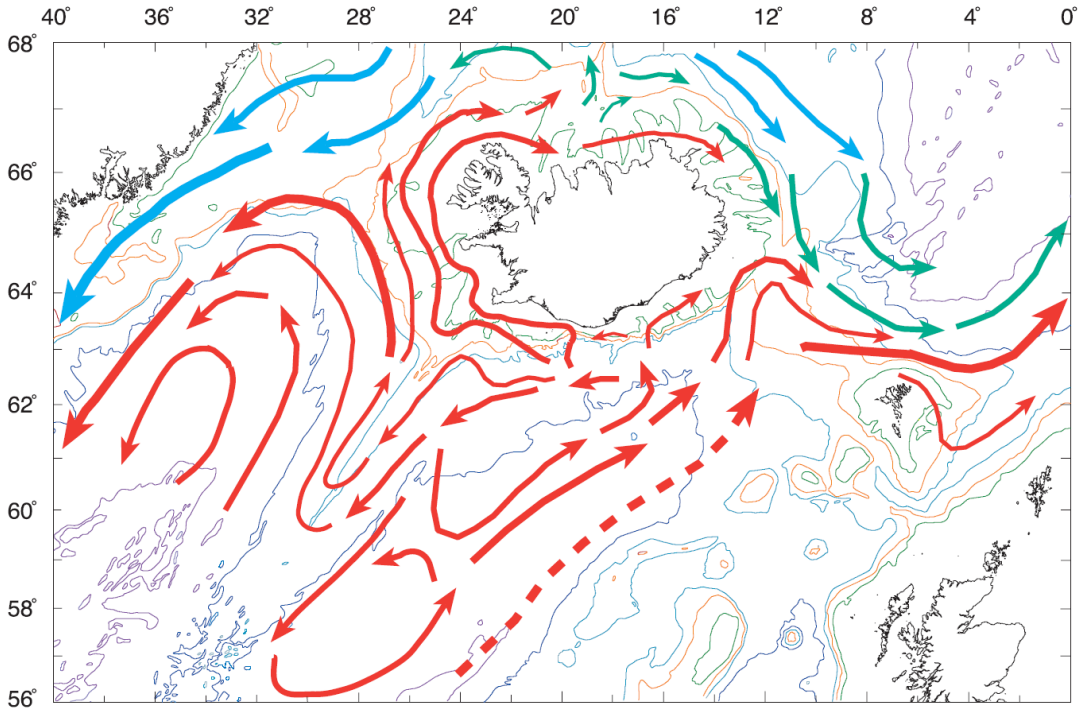

Figure 3. Surface circulation in Icelandic waters, measured via drifter from May 1995 to November 1996. The red, blue, and green arrows represent Atlantic water, Polar water and mixed water, respectively. (Valdimarsson & Malmberg, 1999)

About 5–10 % of the IC flows northward through the Denmark Strait and eventually eastward along the North Icelandic Shelf (Logemann et al., 2013). Then, the North Icelandic Irminger Current (NIIC) transports warm and saline Atlantic waters through the Denmark Strait toward the north of Iceland (Logemann & Harms, 2006). Logemann and Harms (2006) used a model with a high spatial resolution to simulate the NIIC around Iceland. Their results demonstrated that a part of NIIC recirculates in between sections 4 and 5 of its pathway (Figure 4). They stated that the NIIC, flowing eastward, has a significant effect, as a heat source, to the area along the coast and the variation of temperature over the region.

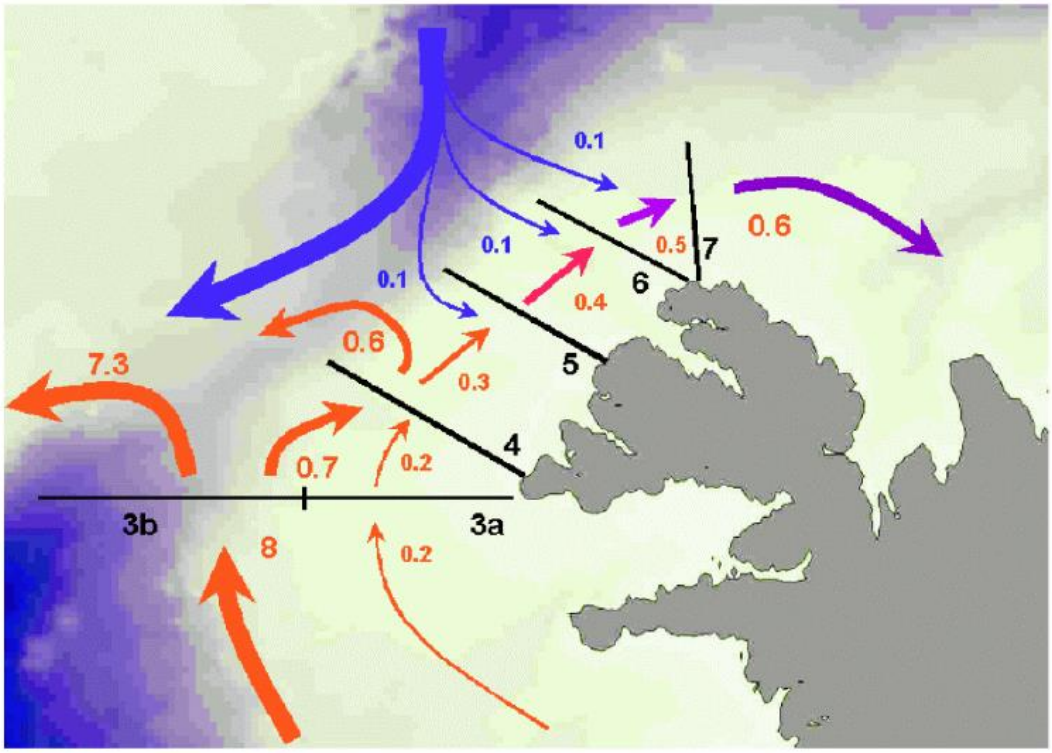

Figure 4. Simulated mean flow of the NIIC and its pathway, 1997–2003. The red and blue arrows represent warm and cold currents, respectively and the black and colored numbers represent sections and Sverdrup rates respectively. (Logemann & Harms, 2006)

As can be seen, in between sections 4 and 5, the area of interest in this research is mostly influenced by the NIIC, which is the prevailing warm current over the Westfjords region. Jónsson and Valdimarsson (2012) presented the North Icelandic Jet (NIJ) as a cold and deep current from the west of the Kolbeinsey Ridge along the northern Icelandic continental slope. The jet is one of the main sources of dense overflow water and appropriates about half of the total overflow transport throughout the region (Våge, Pickart, Spall, Valdimarsson, Jónsson, Torres, Østerhus & Eldevik, 2011).

2.2 Seawater temperature around Iceland

The variability of the seawater temperature around Iceland is primarily related to the currents coming from Atlantic and Polar sources (Astthorssona et al., 2007). Valdimarsson and Malmberg (1999) demonstrated that there are strong horizontal and vertical temperature gradients in Icelandic waters where warm and cold currents meet each other and these are strongest in the northwest and the southeast of the country. Logemann and Harms (2006) presented isotherm lines around Iceland, as illustrated in Figure 5.

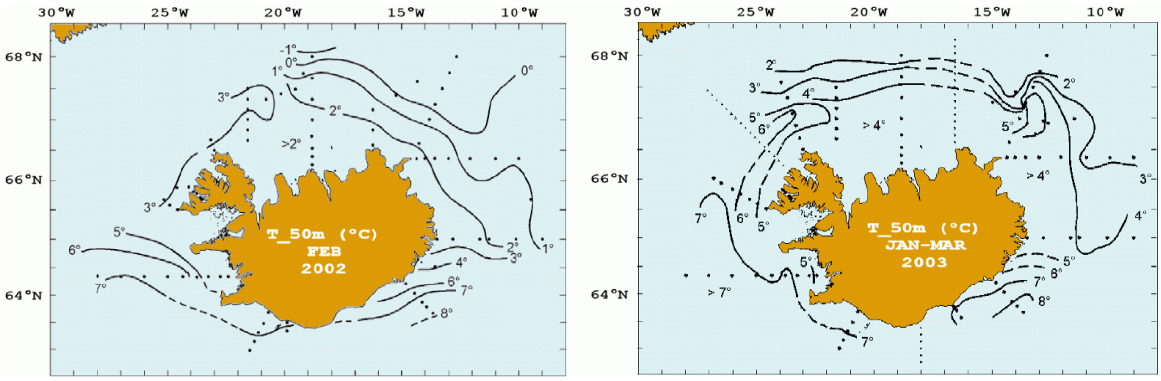

Figure 5. Water temperature measurements taken in February 2002 (left) and from January–March 2003 (right) at a depth of 50 m (Logemann & Harms, 2006)

Studies have shown that during several periods (e.g., from 1972 to 1974, in 1980, from 1984 to 1987, from 1991 to 1994, and from 1999 to 2001), northern Icelandic water was mostly influenced by warm Atlantic water. However, during other periods (e.g., from 1975 to 1979, in 1982, in 1988, and from 1996 to 1998) Polar conditions and during 1981 to 1983, from 1989 to 1990, and in 1995, Arctic influences were recognized over the region (Malmberg & Jonsson, 2002). Jónsson (1999) pointed out in his study that along the south coast of Iceland, the minimum monthly mean temperature occurs sooner, in comparison to the northern coast of the country. Astthorsson et al. (2007) showed that the temperature of the Atlantic water fell between 6-11 °C in the south of Iceland. Hanna, Jónsson, Ólafsson & Valdimarsson (2006) studied Icelandic coastal Sea Surface Temperature (SST). They presented a comprehensive record of long-term Icelandic SST measurements. Jónsson (1999) studied seawater temperatures around

Iceland and analyzed gathered data from seven stations. The results showed that at almost all of the stations, the maximum monthly mean temperature occurred in August. Logemann et al. (2013) simulated seawater temperatures in Icelandic waters. The presented results support observational results based on data from the Marine Research Institute (Anonymous, 2014). The sea water temperatures recorded in 2013 at a depth of 50 m around Iceland are illustrated in Figure 6. As can be seen, in general, the seawater temperatures along the southern coast of the country were warmer than those recorded along the northern coast.

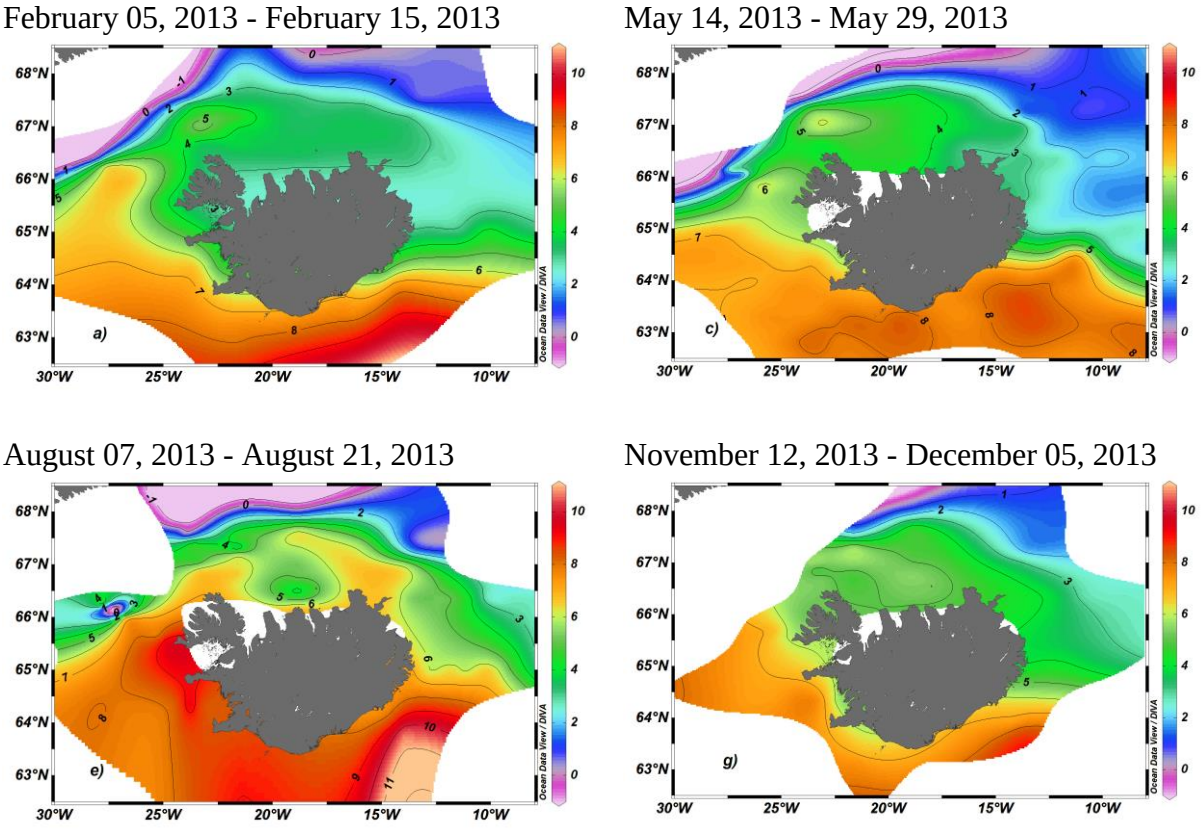

Figure 6. Seawater temperatures around Iceland at a depth of 50 m (Anonymous, 2014)

Þórðardóttir and Eydal (1996) conducted a one-year survey along the northwest coast of Iceland, with regard for the fishing and export industries. The seawater temperatures they measured in Önundarfjörður indicate that, the temperature fluctuated between 1 and 11 °C. The minimum and maximum of the temperatures were recorded in March and August, respectively as shown in Figure 7.

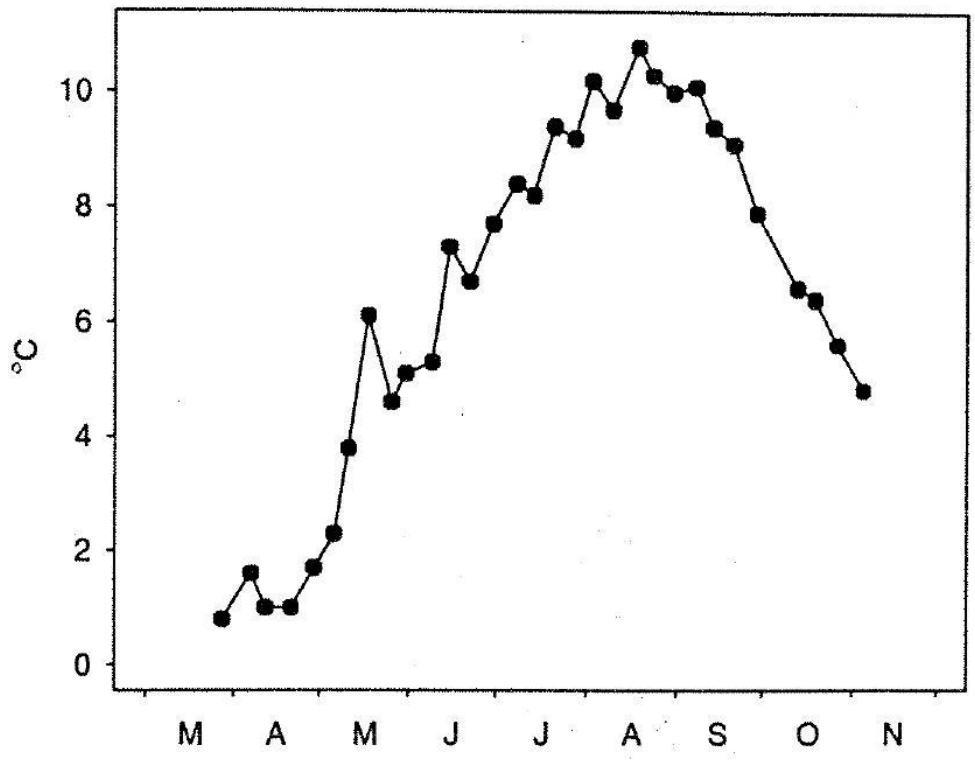

Figure 7. Monthly seawater temperature variation in Önundarfjörður in 1994 (Þórðardóttir & Eydal, 1996)

2.3 Seawater source heat pump systems and case study utilizations

Thermal energy in the seawater can be extracted via seawater source heat pump technology in the countries that are surrounded by the sea. Young, Minsung, Ki, Young and Ho (2014) pointed out that series operation seawater source heat pump system could increase the annual heating performance by at least 8% under certain conditions. They presented the single unit of the system, as shown in Figure 8.

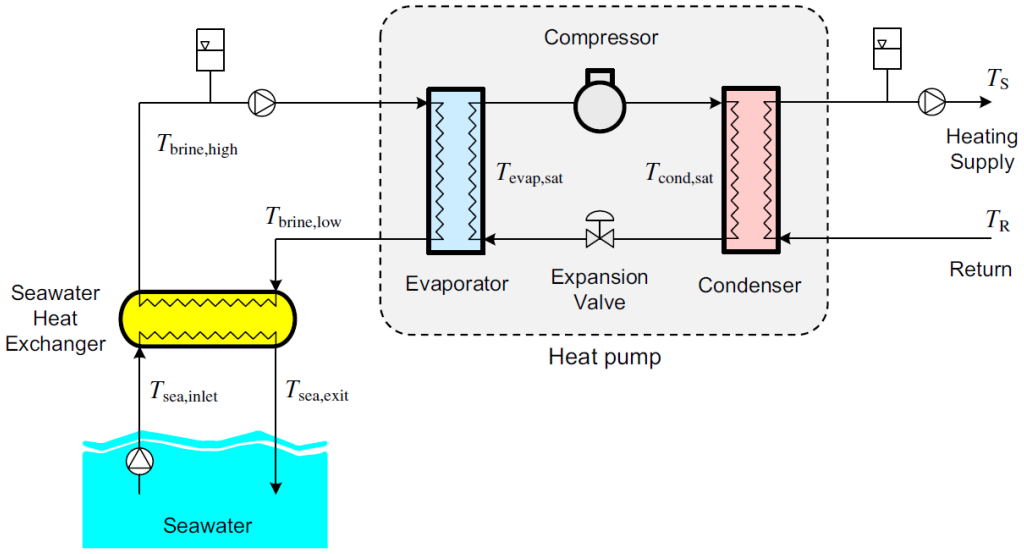

Figure 8. Single unit seawater source heat pump system (Young et al., 2014)

Young et al. (2014) also clarified the operational concept of the single unit seawater source heat pump system as follows: In the first step, seawater with temperature $T_{sea,inlet}$ is directed into the seawater heat exchanger. Afterward, brine seawater is heated up and circulated throughout the system. Then, low T_{brine} is released back into the sea with the temperature of $T_{sea,exit}$.

Zhena, Lin, Shu, Shuang and Zhub (2007) studied energy-savings and the environmental impacts of seawater source heat pump systems. Their results showed that such systems can present meaningful energy savings. They also estimated that a seawater source heat pump system can decrease the standard amount of coal used annually, which brings environmental benefits and reduces air pollution. Hani and Koiv (2012) studied the implementation of heat pump systems in different fields. They analyzed related technologies in order to improve the system's coefficient of performance (COP). They also investigated the feasibility of electrical seawater source heat pump technology and compared it with conventional district heating for within a 5 km radius. Different options of district heating and cooling production and the life cycle costs were considered in this research as well. Chua et al. (2010) studied district heating and cooling using a seawater source heat pumps system in Dalian, China. Their results indicate that the system can reduce the annual energy bill. Wandong, Tianzhen, Shijun and Huan (2014) showed that seawater temperature plays a significant rule in the thermal performance of seawater

source heat pump systems. They also notified that the thermal performance of the system should be taken into account for regions with cold winters.

Moreover, a few examples of operation of seawater source heat pump systems in cold countries are as follow:

In Sweden, heat pump systems are used for different purposes with seawater temperatures within a range of 1.5-2.0 °C (Young et al., 2014). In 2012, the total heating power from several seawater heat pumps in Värtaverket (Ropsten and Nimrod), located in Stockholm, was close to 340 MW. A system operates with 3 °C seawater from a depth of 15 m (Friotherm brochure, no date; Värme samägt, 2012). At Ropsten-1 in Stockholm, six two-stages heat pump compressors were used. The system supplies around 150 MW of heating power in general. Furthermore, at Ropsten-3, another heat pump system, with a capacity of 100 MW, is in operation (Ásmundsson et al., 2013). In Norway, a heat pump system operates with seawater at a range of 4-7 °C to supply the district heating for an area of about 15 km^2. At Nordfjordeid in Sognog Fjordane, Norway, seawater from 50 m depth and within a range of 8-10 °C is used to operate around 40 heat pumps in order to supply 8.5 GWh of heating energy. In Trondheim, Norway, about 800 kW of seawater sourced heating power is supplied by a 1.1 MW heat pump for one of the largest water parks in Scandinavia (Ásmundsson et al., 2013). In the Faroe Islands, a seawater source heat pump system has been utilized for several purposes, such as public and private district heating. In Thorshavn, a home for the elderly (Boðanesheimið) is heated with four heat pumps, producing in total 54 kW, which extract heat from the ocean via a closed glycol loop connected to a seawater heat exchanger located at the shore. At the Betesta church in Klaksvík, a carbon dioxide (CO_2) heat pump producing roughly 100 kW, has been assembled by a marine engineer, Esmar Müller. The system extracts heat from seawater in a single stage and uses three Dorin reciprocating compressors (R. Ásmundsson, personal communication, 2016). In Japan, in some regions such as Fukuoka Seaside Momochi, the Osaka Nanko Cosmosquare Area, and Sunport Takamatsu, seawater source heat pumps have been operated for district heating and cooling since 1993 (Young et al., 2014). Furthermore, several countries and regions, such as Alaska in the United States, Canada, China, and Korea, are using seawater source heat pump systems for heating and cooling purposes.

3 Definition of Renewable Energy

Renewable energy is a form of energy that is obtained from sources that can be replenished naturally on a continual basis (Edenhofer, Pichs-Madruga, Sokona, Seyboth, Matschoss, Kadner, Zwickel, Eickemeier, Hansen, Schlömer & von Stechow, 2011). Renewable energy technologies generate useful energy from the natural, renewable sources of energy. The technologies can supply heat and electricity, as well as mechanical and chemical power (National Renewable Energy Laboratory, 2001). Although most renewable forms of energy are derived from the sun, tidal and geothermal energy originate from different sources (Jackson, 2000).

3.1 Ocean Energy

The oceans have a reputation for yielding remarkable sources of renewable energy in many different forms. In general, ocean energy is in the form of potential, kinetic, thermal, and chemical energy (Edenhofer et al., 2011), which originate from solar energy and gravitational forces (Jackson, 2000). Oceans absorb energy from sunlight. Stored heat in the seawater is an enormous source of renewable energy from which thermal energy can easily be generated using heat pump system technology (Hani & Koiv, 2012).

Ocean energy can be utilized for many applications, including space heating as well as cooling and generating electricity (National Renewable Energy Laboratory, 2001). In order to reduce spatial conflict between MRE installations and other marine activities, such as fishing activities, shipping, and marine protected areas, the areas of interest should be carefully investigated and assessed (Bollmann, Bosch, Colijn, Ebinghaus, Froese, Güssow, Khalilian, Krastel, Körtzinger, Langenbuch, Latif, Matthiessen, Melzner, Oschlies, Petersen, Proelß, Quaas, Reichenbach, Requate, Reusch, Rosenstiel, Schmidt, Schrottke, Sichelschmidt, Siebert, Soltwedel, Sommer,

Stattegger, Sterr, Sturm, Treude, Vafeidis, van Bernem, van Beusekom, Voss, Visbeck, Wahl, Wallmann & Weinberger, 2010).

3.1.1 Seawater source heat pump system

Today, the consumption of energy for supplying heat is increasing (Eisentraut & Brown, 2104). A Water Source Heat Pump (WSHP) system applies water, including seawater, as a source of heat energy to provide useable heat (Sustainable Energy Authority of Ireland, no date). The system transfers heat from the heat source, which is at a low temperature, into a district heating system or heat sink with a higher temperature by using an external source of energy (Eisentraut & Brown, 2014). The availability of the heat source, the range of temperatures, and the investment costs are the important factors in the successful implementation of such a system (Forsén, 2005). Figure 9 shows a WSHP schematically.

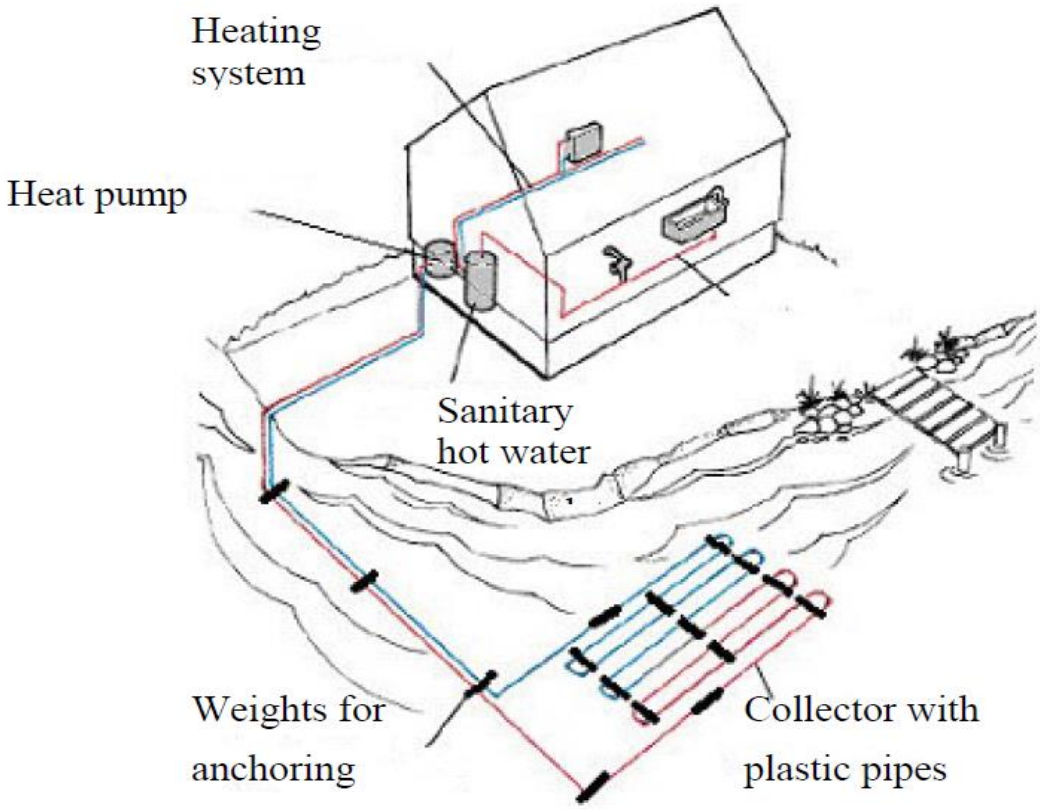

Figure 9. Major components of a water source heat pump (Forsén, 2005)

The system contains two main parts: a water heat exchanger by which heat is delivered to the heat pump and the heat pump that heats the water. In WSHP systems, water loops are inseparable components of the system. The looping system links together different parts, such as the heat pumps, the heat rejecter (i.e., a cooling tower), the heat exchanger, the heat adder (i.e., a boiler), circulation pumps, and related accessories (Murphy, 2007). Depending on the utilization of the source, WSHPs are categorized as closed-loop and open-loop systems. In an open-loop system, the water flows through the heat pump to extract latent heat from the water. Afterward, the water is discharged out of the system. In a closed-loop system, pipes and heat exchange panels are placed directly into the water in order to absorb and then extract heat energy. In a closed-loop system, a mixture of fluids such as water and anti-freeze are applied. In this system, the heat source is never used directly. Figure 10 shows closed-loop and open-loop systems. In general, open-loop systems need more maintenance in comparison to closed-loop systems (Sustainable Energy Authority of Ireland, no date).

Figure 10. Open-loop system (left) and closed-loop system (right) of WSHP (Sustainable Energy Authority of Ireland, no date)

Generally, WSHPs for district heating and cooling systems are not only major feats of engineering; they also require consideration of economic and management factors (Xiang-li, Lin & Hai-wen, 2010).

3.1.2 Heat Pumps

Today, heat pumps are among the most energy-efficient devices. Heat pumps are able to supply three to six units of thermal energy services in absolute terms by consuming one unit of energy. Regarding the EU Directive on the promotion of renewable energy, heat pump systems are known as a renewable energy technology (International Renewable Energy Agency, 2013). They are the only systems that include a process in which a percentage of the heat produced recirculates back into the system to produce useful outcomes, such as space heating, hot water, and even desalination. This ability improves energy efficiency and eliminates negative environmental impacts of the system (Chua, Chou & Yang, 2010).

According to the Directive 2010/31/EU of the European Parliament and Article 2 of the Council of 19 May 2010 on the Energy Performance of Buildings (EPBD), heat pumps are defined in the following terms:

> Heat pump means a machine, a device or installation that transfers heat from natural surroundings such as air, water or ground to buildings or industrial applications by reversing the natural flow of heat such that it flows from a lower to a higher temperature. For reversible heat pumps, it may also move heat from the building to the natural surroundings. (Borre, 2011, p. 1)

Borre (2011) also defines heat pumps as

> A machine, device or installation using renewable natural energy sources from aerothermal, geothermal or hydrothermal heat or non-natural processed wasted heat from water or air and which transfers it to buildings or industrial applications by reversing the natural flow of heat such that it flows from a lower to a higher useful temperature. Primary energy input from electricity, gas or fuel is needed to drive this process. In extreme climatic conditions, additional heating device must compensate the reduced heat production from heat pumps. Only heat pumps with an output that

significantly exceeds the primary energy needed to drive them and the additional heating device energy should be considered. (p. 2)

Heat pumps use heat from different sources of energy, as shown in Figure 11.

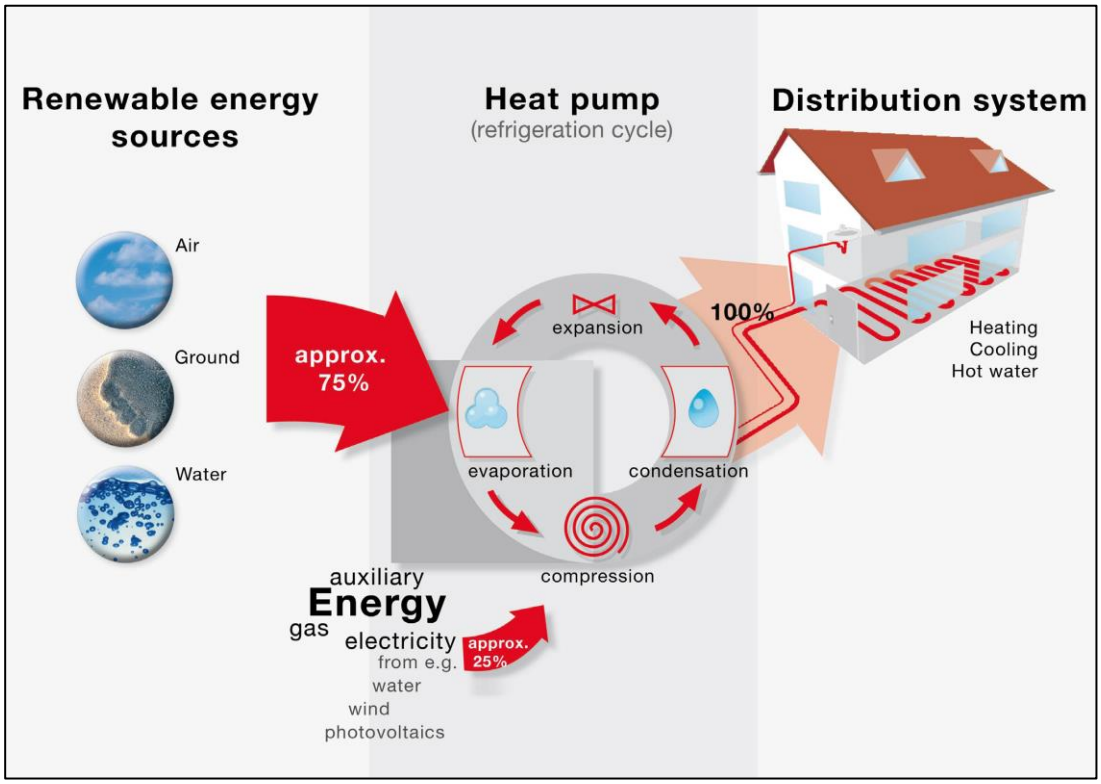

Figure 11. Schematic operation of a heat pump system (Borre, 2011)

Moreover, point 31 of the European Directives mentions renewable energy usage by heat pumps as follow:

> Heat pumps enabling the use of aerothermal, geothermal or hydrothermal heat at a useful temperature level need electricity or other auxiliary energy to function. The energy used to drive heat pumps should therefore be deducted from the total usable heat. Only heat pumps with an output that significantly exceeds the primary energy needed to drive it should be taken into account. (Borre, 2011, p. 1)

Heat pumps can be used for district heating as well as cooling, hot water, swimming pools, sidewalk snow melt, fishing activities, and industrial facilities such as conditioners and refrigerators (Forsén, 2005).

3.1.3 Principles of heat pump operation

Heat pumps operate on the second law of thermodynamics, which is based on the Carnot principle developed by French scientist Nicolas Léonard Sadi Carnot in 1824. Technically, in a complete cycle of heat pump operations, mechanical energy is obtained from thermal energy (International Renewable Energy Agency, 2013). The Carnot cycle comprised four phases: isothermal expansion, contraction, thermally isolated expansion, and contraction. The phases for non ideal refrigeration cycle are shown in Figure 12.

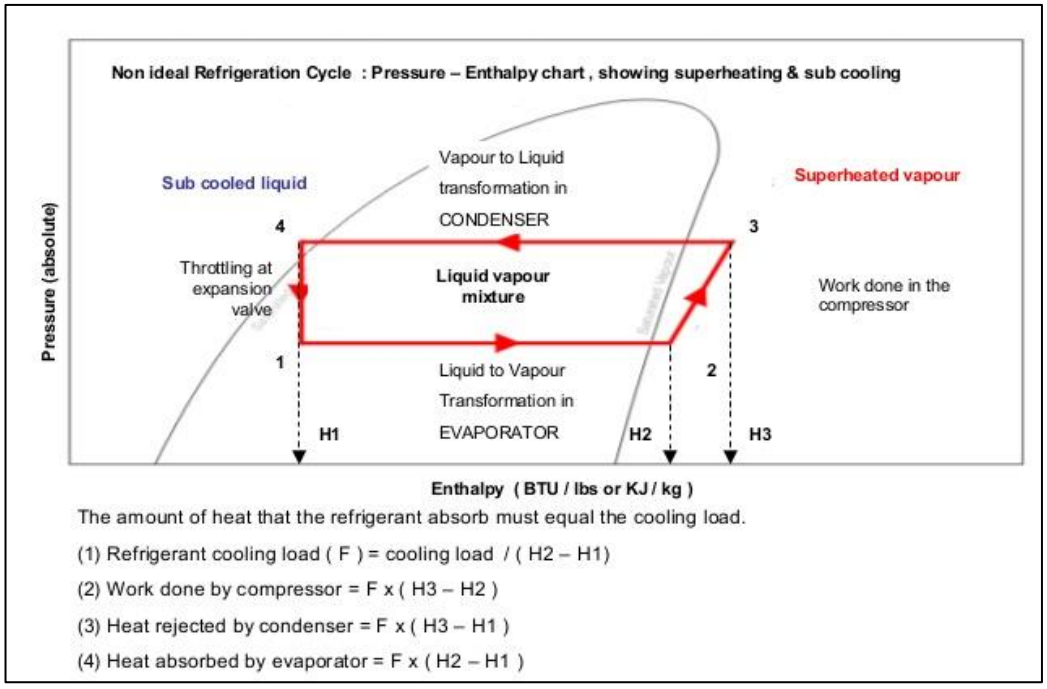

Figure 12. Carnot cycle (Hossain, 2014)

Also for the operation of heat pump system, four phases of the Carnot cycle are defined as follows (Denker, Modern Thermodynamics, 2005):

Phase 1_ Isothermal expansion: The gas is expanded by the absorption of the heat reservoir (Q_H) at a temperature of (T_1). Since the stage is isothermal, the temperature of the gas does not change, but it leads to work on surroundings. In this stage, the entropy of gas is $\Delta S = \frac{Q_H}{T_1}$.

Phase 2_ Isentropic expansion: The gas continues expanding and its temperature drops to (T_2). In this stage the gas also works on surroundings while the entropy does not change.

Phase 3_ Isothermal compression: Surroundings work on the gas and the gas compressed. At a constant lower temperature of gas (T_2) which lead to heat energy of (Q_c). The entropy of the gas is $\Delta S = \frac{Q_c}{T_2}$.

Phase 4_ Isentropic compression: Surroundings continue to work on the gas, and the cycle will be completed. While the entropy of the gas does not change, the internal energy and the temperature (T_1), increase again.

In the Carnot cycle, the ratio of heat and absolute temperature are the same (Erlichson, 1998):

$$\frac{Q_H}{Q_c} = \frac{T_1}{T_2} \qquad [1]$$

Where Q_H, T_1, and Q_C , T_2 are the heat and the temperature of the source and the sink, respectively.

Also, work done per cycle can be calculated as:

$$W = Q_H - Q_c \qquad [2]$$

Furthermore, regarding the first law of thermodynamics and conservation of energy the efficiency of a system is:

$$\eta = \frac{W}{Q_H} \text{ Or } \frac{Q_H - Q_c}{Q_H} \qquad [3]$$

Then, efficiency of the Carnot cycle is obtained as follows:

$$E = \frac{T_1 - T_2}{T_1} \qquad [4]$$

Or

$$\eta_{he} = \frac{T_{hot} - T_{cold}}{T_{hot}} \qquad [5]$$

Where η_{he} is the efficiency of the Carnot cycle. It should be noted that the temperature values are on the Kelvin scale.

There are four key components in a heat pump, including the evaporator, condenser, compressor, and expansion valve. These components are illustrated in Figure 13.

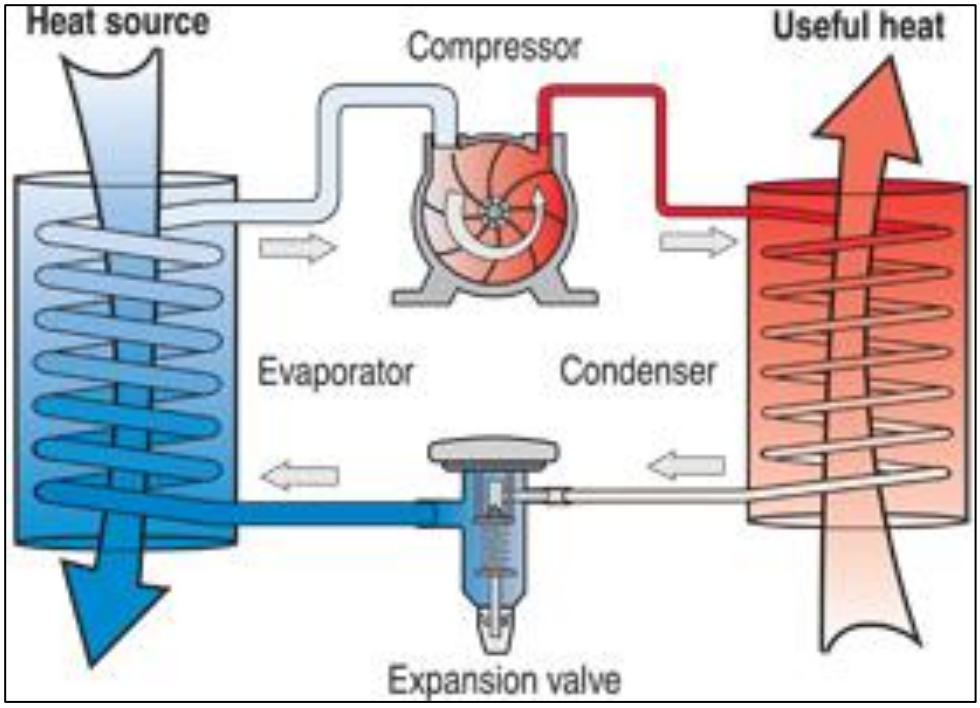

Figure 13. Heat pump components (Heat Pump Center, no date)

In the system, a fluid such as ammonia, clycol, or even potable water are applied as working fluids. Heat pumps have four main stages based on the Carnot cycle in the heating mode of operation. These stages are defined below (Sustainable Energy Authority of Ireland, no date):

Stage 1_ Heat is extracted from a lower temperature heat source, for instance air, water, or ground via a heat exchanger. This external heat energy evaporates refrigerant. Then evaporated refrigerant is delivered to the compressor.

Stage 2_ The compressor raises the pressure, and consequently, the temperature of the refrigerant is increased. The power required for the compressor can be supplied by auxiliary powers such as electricity or gas (Forsén, 2005).

Stage 3_ High pressure with high temperature refrigerant gas transfers its heat energy to the heating system. Then, the temperature of the refrigerant drops and starts converting to liquid via condenser.

Stage 4_ At the final stage, an expansion valve decreases the pressure of the refrigerant. In order to complete the cycle, a mixture of gas/liquid refrigerant with low pressure is delivered to the heat exchanger, and the cycle starts again.

The two major factors by which performance of a heat pump unit is considered includes the performance of the heat pump units and the conditions in which the system works. In the system, thermodynamic perfectibility is defined as the tendency of the current cycle to the ideal cycle in the system. Also, the index of thermodynamic perfectibility is applied to find the efficiency of heat pump units (Haiwen, Lin, Jing, Xin, Zhiyong & Haiyang, 2015). The efficiency of heat pumps has improved notably over the past years. The overall efficiency of a heat pump system is called the Coefficient of Performance (COP). COP is an important performance indicator for the system. COP is defined as a ratio of entire amount of supplied heat to the total power input to the system (Haiwen, Lin, Jing, Xin, Zhiyong & Haiyang, 2015):

$$COP = \frac{\dot{Q}}{\dot{W}} \qquad [6]$$

Where $\dot{Q}$ is the supplied heat power from the source and $\dot{W}$ is the power delivered to the heat pump system.

COP depends on three main factors, including the type of the heat source, the efficiency of the appliance, and the difference between the temperatures of the heat source and the heat sink.

In the heating mode of a heat pump, the COP is more than 1 (Forsén, 2005). The larger the discrepancy in temperature that exists between the heat source and the sink, the lower the COP (International Renewable Energy Agency, 2013).

3.2 The utilization of a heat exchanger

Heat exchangers are the key devices used in order to extract heat from seawater. They transfer heat from one fluid to another when both fluids have different temperatures (Arya & Dhanjibhai, 2015). There are several types of heat exchangers that have been used worldwide. However, for ocean heat extraction, the tube heat exchangers possess several advantages in comparison to other types of heat exchangers. The tube heat exchanger, which is the most accepted heat exchanger in the industry, presents a great deal of promise that can be taken into consideration. The following are the main reasons for which tube heat exchanger has been selected as having the most potential for implementation (MTS Systems Corporation, 2005; Subbarao, no date):

- High availability of information about the design, fabrication, operation, and maintainence
- Ability to tolerate high pressure and to transfer a high ratio of heat
- Relatively high degree of adaptation to the oceanographic conditions
- Simple manufacturing and accessibility to the materials in a wide variety of sizes
- Easy maintenance, repairs, replacement, and cleaning
- Inexpensive accessories in comparison to other types of heat exchangers
- Little, if any, maintenance during its long lifespan of operation
- Allows utilization of free seawater flow access directly to the tubes, i.e. the tube heat exchanger can be designed without a shell with forced seawater flow

3.2.1 The principal components of a heat exchanger

It is also vital for decision makers to acquire general insight into the mechanical features of a heat exchanger prior to making any decision to implement such a device. In this regard, major components of the heat exchanger will be described in this section.

Tube bundle

The tube bundle is the part of the heat exchanger that consists of a set of tubes, tube sheets, baffles, tie rods, spacers, and sliding strips. The tube is the basic and the most important component of a heat exchanger. Tubes transfer heat between fluids that are flowing both outside and inside of the tube. The tubes can be categorized as different types, such as plain or longitudinally finned (Mukherjee, 1998). In order to transfer heat efficiently, the maximum number of tubes in a heat exchanger are applied. Tubing can be fabricated to be either seamless or welded. For the tubing, some criteria should be taken into account, including the number of tubes, which depends directly on the rate of flowing fluids and pressure conditions, tube diameter, tube materials, tube thickness, straightness of the tubes, tube passes, and tube patterns (Arya & Dhanjibhai, 2015). Tube thickness plays a main role in high-pressure and corrosive conditions. The angles between tubes comprise the tube pattern, as illustrated in Figure 14. The shortest distance between the centers of each tube is called the tube pitch. Pressure conditions and velocity control, heat transfers, and mechanical cleaning all are dependent on the geometry of the tube pitch in the heat exchanger (Mukherjee, 1998).

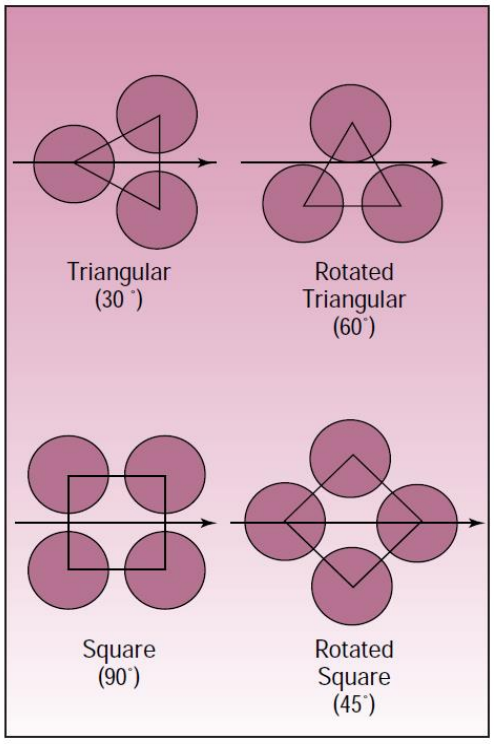

Figure 14. Tube patterns and tube pitch (Mukherjee, 1998)

Tube sheets

Another component of the heat exchanger is the tube sheet. The tube sheet is a part of the device through which tubes are inserted. Tube sheets are made in the form of round plates of metal or forgings drilled and grooved. Depending on the pattern of tubes in the heat exchanger, drilled holes in the tube sheet are formed into either triangular or square shapes. In some cases, the heat exchangers also can operate without tube sheets. The thickness, diameter, and the material of the tube sheet play important roles in the quality of this mechanical part.

Baffle

In a heat exchanger, baffles support the tubes. The plate baffle and rod baffle are two types of baffle. Baffles serve different functions in the heat exchangers (Mukherjee, 1998), by doing the following:

- Supporting the tubes
- Maintaining space between the tubes
- Directing the flowing fluid through the tubes and shell
- Improving the transfer of the heat between the flow on the outside and inner side of the tubes
- Preventing failure of the tube against vibration and sagging

The fabrication of the baffle in the tube bundle is related to the heat transfer coefficient of the system. The number of baffles and baffle spacing are the two main characteristics of the baffle in a heat exchanger. Figure 15 shows baffle spacing in a heat exchanger.

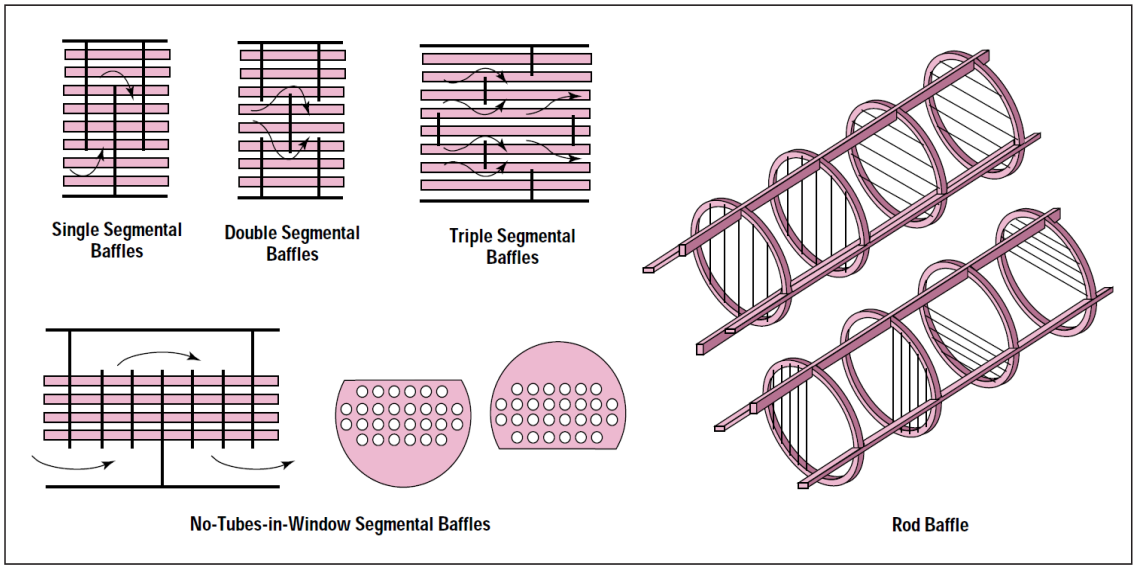

Figure 15. Baffle spacing in a heat exchanger (Mukherjee, 1998)

Moreover, based on the type of the heat exchanger, the following components are used in the system as well:

- Tie-rods and spacers
- Channel cover
- Pass partition plates
- Nozzles
- Impingement plate
- Longitudinal baffle
- Connections
- Sealing strips
- Supports
- Foundation
- Overall length
- Bolt holes

Aforementioned equipment, should be taken into account for implementation of the seawater source heat pump system in Önundarfjörður.

Types of material

One of the crucial factors in the manufacturing, operation, and maintenance of the heat exchangers is the selection of materials. The materials used must reach the relevant standards, codes, and ordinances that are in place. To identify appropriate materials and alloys for the manufacturing of the heat exchanger, the following criteria should be assessed (EZGİ, 2014 ; Farhami & Bozorgian, 2011):

- Environmental condition and location of the device in the field
- Availability of the material
- Initial cost of the material
- Political considerations
- Previous experiences with materials in similar situations
- Maintenance and failure cost
- Water quality, such as purity, pH level, etc.

Careful consideration of the aforementioned criteria prior to the installation of a seawater source heat pump will reduce the risks of corrosion, fouling, fatigue, erosion, and microbiological influenced corrosion (MIC).

4 Description of the area of study

Flateyri is a small town with a geographical positon of N66° 3' 0.976" and W23° 30' 46.205". As shown in Figure 16, the town is located in the Westfjords region in the northwest corner of Iceland. The town is 482 km by road from Reykjavík, the capital of Iceland.

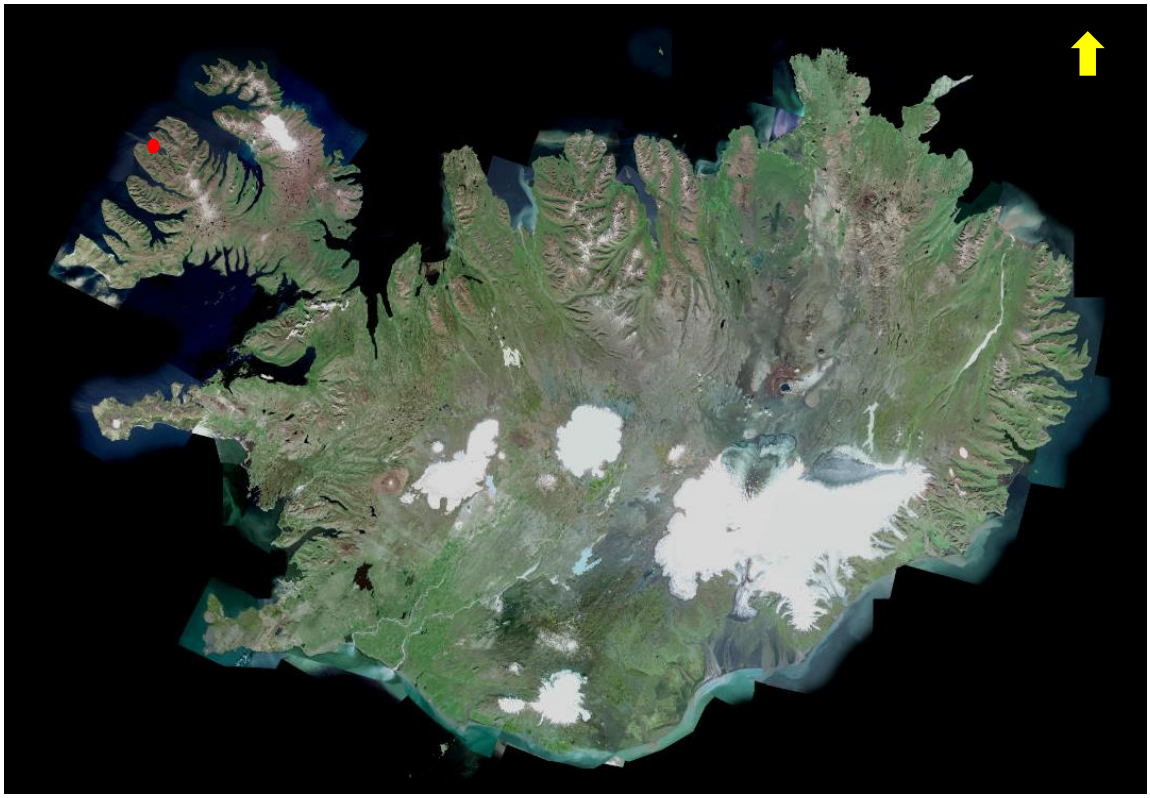

Figure 16. The red dot mark is the location of Flateyri (Kortasjá, 2016)

The town is surrounded by steep mountains. Flateyri (Figure 17) is the largest settlement on the coast of Önundarfjörður.

Figure 17. Flateyri (MATS, 2016)

The town also has a history of whaling, shark-hunting, and fishing activities. In 2015, the population of Flateyri was 206.

There is an active port in Flateyri. The area of the port is around 32,600 m^2. The port is protected with a rubble-mound breakwater and seawall. Although the port has multiple purposes, but the main activities are related to fishing. The port has loading and unloading facilities, two landing cranes, a floating deck, a concrete pier, and an 80 m long wharf purposed for cruise ship landings and cargo. In Önundarfjörður, there are 47 vessels registered with Flateyri as their home port. The largest boat with the Flateyri as its home port is 35.98 m with gross tonnage of 275.37 ton (The Directorate of Fisheries, no date). Bigger vessels such as cruise ships also operate in the

fjord occasionally. In Önundarfjörður, the safe distance for navigation is around 150-200 m from the shoreline (G. Kristjánsson, personal communication, April 7, 2016).

Observation data from the weather station located in Flateyri, indicate that the area of Önundarfjörður is well protected against the wind. Figure 18 and Figure 19 show time series of meteorological data from the station for one year of measurements, from April 1, 2015 to April 1, 2016, which are contemporaneous with the present research. The meteorological raw data are available in the Icelandic Meteorological Office (IMO).

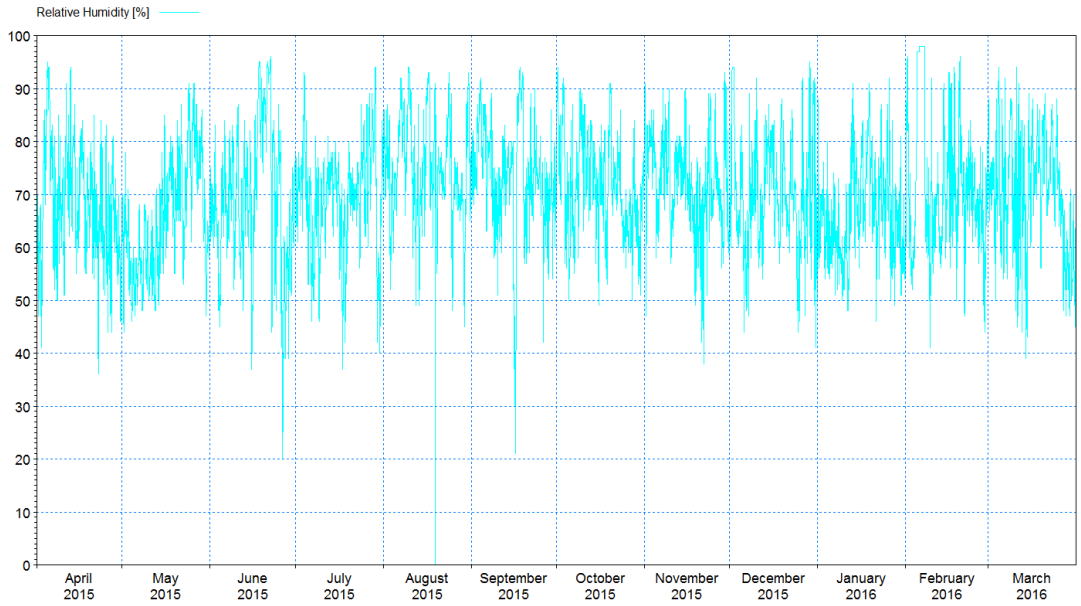

Figure 18. Monthly recorded relative humidity at the Flateyri weather station

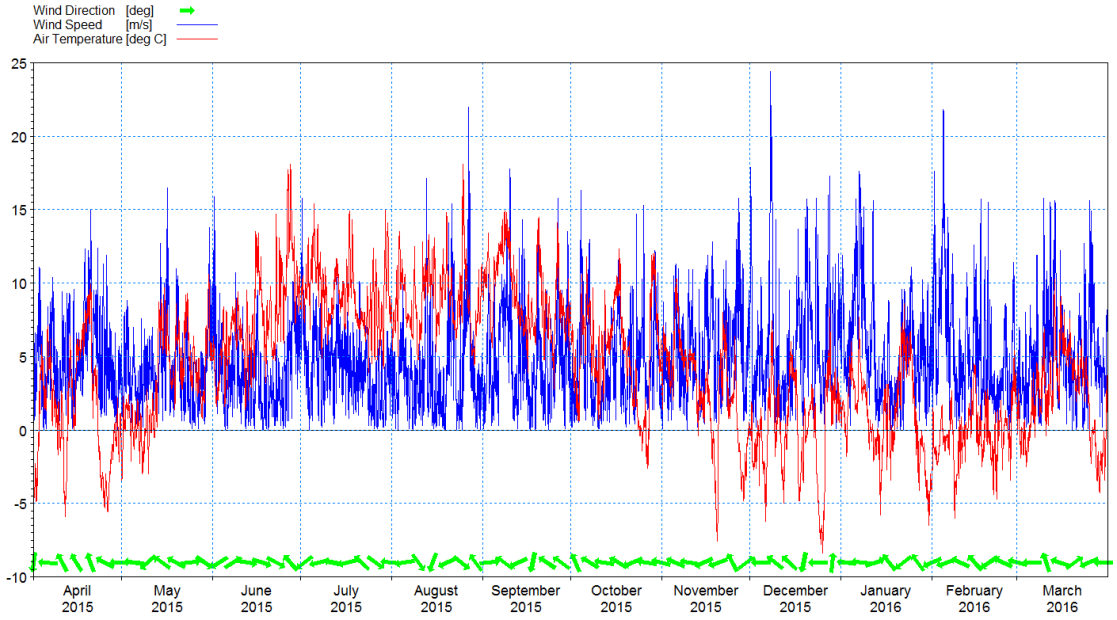

Figure 19. Monthly wind data and air temperature at the Flateyri weather station

As shown in the last two figures, the air temperature falls to below zero on the Celsius scale in the winter time. Also, with increase of the air temperature, the relative humidity decreased in the area. A descriptive presentation of wind, such as wind speed and wind direction over the area, is plotted in Figure 20 as a wind rose diagram.

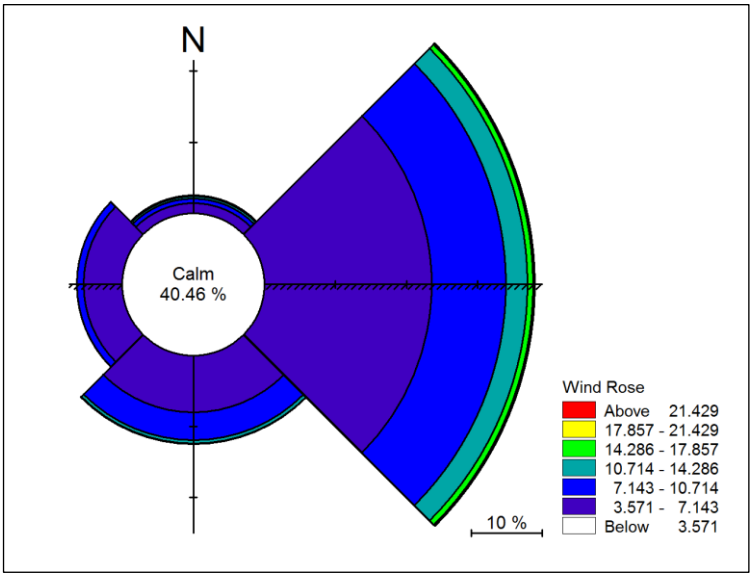

Figure 20. Wind rose plot of Flateyri from April 1, 2015 to April 1, 2016

As depicted in Figure 20, the distribution of the rose wind shows that the east and southeast are as the prominent sectors of wind. Also, the maximum and average wind speed are 24.4 m/s and 4.84 m/s respectively.

In Flateyri, the major sources of energy are provided via electricity and oil. For space heating and the supply of hot water, district heating has been used in the town. The utilization of district heating is known as an efficient way to distribute heat. In a district heating system, water is heated and then distributed throughout network piping. District heating is an economical system to service residential as well as industrial sectors (Baker & Schaefermeyer, 2013). Figure 21 depicts a screenshot of the district heating system in Flateyri, which is monitored by the regional power utility, Orkubú Vestfjarða.

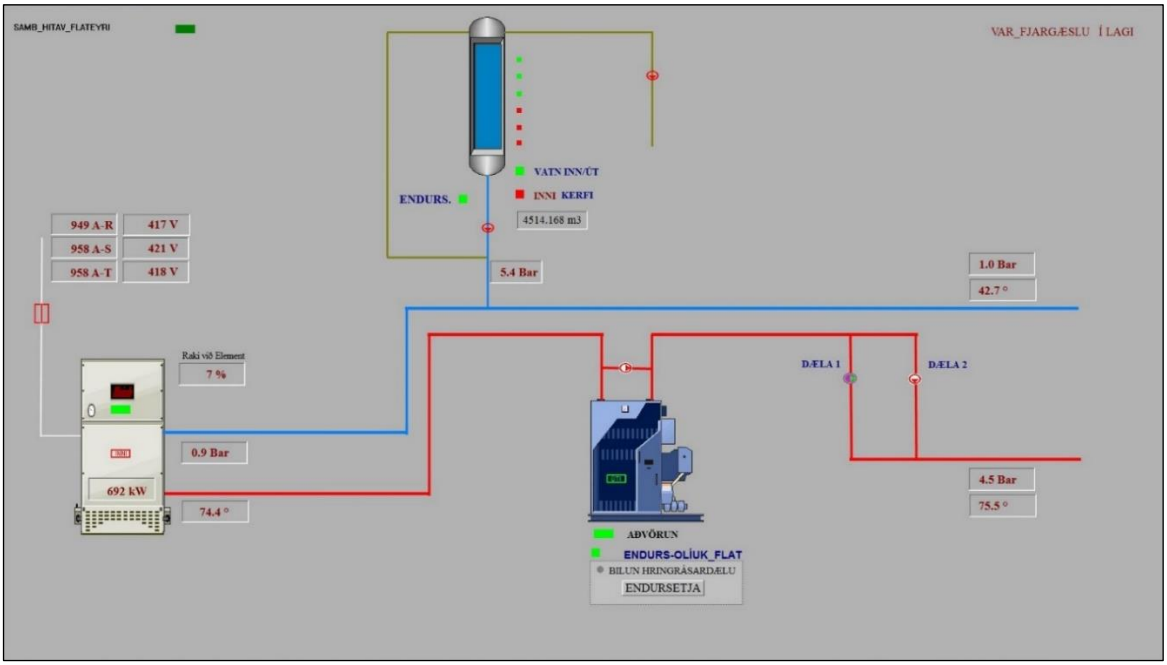

Figure 21. Schematic diagram of the district heating system for Flateyri (Orkubú Vestfjarða, 2016)

As shown in the figure, hot water is distributed throughout the closed, insulated piping system at 75.5 °C and re-circulated back to the district heating at 42.7 °C. In the system, hot water is supplied via an electrical boiler. However, an oil boiler is also added to the system in necessary

conditions as an auxiliary boiler. In Flateyri, both electricity and oil are used to supply hot water and space heating for private users, industries, and the public sector, in addition to other user as categorized in Table 2.

Table 2. Total consumption of electricity for space heating and hot water in Flateyri in 2015 (Orkubú Vestfjarða, 2016)

Consumption of electricity	(kWh)	Consumption of electricity to supply hot water	(kWh)
Private users	85716	Private users	2470285
Industries	130761	Industries and swimming pool	1880997
Public sector and other users	727567	Other users	499059
Total	963574	Total	4522590
Total		5486164	

Moreover, Table 3 describes the monthly amount of electricity consumption and oil usage in order to provide electricity for the town in 2015.

Table 3. Monthly amount of oil and electricity demands in Flateyri in 2015 (Orkubú Vestfjarða, 2016)

Month	Oil (liter)	Electricity from oil (kWh)	Electricity (kWh)
January	437	3,715	592,364
February	2,616	22,236	527,535
March	1,262	10,727	551,368
April	760	6,460	521,810
May	1,009	8,577	449,119
June	204	1,734	352,266
July	313	2,661	344,914
August	160	1,360	355,088
September	6,053	51,451	327,605
October	458	3,893	497,516
Novemver	93	791	550,944
December	13,075	111,138	469,179
Total	26,440	224,740	5,539,708

Table 3 shows that oil supplies around 4% of the energy consumed in Flateyri. The reasons for the small discrepancy between the total amount of electricity consumption presented in Table 2 and that presented in Table 3 are the energy loss that occurs during the distribution of energy throughout the network piping, as well as interconnection and any possible leakage (S. Sólbergsson, personal communication, April 22, 2016).

Figure 22 shows the air temperatures in Flateyri in 2015. As shown in the figure, the area experiences an ambient air temperature below zero on the Celsius scale in eight months of the year.

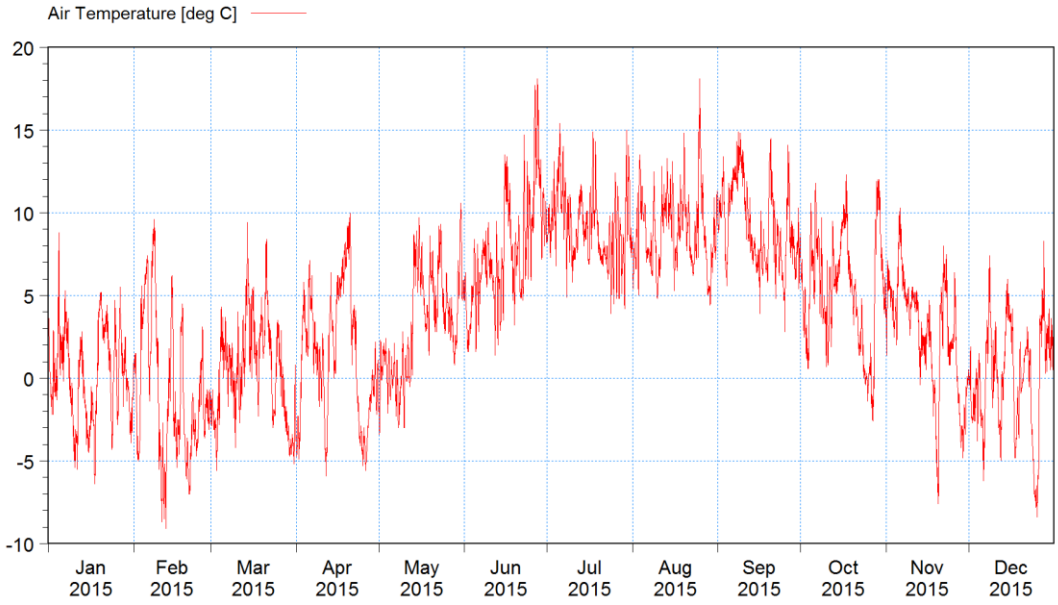

Figure 22. Monthly air temperature in Flateyri

The maximum, average, and minimum recorded air temperatures in 2015 were 18.1°C, 3.9°C and -9.1°C, respectively.

As depicted in Figure 23, the maximums consumption of electricity in the town occur in the early months and last months of the year, when air temperatures are generally below zero.

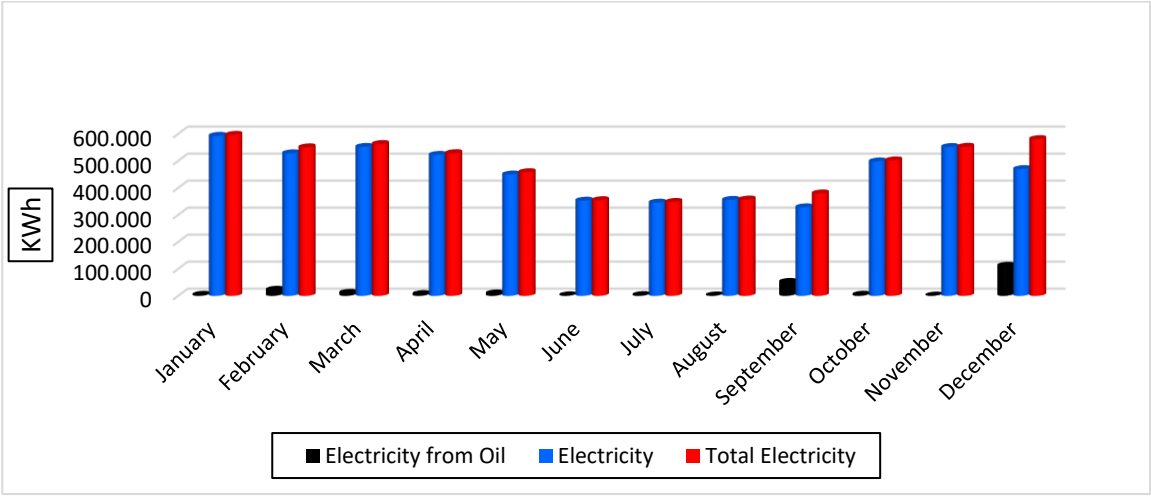

Figure 23. Monthly amount of energy demands in Flateyri in 2015 (Orkubú Vestfjarða, 2016)

As can be seen, the heating demand in the town is directly related to the weather conditions.

5 Methodology

5.1 Tools and equipment used for field measurements

In this research, the in-situ seawater temperature is measured by two different types of instruments. The instruments were moored in Önundarfjörður. The moorings were deployed accurately via Global Positioning System (GPS). The period of measurement was one year, beginning April 1, 2015 and ending April 1, 2016. Table 4 provides basic information for the four locations, hereafter called A, B, C, and D.

Table 4. Location of and mooring information for the instruments

Location	Position			Bottom depth	Type of Instrument
	Latitude	Longitude	Depth		
A	66° 2.718'N	23° 29.803'W	• Measurement at 7 depths from 1-10 m • The interval in between sensors is 1.5 m	15.5 m	SM4
B	66° 2.670'N	23° 30.370'W	• Measurement at 1 depth • 1.5 m above the bottom	16.2 m	Starmon mini
C	66° 2.879'N	23° 31.389'W	• Measurement at 1 depth • 1.5 m above the bottom	17.6 m	Starmon mini
D	66° 2.517'N	23° 34.137'W	• Measurement at 1 depth • At depth of 8 m	21.5 m	Starmon mini

The locations of the instruments are pictured in Figure 24.

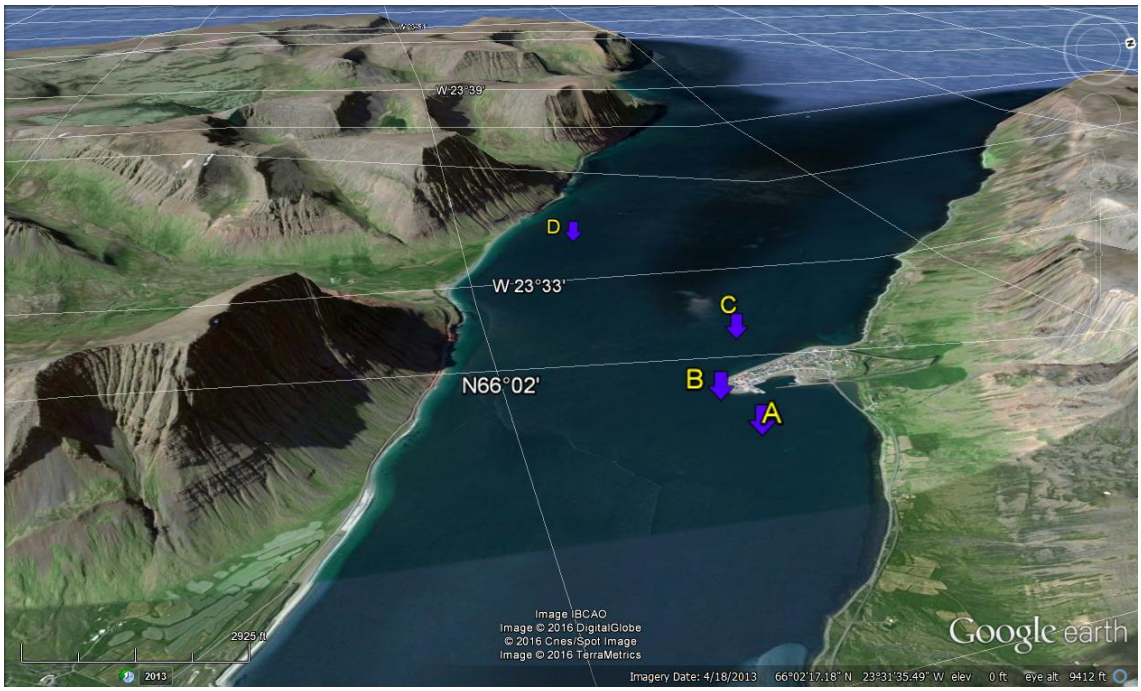

Figure 24. Location of instruments in Önundarfjörður

Figure 25 illustrates the 2D bathymetry of the fjord in order to discern the locations of the instruments for measuring seawater temperatures.

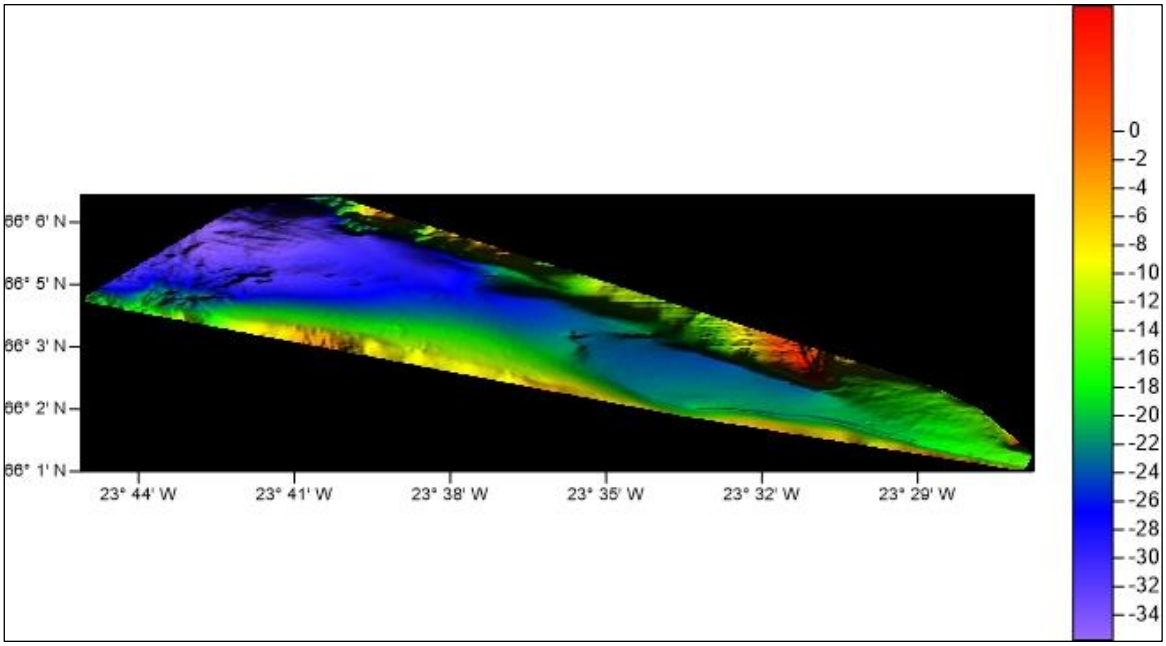

Figure 25. Plotted 2D bathymetry of Önundarfjörður, Using Surfer13

As can be seen from Table 4, location D is located in the deepest area relative to the other locations.

At location A, the instrument was attached to an aquaculture pen, as shown in Figure 26. Location A is the innermost place in the fjord in this research.

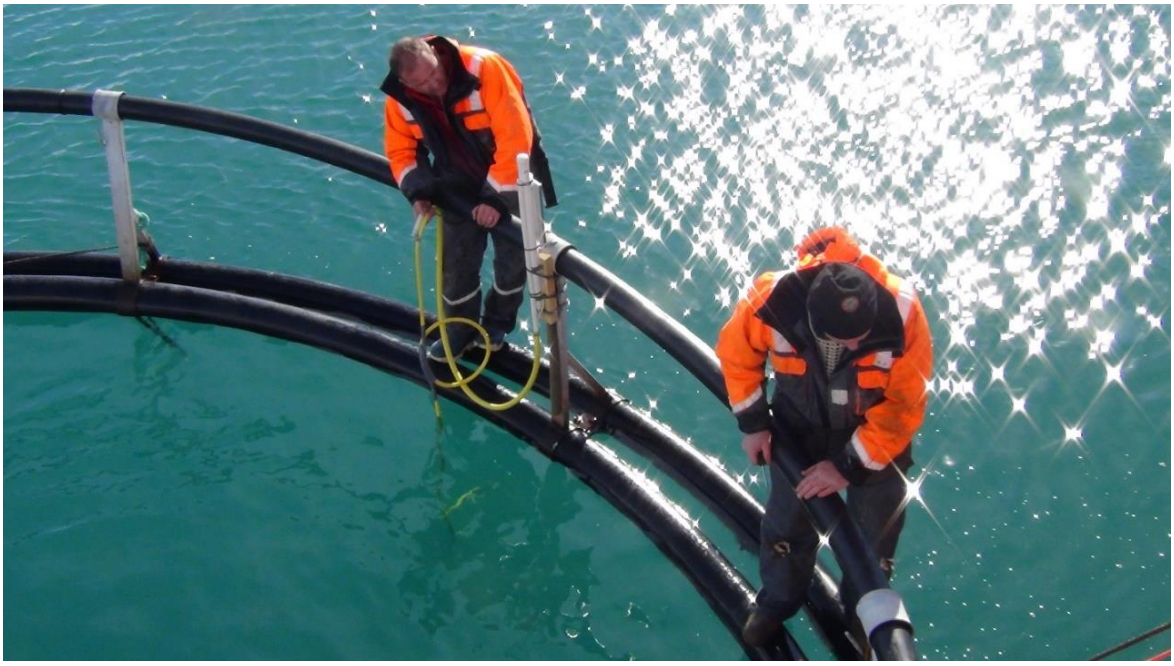

Figure 26. Attaching the instrument to the aquaculture pen at location A

At location B, the instrument was anchored to the bottom and attached to a rope located 1.5 m above the bottom. The instrument was chained to a concrete block on a rubble-mound seawall as shown in Figure 27. Location B is in front of the tip of the Flateyri peninsula and near to the port.

Figure 27. Chaining the instrument to the block at location B

At location C, the instrument was anchored to the bottom and attached to a rope 1.5 m above the bottom of the fjord. The instrument was marked with floatation buoy on the surface of the water, as shown in Figure 28. This location is at the northwest of Flateyri, along the north shore of Önundarfjörður.

Figure 28. Floating buoy at location C

At location D, an instrument was attached to an aquaculture pen at a depth of -8 m. Location D is off the southern shoreline of Önundarfjörður, near the mouth of the fjord and furthest from

Flateyri. This location was more subject to open ocean in comparison to the other tested locations in the fjord.

5.1.1 Seawater Temperature Recorder-Starmon mini

The seawater temperature was measured via Starmon mini at locations B, C, and D. Starmon mini instruments are reliable and accurate in recording seawater temperature. The instruments were covered by plastic or titanium waterproof cylinders (Figure 29) and manufactured by STAR-ODDI Ltd. in Iceland (Star ODDI Company, no date).

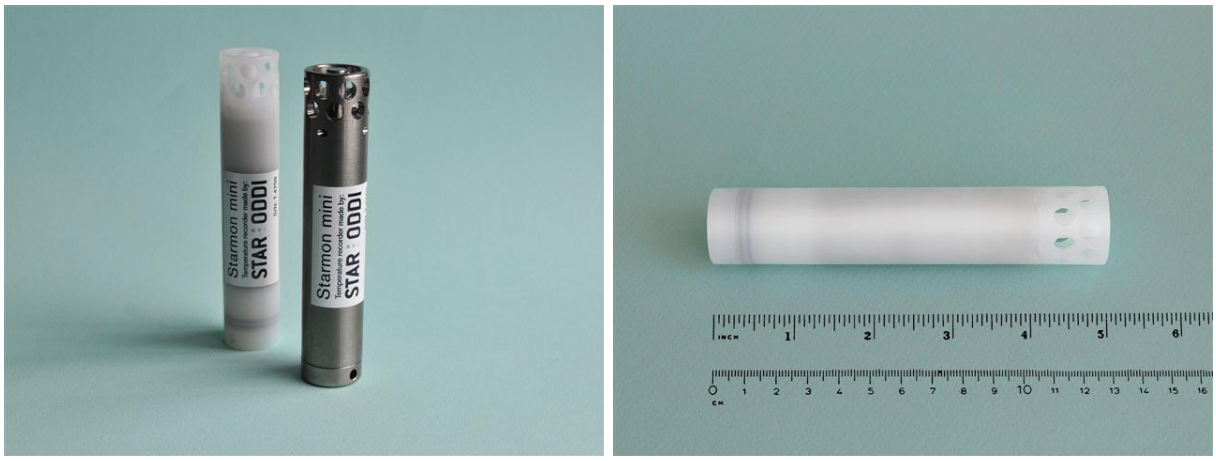

Figure 29. Starmon mini, underwater temperature recorder (Star ODDI Company, no date)

In order to protect the instruments in rough environmental and high pressure conditions, a non-corrosive, stainless steel protective housing (Figure 30) was used. The housing also helps for the better attachment of the recorder to the moorings facilities (Star ODDI Company, no date).

Figure 30. Stainless steel protective housing (Star ODDI Company, no date)

For transferring the recorded data to a PC computer, a communication cable was used. The technical specifications of the instrument are detailed in Appendix A.

5.1.2 Seawater temperature recorder- SM4

Another instrument that was used for measuring seawater temperature at location A, is developed by POLS Engineering Company in Iceland. The instrument, hereafter called SM4, has a series of DS18B20 thermometers (Ingólfsson, Grimsdottir & Jónsson, no date). The DS18B20 has a central microprocessor and required power can be directly derived from the same data line. One microprocessor controls many installed DS18B20s in different places. Technical features of the thermometer are detailed in Appendix B. In the SM4, thermistors are fixed throughout the cable at specific interval. The instrument consisted of eight thermometers, and the first one was placed at +1 m above the surface water. The following one was at a depth of -1 m and the rest were placed at 1.5 m interval through the cable. As depicted in Figure 31, one thermometer was deployed in every small circle.

Figure 31. SM4 in laboratory

During measurement, the recorded data transferred continuously by a wireless Global System for Mobile Communications (GSM) telephone connection to a central computer. The real-time output are displayed as a seawater temperature profile on the website [1] as depicted in Figure 32.

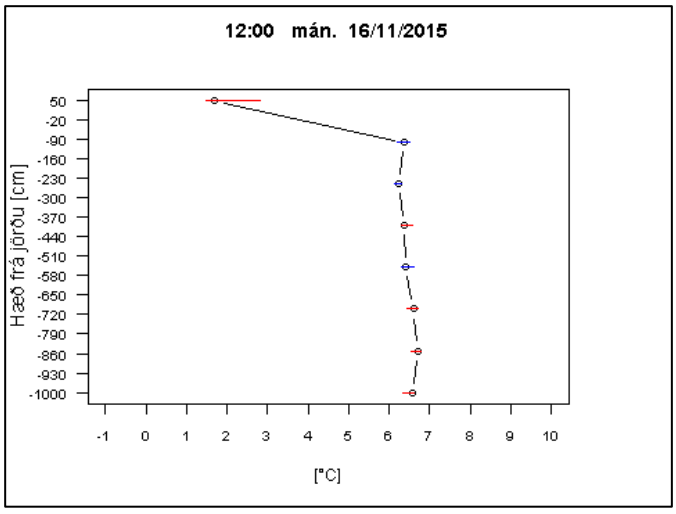

Figure 32. Graphed water temperature profile measured by the SM4 on November 16, 2015

[1] http://data.snowsense.is/snwebh2o/sngraph.php?ID=214

Since 2006, the SM4 has been mostly used for ice, snow, and avalanche applications, as well as weather forecasting in Iceland (Jónsson, Grimsdottir, Breien, Kristensen & Zeinali, 2014). However, there is a history of seawater temperature measurements via the instruments placed in Ísafjörður bay, Skutulsfjörður, and Dýrafjörður. In order to reassure the accuracy of the instrument, both the Starmon mini and the SM4 were placed at the same depth in location A from April 1, 2015, to June 15, 2015. The comparison between the instruments indicated that SM4 recorded less data than Starmon mini (by about 2%) during the period of measurement. Missing data were considered as null data in order to complete the comparison. As illustrated in Figure 33, unanimous trends in peaks and falls confirmed the reliability of the SM4 for the purposes of this research. Figure 34 shows the good qualitative correlation between data, with consistency between the two instruments.

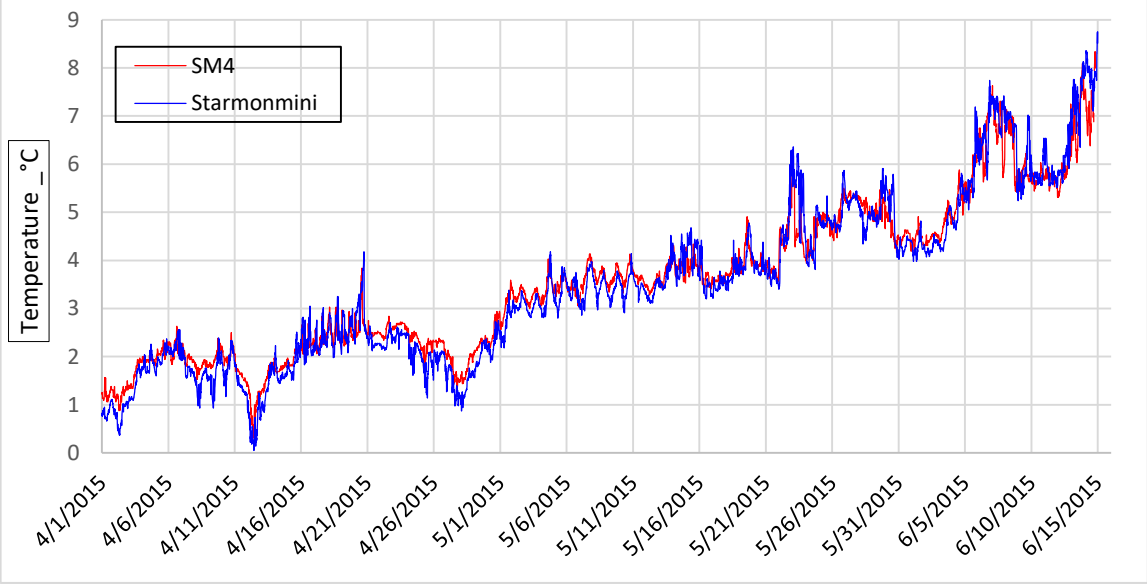

Figure 33. Comparison of the trend in data collected by the SM4 and the Starmon mini

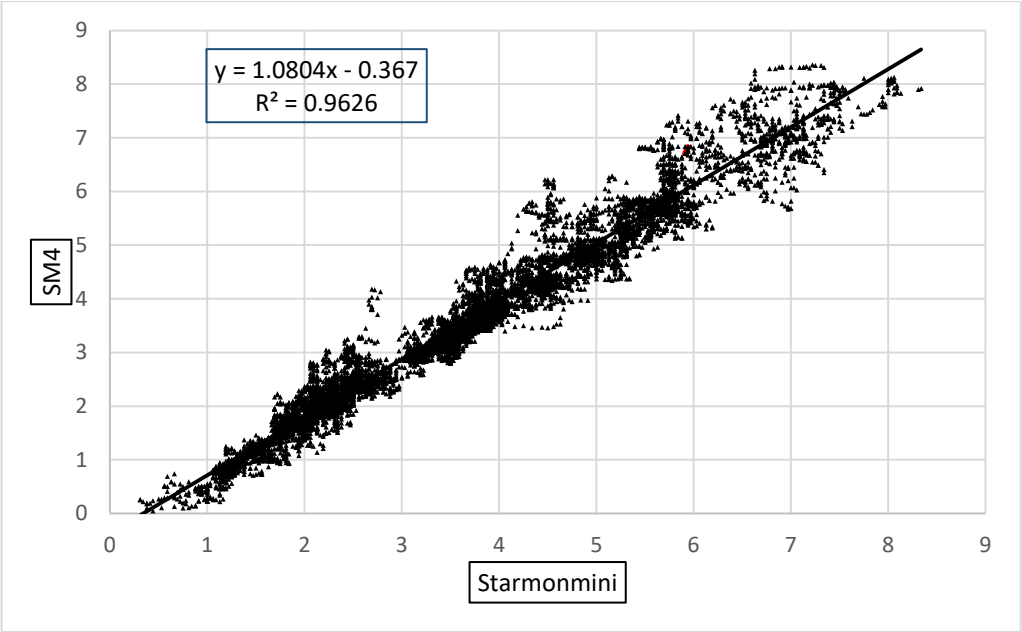

Figure 34. Correlation between the data collected by the SM4 and the Starmon mini

The results of the comparisons reveal that the SM4 is a reliable instrument that is able to measure seawater temperature with acceptable accuracy for the present research. Additional instruments and tools used in field measurements, such as rope, floating buoys, chains, and anchors, are pictured in Figure 35.

Figure 35. Additional instruments and tools for field measurements

5.2 Tools and software for numerical simulation

The major aim of the modeling is to arrive at a plausible overview of the oceanographic conditions in Önundarfjörður. In this research, two-dimensional (2D) and three-dimensional (3D) features of the seabed in Önundarfjörður were plotted with the software Surfer13, developed by the American company Golden Software. Surfer13 offers 2D and 3D high resolution modeling, including contour mapping, modeling bathymetry, gridding, and analyzing surfaces. The features of the model can also be customized by a modeler. Basically, the initial data for the Surfer13 are X, Y, and Z data, which represent latitude, longitude, and altitude or depth, respectively (Golden Software Company, no date). The raw bathymetry data were obtained from the hydrographic department of the Icelandic Coast Guard.

The oceanographic parameters of Önundarfjörður were simulated via the commercial software MIKE21 and MIKE3 Flow Model, developed by the Danish Hydraulic Institute (DHI). These two types of modules are versatile tool for 2D and 3D simulation based on flexible mesh (DHI, 2016). The software used had several advantages in comparison to other software, such as the ability to represent actual conditions of interest parameters in the area and the flexibility of mesh for modeling, which aided in the achievement of accurate results. The main numerical solutions for the modeling system included incompressible Reynolds averaged Navier-Stokes equations, Boussinesq, and hydrostatic pressure. Furthermore, the model included continuity equations, momentum equations, temperature equations, salinity equations, and density equations. In these modules, the simulations of water level variations and flows were based on a variety of forcing functions (DHI, 2016). Moreover, the following factors were considered in the simulations:

- Bed resistance
- Eddy viscosity
- Tidal potential
- Wind shear stress
- Coriolis force
- Momentum dispersion

- Flooding and drying

5.2.1 3D governing equations in Cartesian coordinates

In the shallow water conditions, the principle equation was the incompressible Reynolds averaged Navier-Stokes with respect to Boussinesq and hydrostatic pressure.

The local continuity equation is presented as:

$$\frac{\partial u}{\partial x}+\frac{\partial v}{\partial y}+\frac{\partial w}{\partial z}=S \quad [7]$$

And the two horizontal momentum equations for X and Y components are:

$$\frac{\partial u}{\partial t}+\frac{\partial u^2}{\partial x}+\frac{\partial wu}{\partial y}+\frac{\partial wu}{\partial z}=$$

$$fv-g\frac{\partial \eta}{\partial x}-\frac{1}{\rho_0}\frac{\partial p_a}{\partial x}-\frac{g}{\rho_0}\int_z^\eta \frac{\partial \rho}{\partial x}dz-\frac{1}{\rho_0 h}\left(\frac{\partial s_{xx}}{\partial x}+\frac{\partial s_{xy}}{\partial y}\right)+F_u+\frac{\partial}{\partial z}\left(v_t\frac{\partial u}{\partial z}\right)+u_sS \quad [8]$$

$$\frac{\partial v}{\partial t}+\frac{\partial v^2}{\partial y}+\frac{\partial uv}{\partial x}+\frac{\partial wv}{\partial z}=$$

$$-fu-g\frac{\partial \eta}{\partial y}-\frac{1}{\rho_0}\frac{\partial p_a}{\partial y}-\frac{g}{p_0}\int_z^\eta \frac{\partial \rho}{\partial y}dz-\frac{1}{\rho_0 h}\left(\frac{\partial s_{yx}}{\partial x}+\frac{\partial s_{yy}}{\partial y}\right)+F_v+\frac{\partial}{\partial z}\left(v_t\frac{\partial v}{\partial z}\right)+v_sS \quad [9]$$

Where t is the time; x, y and z are the Cartesian coordinate; η is the surface elevation; d is the still water depth; $h=\eta+d$ is the total water depth; *u, v* and *w* are the velocity components in the x, y and z direction; $f=2\Omega sin\phi$ is the Coriolis parameter (Ω is the angular rate of revolution and ϕ the geographic latitude); g is the gravitational acceleration; ρ is the water density; S_{xx}, S_{xy}, S_{yx} and S_{yy} are components of the radiation stress tensor; v_t is the vertical turbulent or eddy viscosity, P_a is the atmospheric pressure; ρ_o is the reference density of water. S is the magnitude of the discharge due to point sources, and (*us*, *vs*) is the velocity by which the water is discharged into the ambient water (DHI, 2016).

The surface and bottom boundary condition for *u, v* and *w* are:

At $z=\eta$:

$$\frac{\partial \eta}{\partial t}+u\frac{\partial \eta}{\partial x}+v\frac{\partial \eta}{\partial x}-w=0\,,\left(\frac{\partial u}{\partial z},\frac{\partial v}{\partial z}\right)=\frac{1}{\rho_0 v_t}\left(\tau_{sx},\tau_{sy}\right) \quad [10]$$

At $z=-d$:

$$u\frac{\partial d}{\partial x}+v\frac{\partial d}{\partial y}+w=0\,,\left(\frac{\partial u}{\partial z},\frac{\partial v}{\partial z}\right)=\frac{1}{\rho_0 v_t}\left(\tau_{bx},\tau_{by}\right) \quad [11]$$

(τ_{sx}, τ_{sy}) and (τ_{bx}, τ_{by}) are as the x and y components of the surface wind and bottom stresses. From the kinematic boundary condition at the surface, the water depth, h, is achievable, while the velocity is considered with momentum and continuity equations (DHI, 2016). The vertical integration of the local continuity equation is:

$$\frac{\partial h}{\partial t}+\frac{\partial h\bar{u}}{\partial x}+\frac{\partial h\bar{v}}{\partial y}=hS+\hat{P}-\hat{E} \quad [12]$$

where $\hat{P}$ and $\hat{E}$ represent precipitation and evaporation and $\bar{u}$ and $\bar{v}$ are the depth averaged velocities:

$$h\bar{u}=\int_{-d}^{\eta}udz\,,h\bar{v}=\int_{-d}^{\eta}vdz \quad [13]$$

Moreover, the fluid is considered to be incompressible. The density, ρ, depends on temperature, *T*, and salinity, *s*, as follows:

$$\rho=\rho(T,s) \quad [14]$$

Transport equation for salt and temperature

Regarding the transport diffusion equation, the transport of temperature and salinity can be defined as follows:

$$\frac{\partial T}{\partial t}+\frac{\partial uT}{\partial x}+\frac{\partial vT}{\partial y}+\frac{\partial wT}{\partial z}=F_T+\frac{\partial}{\partial z}\left(D_v\frac{\partial T}{\partial z}\right)+\widehat{H}+T_sS \quad [15]$$

$$\frac{\partial s}{\partial t}+\frac{\partial us}{\partial x}+\frac{\partial vs}{\partial y}+\frac{\partial ws}{\partial z}=F_s+\frac{\partial}{\partial z}\left(D_v\frac{\partial s}{\partial z}\right)+s_sS \quad [16]$$

Where D_v is the vertical turbulent diffusion coefficient. $\widehat{H}$ represents the source which is exchanging heat with the atmosphere. T_s and S_s are the temperature of the source and the salinity of the source, respectively. F is the horizontal diffusion, which is described as follows:

$$(F_T,F_s)=\left[\frac{\partial}{\partial x}\left(D_h\frac{\partial}{\partial x}\right)+\frac{\partial}{\partial y}\left(D_h\frac{\partial}{\partial y}\right)\right](T,s) \quad [17]$$

D_h is the horizontal diffusion coefficient related to the eddy viscosity as shown below:

$$D_h = \frac{A}{\sigma_T}\ , D_v = \frac{v_t}{\sigma_T} \quad [18]$$

Where σ_T is the Prandtl number.

Transport equation for a scalar quantity

The conservation equation of scalar quantity is defined as follows:

$$\frac{\partial C}{\partial t} + \frac{\partial uC}{\partial x} + \frac{\partial vC}{\partial y} + \frac{\partial wC}{\partial z} = F_c + \frac{\partial}{\partial z}\left(D_v \frac{\partial C}{\partial z}\right) - k_p C + C_s S \quad [19]$$

Where C represents the concentration of the scalar quantity, k_p is the linear decay rate, C_s is the concentration of the scalar quantity at the source, D_v is the coefficient of vertical diffusion and F_c is horizontal diffusion, which is:

$$F_c = \left[\frac{\partial}{\partial x}\left(D_h \frac{\partial}{\partial x}\right) + \frac{\partial}{\partial y}\left(D_h \frac{\partial}{\partial y}\right)\right] C \quad [20]$$

Where D_h is the coefficient of horizontal diffusion (DHI, 2016).

5.2.2 2D governing equations in Cartesian coordinates

Two-dimensional shallow water equations are achievable with respect to integration of the horizontal momentum equations and the continuity equation over depth $h = \eta + d$ as follows:

$$\frac{\partial h}{\partial t} + \frac{\partial h\bar{u}}{\partial x} + \frac{\partial h\bar{v}}{\partial y} = hS \quad [21]$$

$$\frac{\partial h\bar{u}}{\partial t} + \frac{\partial h\bar{u}^2}{\partial x} + \frac{\partial h\bar{v}\bar{u}}{\partial y} = f\bar{v}h - gh\frac{\partial \eta}{\partial x} - \frac{h}{\rho_0}\frac{\partial p_a}{\partial x} - \frac{gh^2}{2\rho_0}\frac{\partial \rho}{\partial x} + \frac{\tau_{sx}}{\rho_0} - \frac{\tau_{bx}}{\rho_0} - \frac{1}{\rho_0}\left(\frac{\partial s_{xx}}{\partial x} + \frac{\partial s_{xy}}{\partial y}\right) + \frac{\partial}{\partial x}(hT_{xx}) + \frac{\partial}{\partial y}\left(hT_{xy}\right) + hu_s S \quad [22]$$

$$\frac{\partial h\bar{v}}{\partial t} + \frac{\partial h\bar{u}\bar{v}}{\partial x} + \frac{\partial h\bar{v}^2}{\partial y} = -f\bar{u}h - gh\frac{\partial \eta}{\partial y} - \frac{h}{\rho_0}\frac{\partial p_a}{\partial y} - \frac{gh^2}{2\rho_0}\frac{\partial \rho}{\partial y} + \frac{\tau_{sy}}{\rho_0} - \frac{\tau_{by}}{\rho_0} - \frac{1}{\rho_0}\left(\frac{\partial s_{yx}}{\partial x} + \frac{\partial s_{yy}}{\partial y}\right) + \frac{\partial}{\partial x}\left(hT_{xy}\right) + \frac{\partial}{\partial y}\left(hT_{yy}\right) + hv_s S \quad [23]$$

The overbar is the depth average value. $\bar{u}$ and $\bar{v}$ are the depth-averaged velocities which are obtain from:

$$h\bar{u} = \int_{-d}^{\eta} u dz\,,\ h\bar{v} = \int_{-d}^{\eta} v dz \qquad [24]$$

The lateral stresses T_{ij} comprise viscous friction, turbulent friction, and differential advection. According to the depth average velocity gradients and the eddy viscosity formulation, lateral stresses are (DHI, 2016):

$$T_{xx} = 2A\frac{\partial \bar{u}}{\partial x}\,, T_{xy} = A\left(\frac{\partial \bar{u}}{\partial y} + \frac{\partial \bar{v}}{\partial x}\right)\,, T_{yy} = 2A\frac{\partial \bar{v}}{\partial y} \qquad [25]$$

Transport equations for salt and temperature

Integrating the transport equations for salt and temperature over depth, the two-dimensional transport equations are derived as shown below:

$$\frac{\partial h\bar{T}}{\partial t} + \frac{\partial h\bar{u}\bar{T}}{\partial x} + \frac{\partial h\bar{v}\bar{T}}{\partial y} = hF_T + h\widehat{H} + hT_sS \qquad [26]$$

$$\frac{\partial h\bar{s}}{\partial t} + \frac{\partial h\bar{u}\bar{s}}{\partial x} + \frac{\partial h\bar{v}\bar{s}}{\partial y} = hF_s + hS_sS \qquad [27]$$

Where $\bar{T}$ and $\bar{s}$ is the depth average of temperature and salinity, respectively (DHI, 2016).

Transport equations for a scalar quantity

The two-dimensional transport equations in depth average for a scalar quantity are:

$$\frac{\partial h\bar{C}}{\partial t} + \frac{\partial h\bar{u}\bar{C}}{\partial x} + \frac{\partial h\bar{v}\bar{C}}{\partial y} = hF_c - hk_p\bar{C} + hC_sS \qquad [28]$$

Where $\bar{C}$ is the depth average scalar quantity.

5.2.3 Time integration

In terms of the general form of equation as $\frac{\partial U}{\partial t} = G(U)$ in 2D simulation, for the time integration there are lower and higher order methods, such as Euler and Runge Kutta, respectively.

In the Euler method:

$$U_{n+1} = U_n + \Delta t G(U_n) \qquad [29]$$

In the Runge Kutta method:

$$U_{n+\frac{1}{2}} = U_n + \frac{1}{2}\Delta t G(U_n) \quad [30]$$

$$U_{n+1} = U_n + \Delta t G\left(U_{n+\frac{1}{2}}\right) \quad [31]$$

Where Δt is the time step interval.

5.2.4 Courant-Friedrich-Levy (CFL) number

In Cartesian coordinates, the CFL for the shallow water equation is described as:

$$CFL_{HD} = \left(\sqrt{gh} + |u|\right)\frac{\Delta t}{\Delta x} + \left(\sqrt{gh} + |v|\right)\frac{\Delta t}{\Delta y} \quad [32]$$

Where h is the total water depth; u is x direction and v is y direction velocity components; g is the gravitational acceleration; Δx and Δy are length scale; Δt is time step interval;

Furthermore, in Cartesian coordinates the CFL number for the transport equations is (DHI, 2016):

$$CFL_{AD} = |u|\frac{\Delta t}{\Delta x} + |v|\frac{\Delta t}{\Delta y} \quad [33]$$

5.2.5 The creation of digitized bathymetry

Creating the computational domain and the boundary were the initial tasks for the modeling. The creation of the mesh file was one of the crucial steps in the modeling process, which requires a variety of considerations and modifications. In order to generate mesh with minimum error, a nested approach was considered (DHI, 2016). The resolution was around 200 m. The total number of elements used in the mesh was 4249, with 2298 nodes. The CFL number used was 0.8. A UTM projection system and zone 27 were specified for the model. The mouth of the fjord and the coastline were defined as the model's domain boundaries. Figure 36 shows the generated mesh with scattered bathymetric values of the fjord. The generated mesh improved through smoothing, refining, and analyzing.

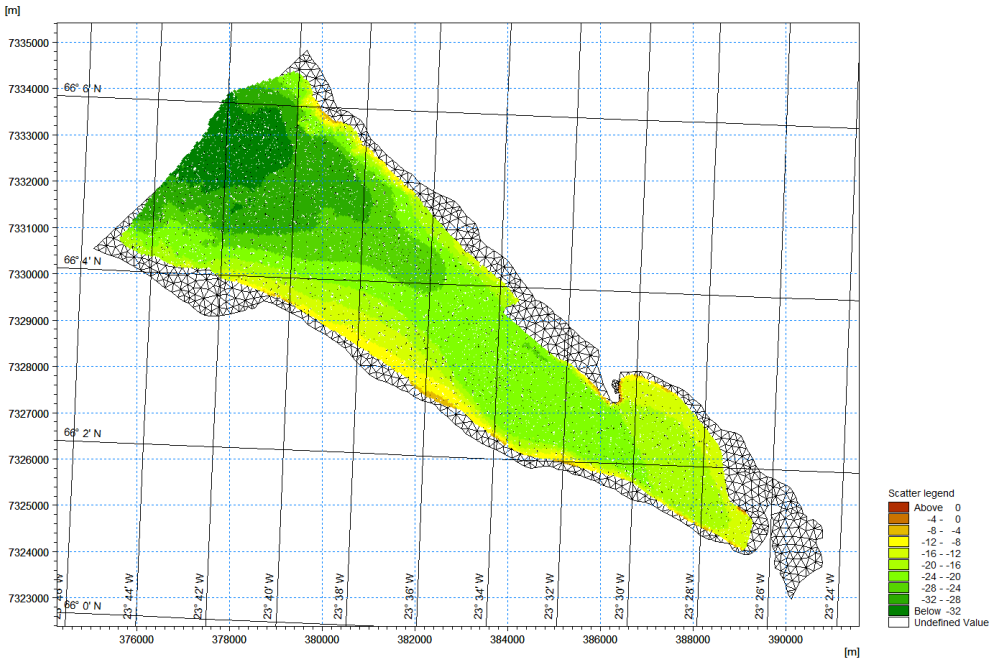

Figure 36. Scattered bathymetry data with mesh file

Figure 37 depicts a comprehensive bathymetry of the fjord, created from interpolated scatter data and generated mesh.

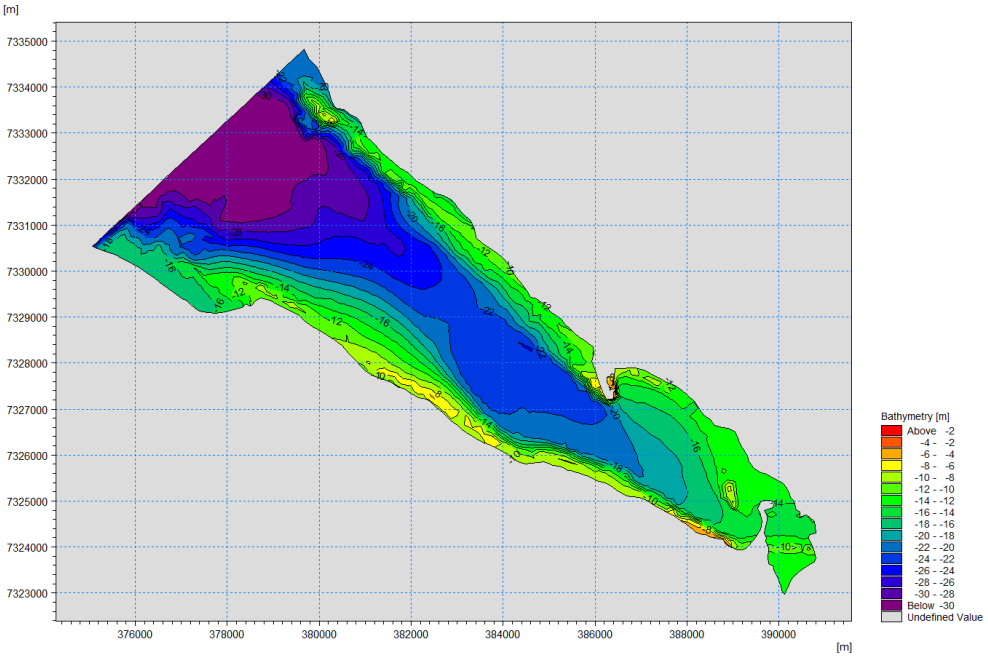

Figure 37. Plotted bathymetry of the fjord

5.2.6 Input parameters

Before setting up the model, it was essential to create the input parameters. To this end, preprocessing of raw meteorological and oceanographic data was performed for the modeling. Meteorological data from an automatic weather station in Flateyri were inputted into the model. The information about the weather station in Flateyri is presented in Appendix C. The station is located next to the port of Flateyri, as marked with a red dot in Figure 38.

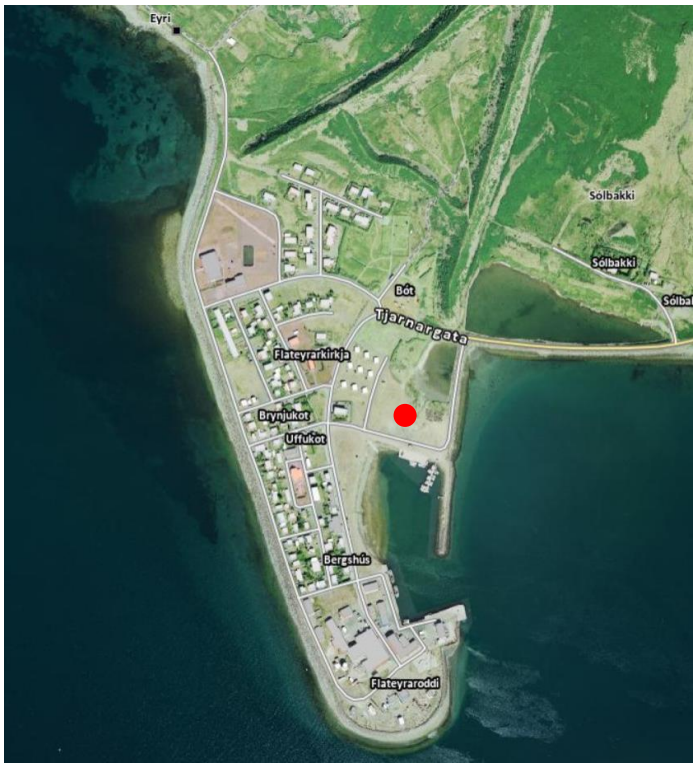

Figure 38. Location of the weather station in Flateyri (www.map.is)

For the model, all the recorded meteorological data by the station included air temperature, relative humidity, wind speed, and wind direction were defined uniform over the domain. Furthermore, the nearest station of measuring sea level to Önundarfjörður is located in Ísafjörður, a town near to Flateyri. However, the data have not been recorded consistently at the station. So, in this research predicted tidal data based on global tidal analysis were used for the modeling. The data were defined as the boundary conditions to the model. A comparison of data collected at the station in Ísafjörður with predicted tidal data demonstrates that both data have

acceptable conformity. Figure 39 shows the predicted tidal elevation for the years 2015 and 2016.

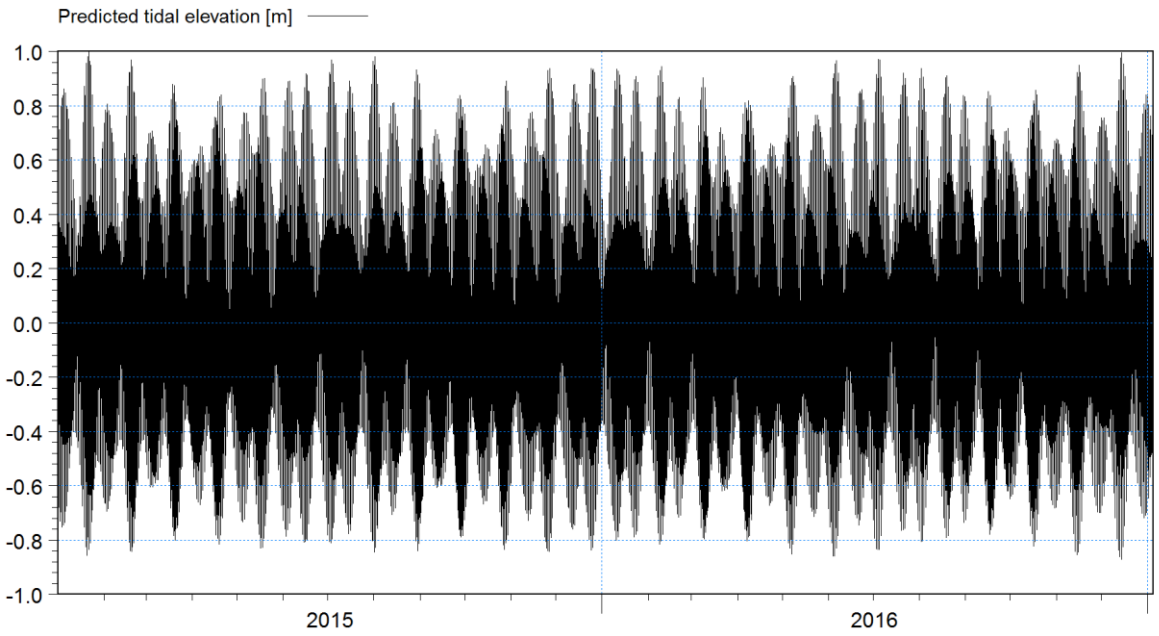

Figure 39. Predicted tide used for the model

The tidal diagram reveals that tidal characteristic of the area were mixed with predominantly semi-diurnal types. With MIKE zero the raw data were processed and put in an acceptable format for the modeling as the input of the model.

Currents played a significant role in the research. In 2013, Náttúrustofa Vestfjarða sporadically measured currents during the periods from July 10 to August 4, September 20 to October 10, and November 28 to December 20. The current meter was located at the position of 66°03.050´ and -23°36.000´ at a depth of 10 m, as shown in Figure 40 (Þórisson, 2013).

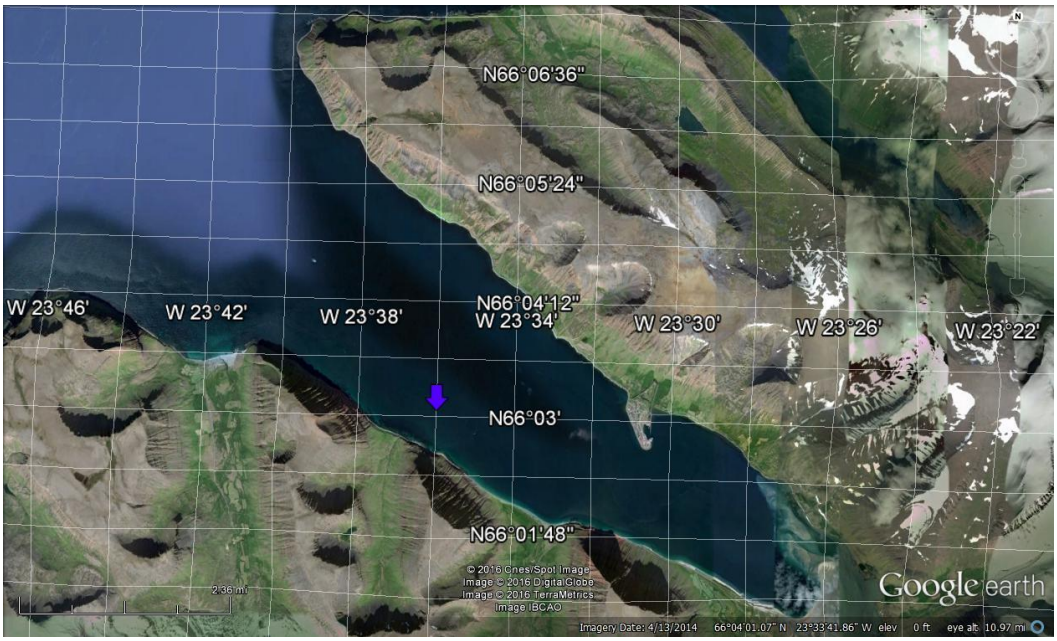

Figure 40. Location of the current meter in Önundarfjörður

The aforementioned current data were used in the calibration of the model. In this regard, the current model in this research was based on the current pattern in Önundarfjörður measured in 2013. Figure 41 shows the current data, including velocity and direction, after despiking of invalid raw data.

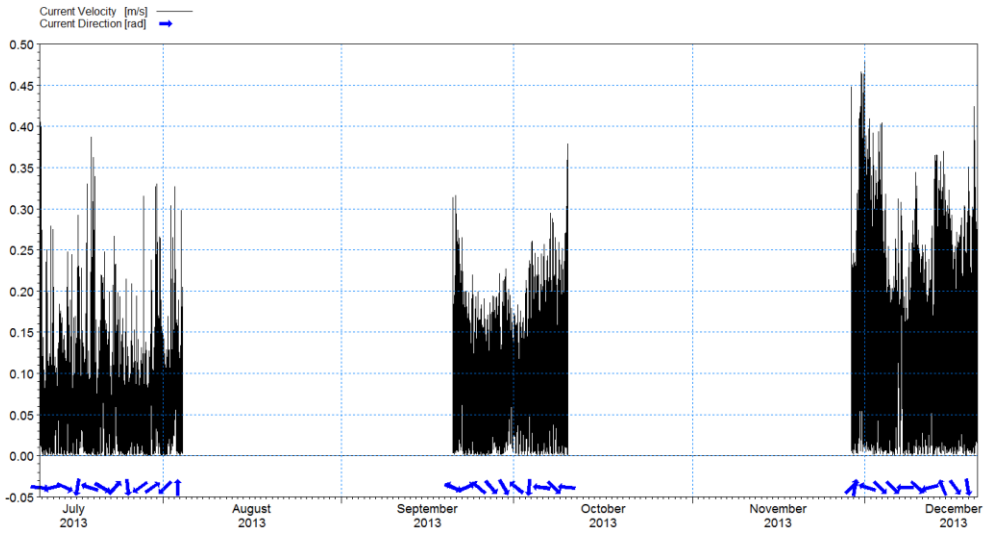

Figure 41. Measured current data in Önundarfjörður

Generally, the calibration of a model is carried out in order to modify the outputs of the model with available measured data (Goyal & Rathod, 2011). The calibration of the model provides accurate simulation of the interest parameters. Accordingly, in this research the model was calibrated using the comprehensive data sets of one year of field measurements plus the available data. The main parameters for the calibration of the current are bed resistance using Manning's number and eddy viscosity using the Smagorinsky formula. Furthermore, for the calibration of the seawater temperature, vertical and horizontal distribution with dispersion coefficient formulation were performed.

6 Results

6.1 Field measurements

In this chapter, measured data will be discussed based on statistical and graphical analysis. Also, the monthly variations of seawater temperature from the surface to the bottom of Önundarfjörður will be investigated. This thesis marks the first time that a continuous seawater temperature has been measured simultaneously at four locations in the fjord.

At location A (see Figure 24), data were recorded at two different intervals, including every 10 minutes and every 60 minutes. The monthly time series of seawater temperatures for one year is illustrated in Figure 42.

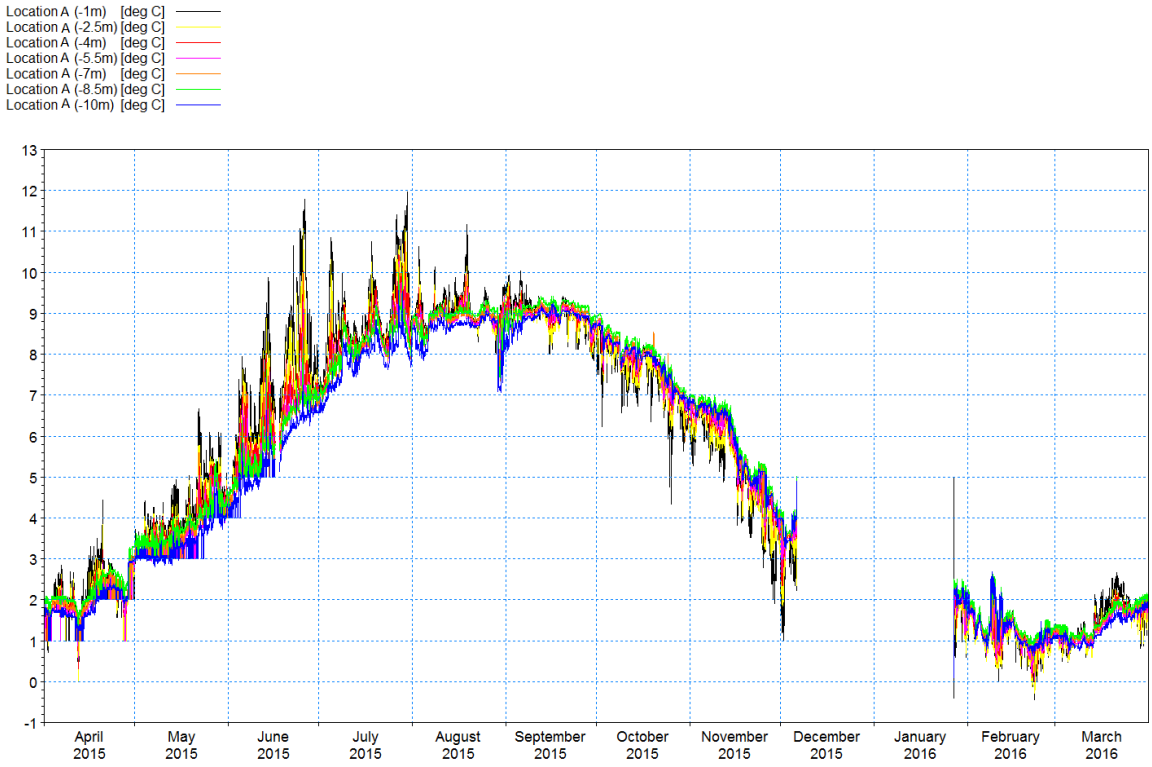

Figure 42. Monthly seawater temperatures at location A

Some gaps in the dataset are explained by battery failure and other technical problems that occurred during the online transfer of data from the instrument to the server. Moreover, the instrument broke down because of harsh weather and sea conditions from early December. However, the instrument was redeployed at the same location in late January. The damaged instrument is shown in Figure 43.

Figure 43. Damaged SM4 instrument

As depicted in the Figure 42, 12.0 °C and -0.4 °C were recorded as the maximum and the minimum seawater temperatures at the depth of -1 m in late July and in February, respectively. Table 5 gives an overview of the data recorded at the individual sensors at location A.

Table 5. Statistical information at location A

Depth (m)	**Minimum (**°C)	**Maximum (**°C)	**Mean (**°C)
-1	-0.4	12.0	4.3
-2.5	-0.2	11.0	4.1
-4	0.0	11.0	4.1
-5.5	0.0	10.2	4.0
-7	0.0	10.1	4.1
-8.5	0.2	10.0	4.2
-10	0.6	9.5	4.0

As illustrated in Figure 42, the water temperatures recorded at the four upper sensors had more fluctuation during the measurements. The sensor at a depth of -1 m recorded the maximum number of fluctuations, likely because surface layers are more influenced by ambient air and are less dense in comparison to isolated, denser water at the bottom. However, tidal mixing and wind reduces stratification and the high variation of seawater temperatures between the layers. The standard deviation during June to July was the largest at this location. Higher temperatures were observed several times during the measurements at the two upper sensors. However, soon after, the temperatures decreased again. As can be seen from Figure 42 during the first half of measurements, from April to the middle of September, four upper sensors recorded higher water temperatures. This trend changed during the second half of the measurements, during which the sensors recorded lower seawater temperatures. At all depths, the minimum temperatures were recorded in February and the maximum temperatures occurred in July. Since September, when the ambient air temperature began decreasing, the temperature of the surface layer fell more in comparison to other layers. In June, three maximums were observed. The maximums were particularly seen in the surface layers, including at depths of -1 m, -2.5 m, and -4 m. In the following month, the maximums were observed again with lower ranges, as shown in Figure 44.

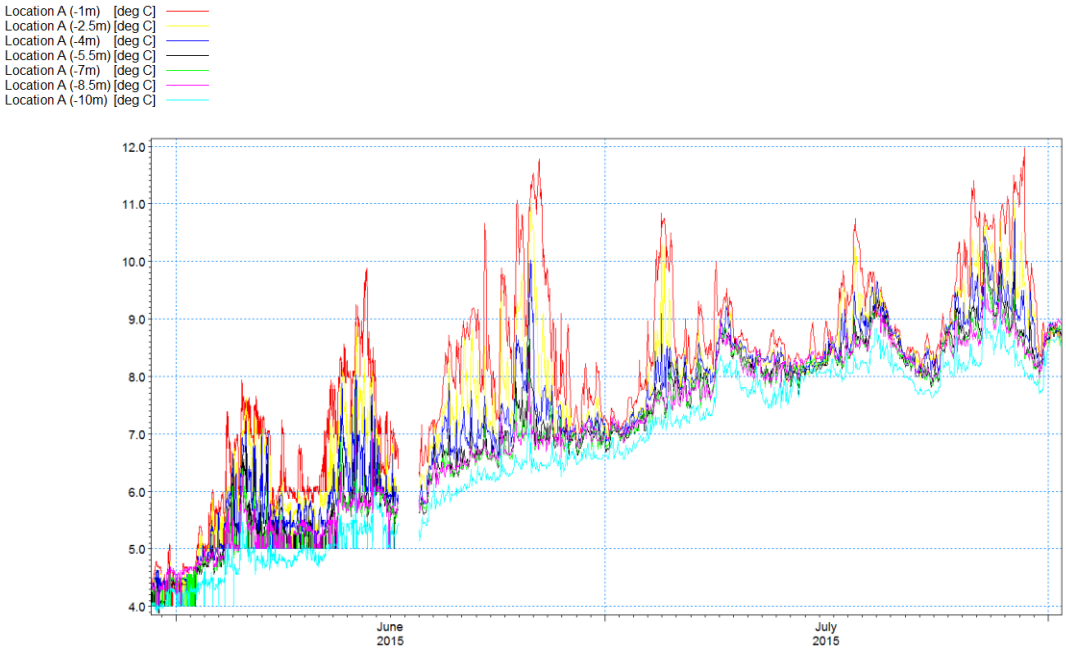

Figure 44. Seawater temperatures at location A in June and July

As illustrated in Figure 44, the water temperatures at the depth of -1 m dropped drastically, by around 4.5°C, at the end of June. In this month, the standard deviation of recorded data at the depth of -1 m was 0.4 °C. Going forward to August, a distinct peak in temperature at the upper layer was observed. At the end of the month, the seawater temperature suddenly fell, mostly in the deeper layers, as depicted in Figure 45.

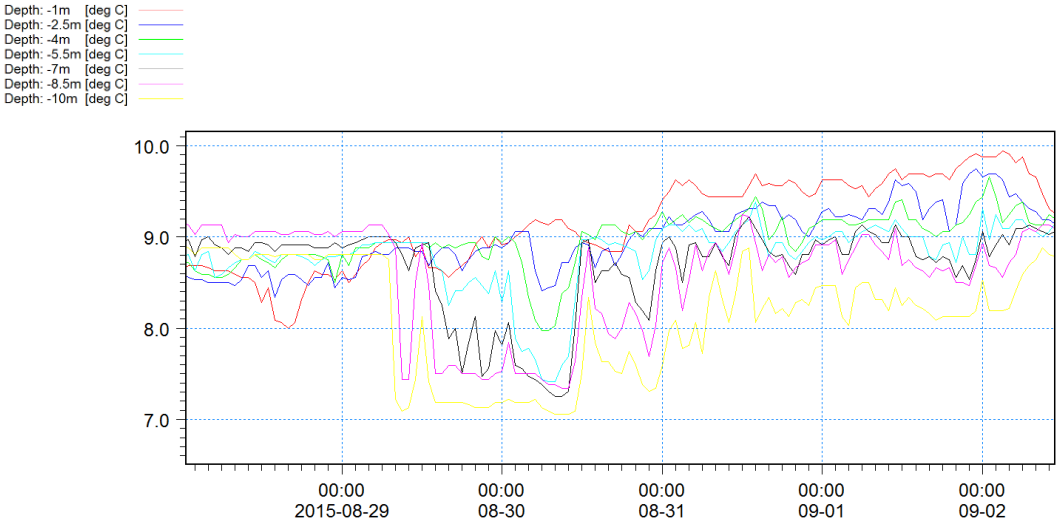

Figure 45. Seawater temperatures at location A from late August to early September

As elucidated in Figure 45, while seawater temperatures at upper layers remained approximately constant, at the depper layers, the temperatures changed suddenly. This episode was observed for data recorded by the lowest sensor, which registered a drop in temperature of more than 1.5 °C. This anomaly is in accordance with data recorded at other locations, where the instruments were placed at the bottom of the fjord. The reason may be explained by a cold front current which flows at the lower layers during this short period of time. This pattern was observed by simulation of the current at the lower layers as well (Figure 70).

Then, the water temperature started rising with a smooth slope until mid-September. Thenceforth, the temperature started falling until the end of period of measurement. However, the seawater temperature at the upper layers dropped several times in October and November. Figure 46 delineates the maximum, average, and minimum seawater temperatures recorded by all seven sensors every month.

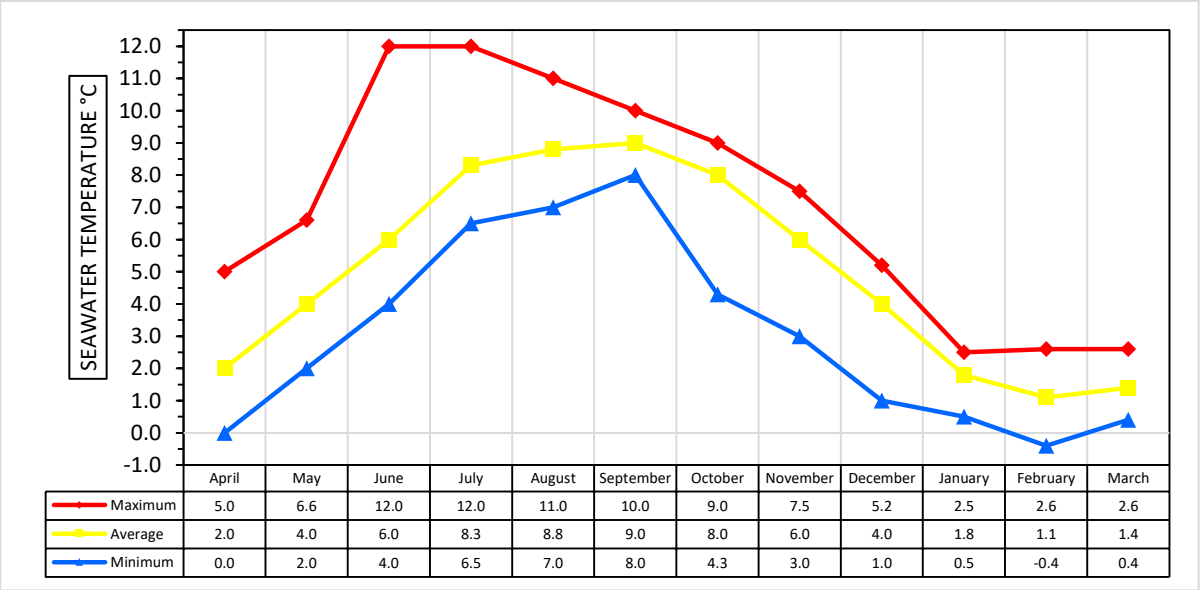

	April	May	June	July	August	September	October	November	December	January	February	March
Maximum	5.0	6.6	12.0	12.0	11.0	10.0	9.0	7.5	5.2	2.5	2.6	2.6
Average	2.0	4.0	6.0	8.3	8.8	9.0	8.0	6.0	4.0	1.8	1.1	1.4
Minimum	0.0	2.0	4.0	6.5	7.0	8.0	4.3	3.0	1.0	0.5	-0.4	0.4

Figure 46. Monthly maximum, average, and minimum seawater temperatures for seven sensors at location A

The monthly time series of seawater temperatures at location B (see Figure 24) from April 1, 2015, to April 1, 2016 is depicted in Figure 47. In this location, the recording interval was every 10 minutes.

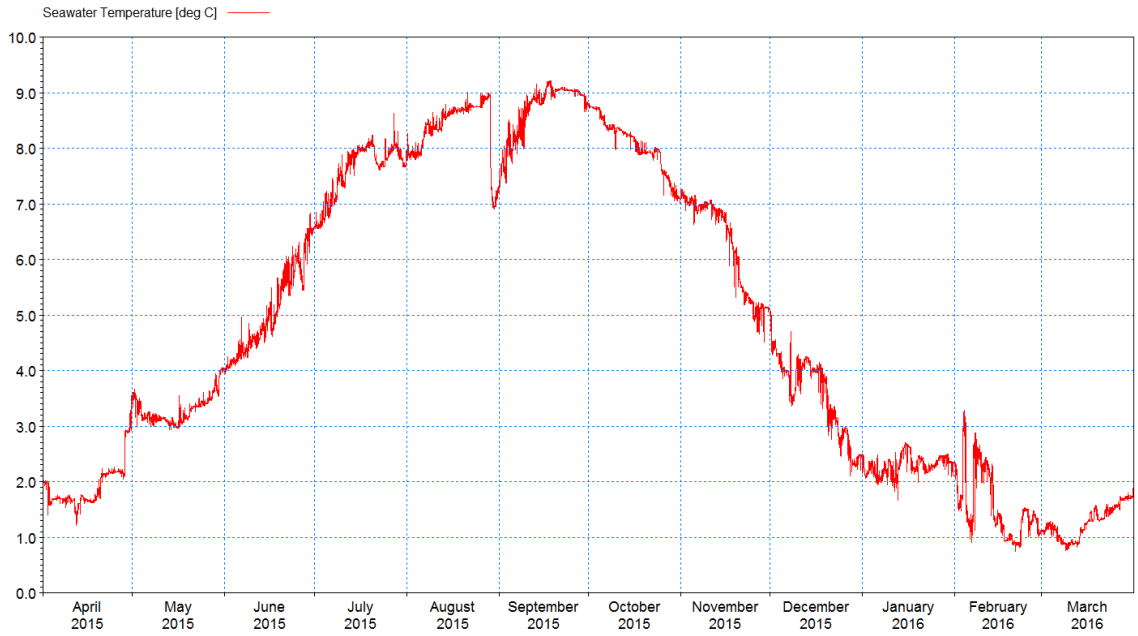

Figure 47. Monthly seawater temperatures at location B

As can be seen from the figure, maximum temperature in the seasonal cycle was 9.21 °C, recorded in September, and the minimum temperature was 0.74 °C, recorded in February. For the whole period of measurement, the average temperature was 5.64 °C with a standard deviation of 2.50 °C. At the beginning of the measurement period, a relative minimum seawater temperature was observed in mid-April. At the end of this month and in early May, the temperature suddenly increased by more than 1.50 °C. After that, the temperature fell to 3.0 °C by mid-May. Then, the seawater temperature started rising from 3.00 °C to 8.00 °C during the following two months, until mid-July. At the end of July the water temperature decreased by less than 0.50 °C. Although the temperature increased in August, at the end of the month the seawater temperature dropped by more than 2.00 °C, a drastic shift. In this month, the standard deviation was 0.50 °C. In September, the temperature began to rise with a steep slope until the middle of the month when the maximum temperature was recorded. Afterward, the temperature had a diminishing pattern, with variable temperature until March. At the end of the period, the seawater temperature remained near constant, at around 2.00 °C. Figure 48 illustrates monthly maximum, average, and minimum seawater temperatures.

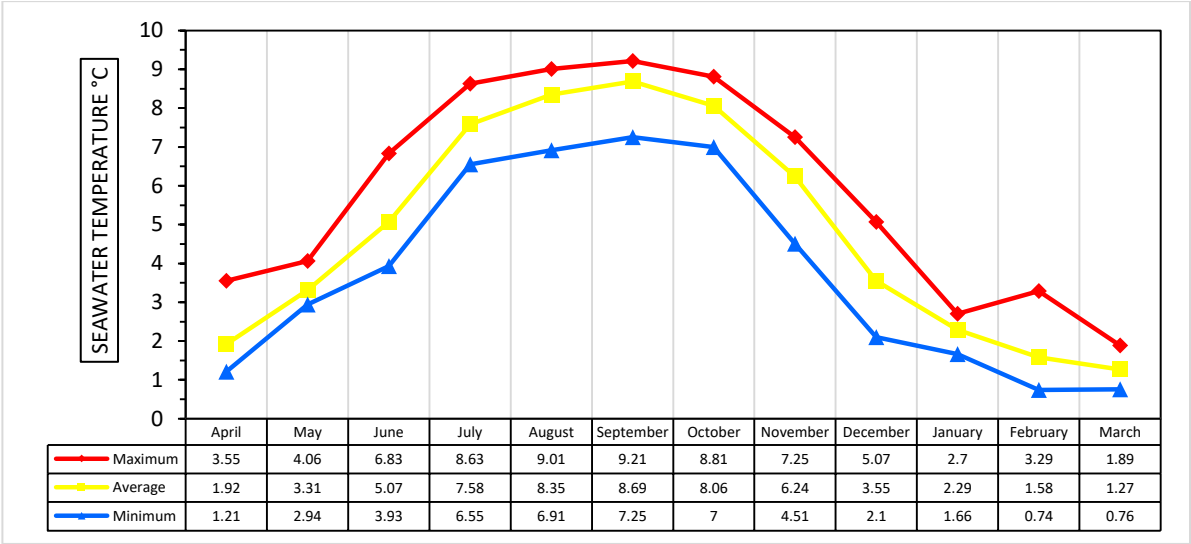

	April	May	June	July	August	September	October	November	December	January	February	March
Maximum	3.55	4.06	6.83	8.63	9.01	9.21	8.81	7.25	5.07	2.7	3.29	1.89
Average	1.92	3.31	5.07	7.58	8.35	8.69	8.06	6.24	3.55	2.29	1.58	1.27
Minimum	1.21	2.94	3.93	6.55	6.91	7.25	7	4.51	2.1	1.66	0.74	0.76

Figure 48. Monthly maximum, average, and minimum seawater temperatures at location B

As shown in the figure, at this location there was no major difference between maximums and minimums of seawater temperature during the year. The monthly maximum and minimum discrepancy of digrams were in February and January respectively.

The monthly time series of seawater temperature at location C (See Figure 24) from April 1, 2015, to April 1, 2016 is shown in Figure 49. In this location, the recording interval was 10 minutes.

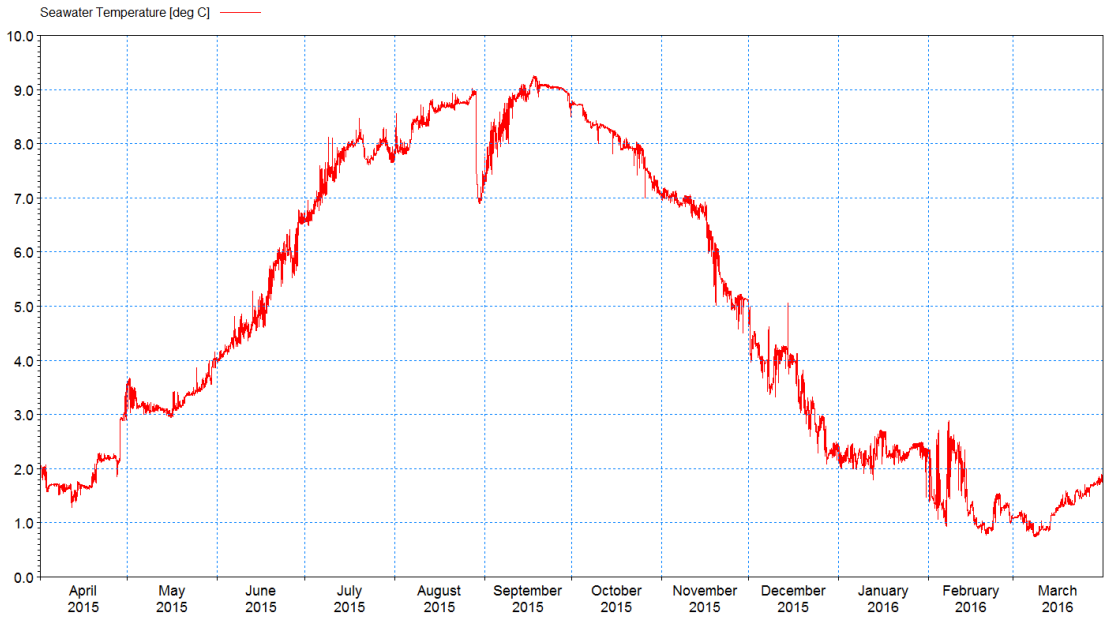

Figure 49. Monthly seawater temperatures at location C

As shown in the figure, the maximum seawater temperature was 9.26 °C, recorded in September, and the minimum temperature was 0.74 °C, recorded in March. For the whole period of measurement, the mean temperature was 6.06 °C and the standard deviation was 2.39 °C. At this location, the seawater temperature significantly increased, with more than 1.50 °C at the end of April and early May. After that, the temperature decreased by around 0.50 °C, nearly constant to the 3.00 °C recorded by mid-May. Then, the temperature continuously started rising with a steep slope, reaching 6.50 °C in June. However, at the end of this month the seawater temperature dropped by around 1.00 °C. Although there was an increasing trend in July, from the latter half, variations in the seawater temperature appeared. There was one anomalous episode in August and in the second half of the month, the seawater temperature fell drastically, by around 2.00 °C within one day. However, after that, temperatures increased again. In mid-September, the temperature increased to a distinct peak of 9.26 °C. In this month, the standard deviation was 0.45 °C. Thenceforth, the seawater temperatures started falling until the end of period. In November, the temperature dropped suddenly more than 1.50 °C. In February the temperature increased again, and a few days later the temperature fell to about 1.00 °C. Figure 50 shows the maximum, average, and minimum seawater temperature recorded each month.

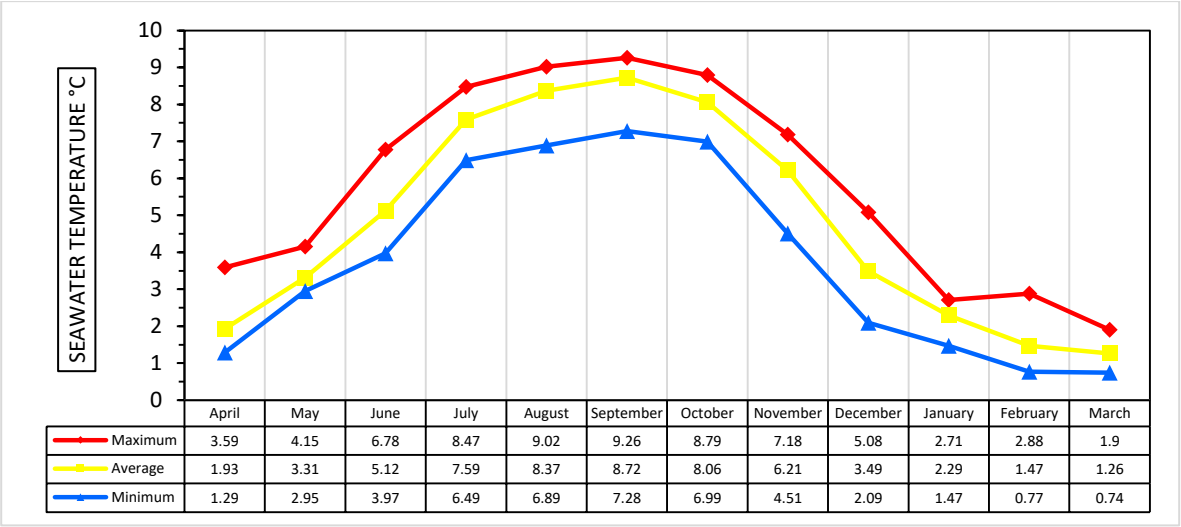

	April	May	June	July	August	September	October	November	December	January	February	March
Maximum	3.59	4.15	6.78	8.47	9.02	9.26	8.79	7.18	5.08	2.71	2.88	1.9
Average	1.93	3.31	5.12	7.59	8.37	8.72	8.06	6.21	3.49	2.29	1.47	1.26
Minimum	1.29	2.95	3.97	6.49	6.89	7.28	6.99	4.51	2.09	1.47	0.77	0.74

Figure 50. Monthly maximum, average, and minimum seawater temperatures at location C

As can be seen from the figure, the trend of maximums and minimums at location C were almost the same as at location B during the year. The monthly maximum and minimum discrepancy of digrams were in February and May respectively.

The monthly time series of seawater temperature at location D (see Figure 24) from April 1, 2015, to April 1, 2016 is illustrated in Figure 51. In this location, the recording interval was 60 minutes.

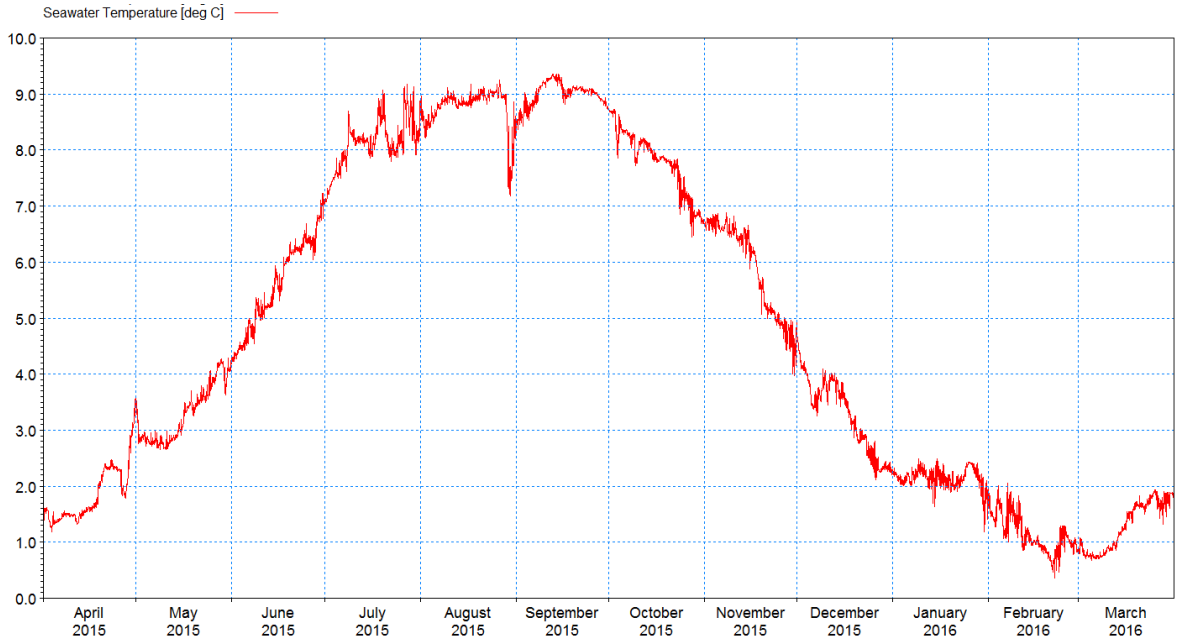

Figure 51. Monthly seawater temperatures at location D

As shown in the graph, the highest temperature of 9.36 °C occurred in September, while the minimum temperature was 0.36 °C in February. For the whole period of measurement, the mean temperature and the standard deviation were 6.16 °C and 2.50 °C, respectively. In early April, the seawater temperature remained nearly constant, but then it increased with a steep slope to 3.60 °C at the end of month. Although the temperature decreased again by mid-May around 3.00 °C, it increased significantly with a steep slope to 8.50 °C in early July. The increasing temperature of the water in July coincided with distinct variation in temperature, with a standard deviation of 0.42 °C from the latter half of the month. In August, the temperature remained mostly in the range 8.50-9.00 °C, but in the second half of month the temperature dropped drastically by more than 1.50 °C within one day. Right after that, at the beginning of September, the temperature increased again. Around mid-September, the temperature increased to the maximum of 9.36 °C. Then, the seawater temperature started falling with a steep slope until the end of the period of measurement, in particular in November. Figure 52 shows monthly maximum, average, and minimum temperatues of seawater at location D.

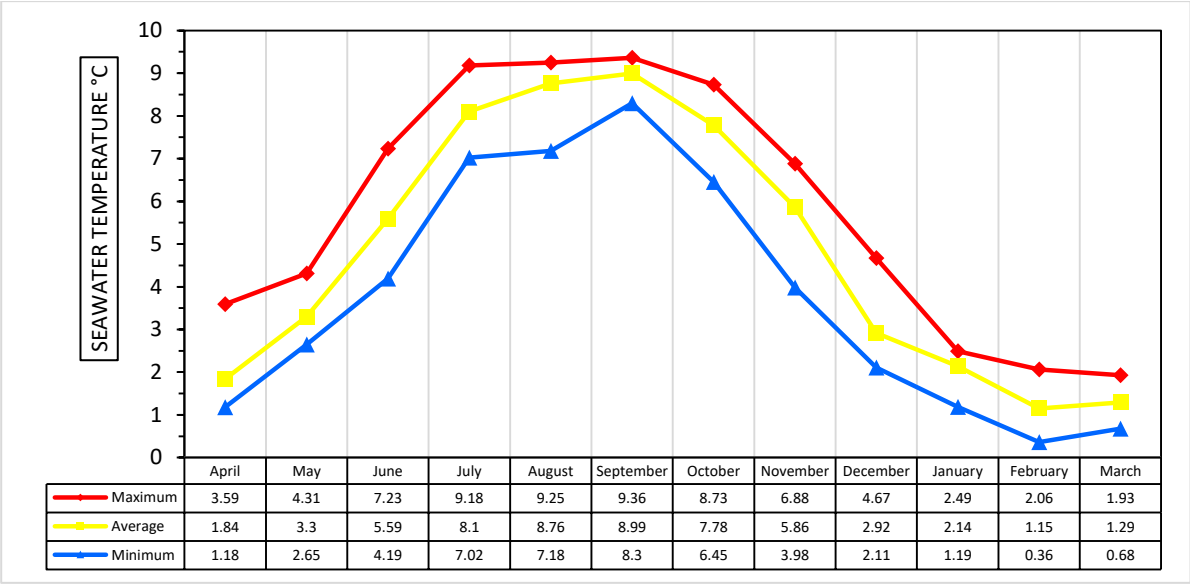

	April	May	June	July	August	September	October	November	December	January	February	March
Maximum	3.59	4.31	7.23	9.18	9.25	9.36	8.73	6.88	4.67	2.49	2.06	1.93
Average	1.84	3.3	5.59	8.1	8.76	8.99	7.78	5.86	2.92	2.14	1.15	1.29
Minimum	1.18	2.65	4.19	7.02	7.18	8.3	6.45	3.98	2.11	1.19	0.36	0.68

Figure 52. Monthly recorded maximum, average, and minimum seawater temperatures in location D

The figure reveals that at this location, the discrepancy between the maximum and minimum was lesser than at other locations, and the seawater had a lower range of temperatures. The monthly maximum and minimum discrepancy of digrams were in August and September, respectively. At this location, the yearly variability was the smallest, with an amplitude of 7.97 °C.

6.2 Bottom features of Önundarfjörður

The seabed, as well as the seawater temperature and current velocity, plays an important role in the implementation of seawater source heat pumps system. Features of the seabed were significant factors in the cost analysis of the utilization of the system. In order to plot the bathymetry of Önundarfjörður, the X, Y, and Z data were defined to be acceptable for the software. Using Surfer13, the 2D bathymetry of Önundarfjörður was plotted (Figure 25). 2D bathymetry allows users to discern possible locations for the implementation of a heat exchanger

in the fjord. Through 3D simulation, the bottom features of Önundarfjörður were carefully scrutinized, and the 3D bathymetry of Önundarfjörður was plotted, as shown from two opposite angles in Figure 53 and Figure 54.

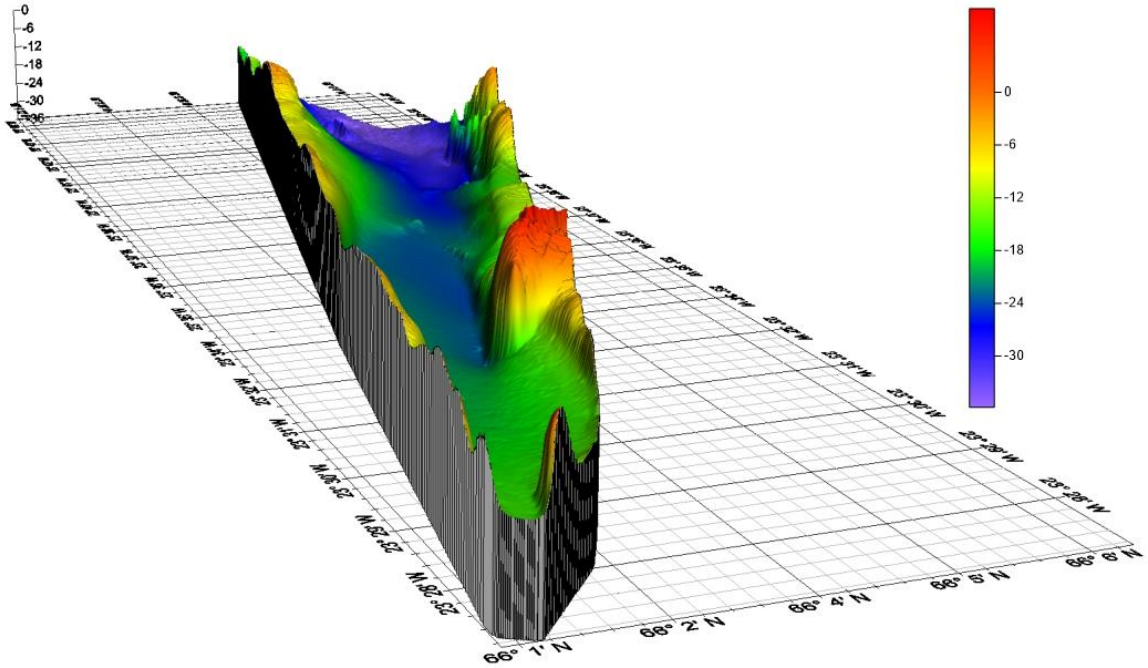

Figure 53. 3D bathymetry of Önundarfjörður, view to the North Atlantic Ocean

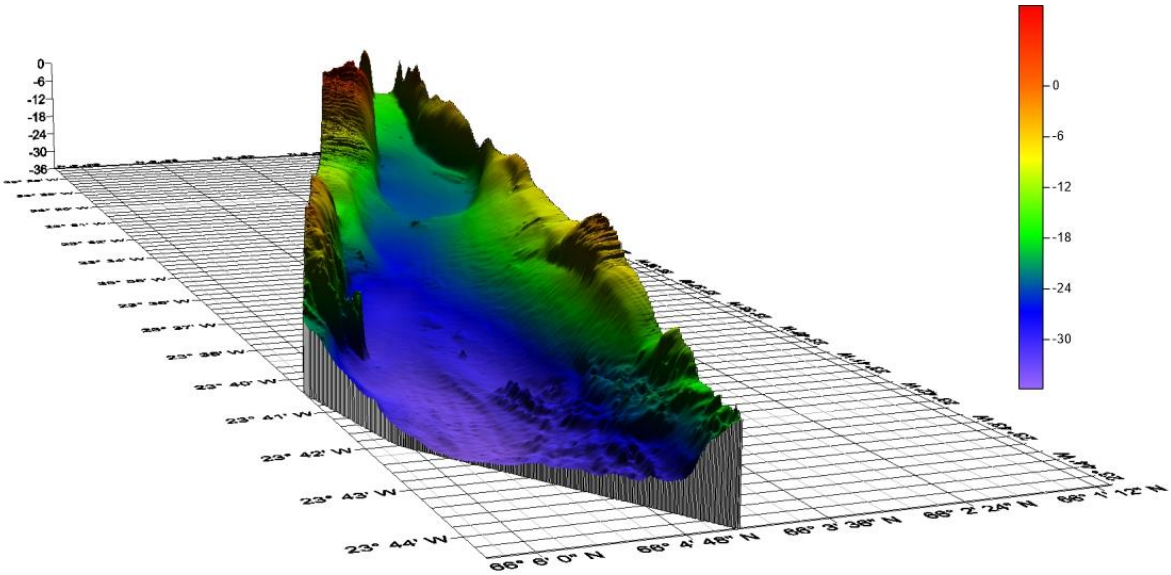

Figure 54. 3D bathymetry of Önundarfjörður, view from the North Atlantic Ocean

As depicted in the last two figures, the northern shore of Önundarfjörður is steeper than the fjord's southern shoreline. The bottom of Önundarfjörður has a smooth slope, and the deepest part is located at the mouth of the fjord with the maximum depth around 36 m.

Figure 53 and Figure 54 delineate that around the port of Flateyri and beside the town, the fjord has the shallowest area.

6.3 Simulation of oceanographic parameters

Oceanographic parameters play noteworthy roles in the present research. Through the art of numerical modeling, better insight of the unknown oceanographic patterns can be acquired. The means of numerical modeling estimates the prevailing conditions of the parameters of interest in the area of study. In this research, the aim of the modeling was to provide accurate linkages between the locations of measurement as well as to assess the parameters of interest in Önundarfjörður.

6.3.1 2-Dimensional simulation of currents

In this research, the simulations of currents in Önundarfjörður were based on data from 2013. The simulated currents represent acceptable contingency with the measured data. However, the outputs of the model indicate that the currents measured have higher velocity in comparison to the simulation results. The results show that a strong vortex usually flows at the mouth of the fjord, as illustrated in Figure 55. Over this area, the maximum current velocity is around 1.6 m/s.

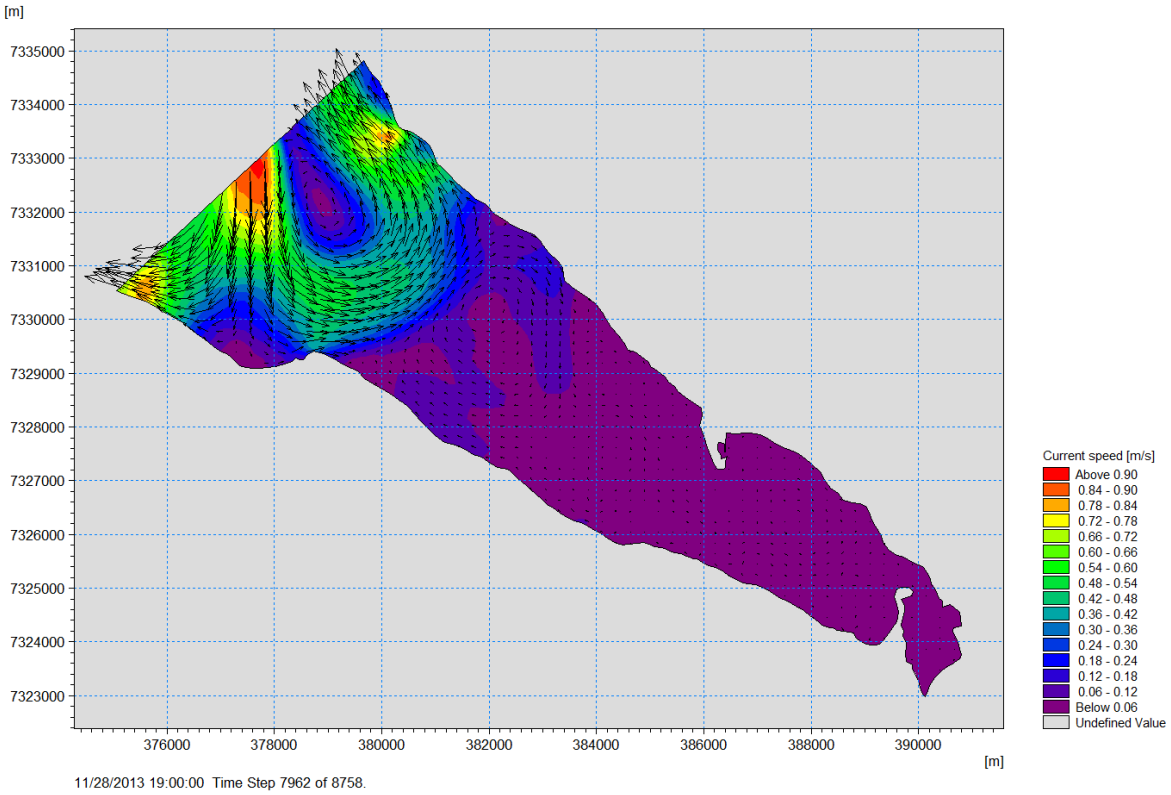

Figure 55. Vortex pattern at the mouth of Önundarfjörður

However, it should be noticed that the creation of the vortex in the mouth of the fjord is influenced by the unstable conditions of the model's boundary. One year of hydrodynamic simulations indicate that during floods and ebb, a higher velocity was observed throughout the area. During flood, the center of the fjord was influenced by a higher velocity, while the shores along the fjord are mostly ebb-dominated, as shown in Figure 56.

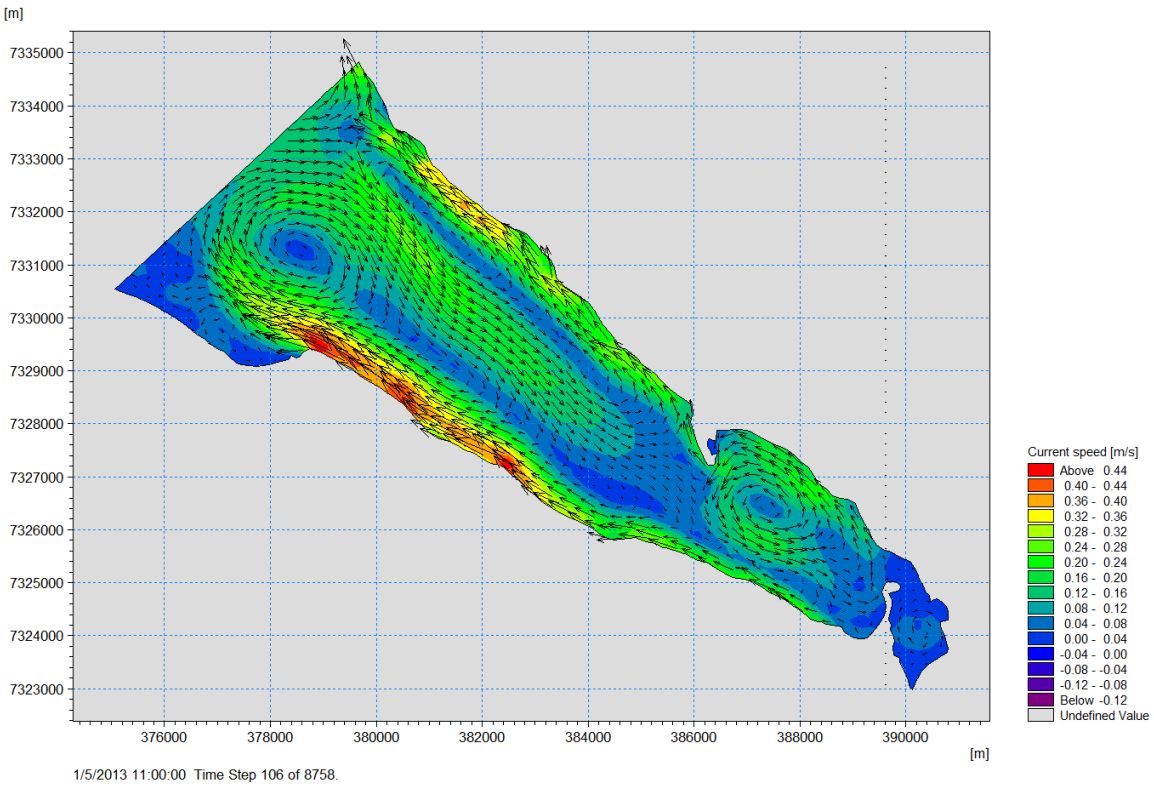

Figure 56. Strong ebb along shorelines

As shown in the figure, during the ebb, the high longshore velocity component flows towards the mouth of the fjord. The results indicate that the magnitude of flood and ebb are not similar throughout the fjord. The simulated depth average current demonstrated that during ebb, the southern shoreline experiences higher velocity in comparison to the northern shoreline. The result shows that the maximum current along the southern and northern shoreline in the fjord is around 0.72 m/s and 0.46 m/s, respectively. Results indicate that the northern longshore of the fjord rarely experiences flood, while strong flood occasionally is observed along the southern shoreline (Figure 57).

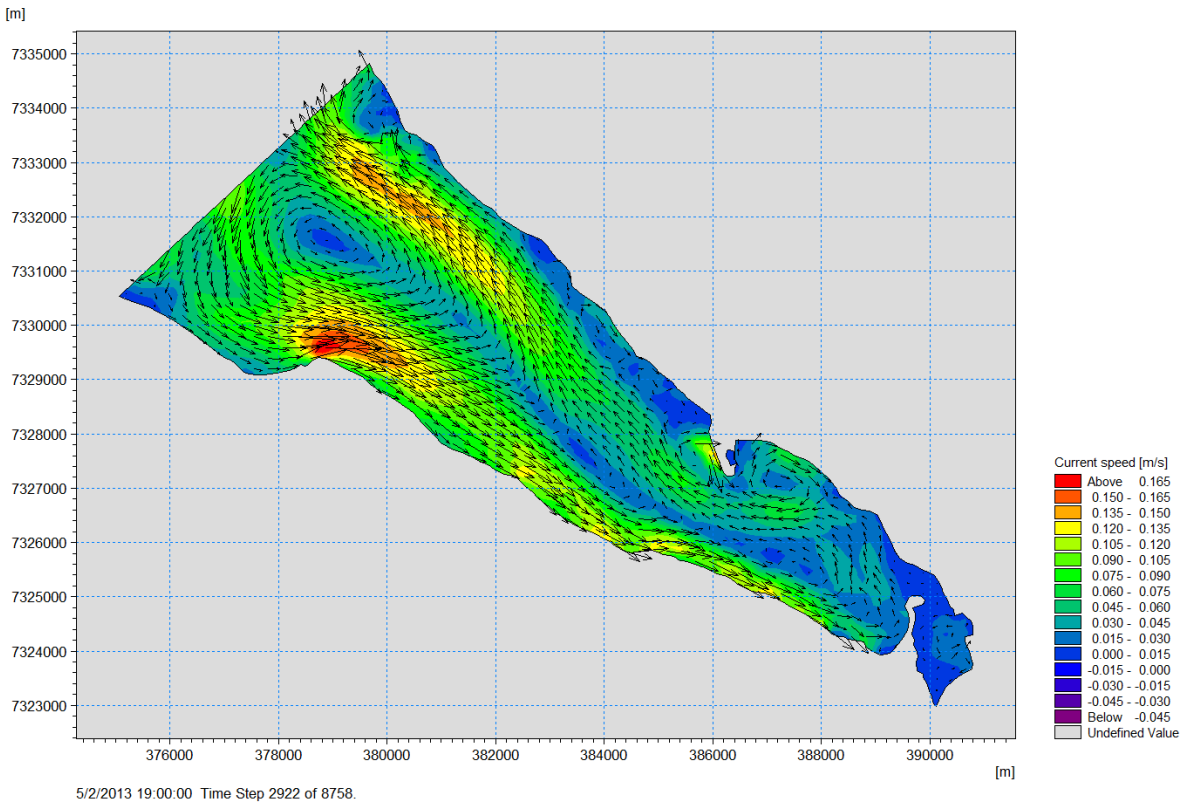

Figure 57. Strong flood and ebb along the southern and the northern shoreline, respectively

The simulation showed that, in general, the currents innermost of the fjord and in front of the port were smaller than at the center and near the mouth of the fjord. Furthermore, several rings were constantly formed in the fjord during the one year simulation. In general, both clockwise and anticlockwise rings at the middle of the fjord were observed, as depicted in Figure 58.

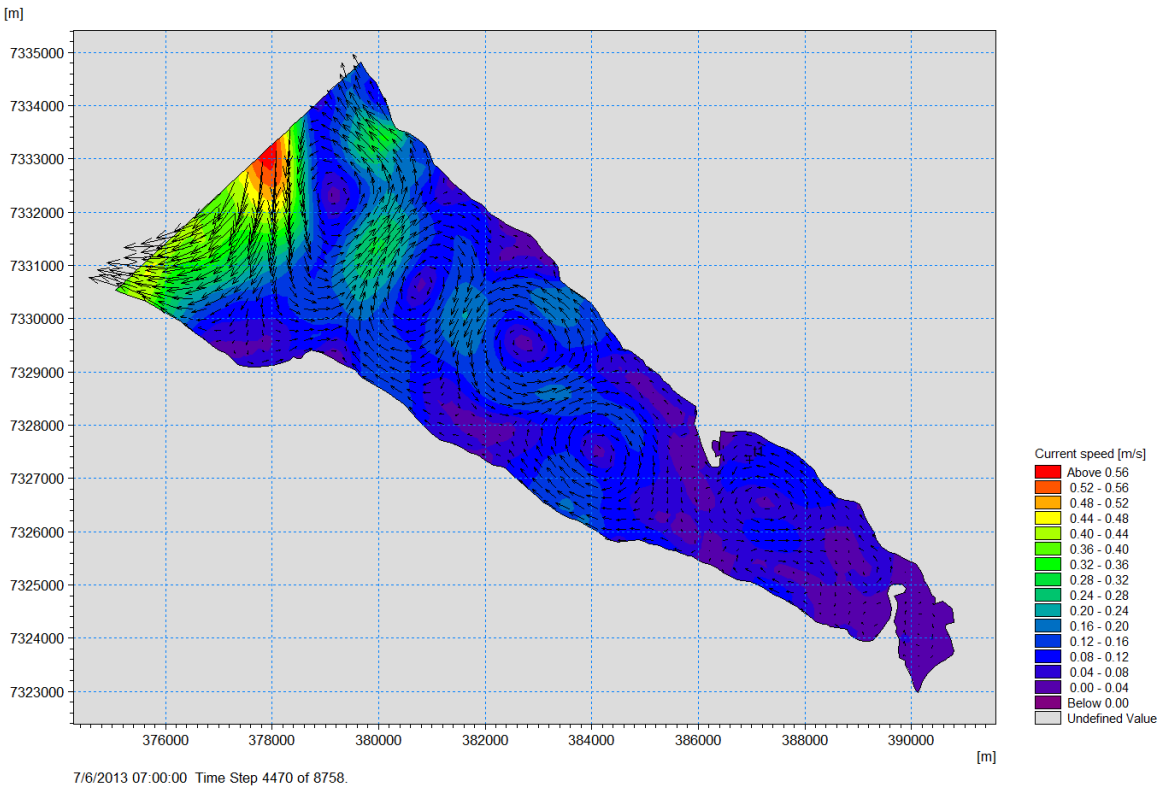

Figure 58. Formation of rings in Önundarfjörður

The main reasons for the formation of the rings in the fjord were prevailing wind patterns, the flow of currents in opposite directions along the northern and southern shorelines, and bottom features.

6.3.2 2-Dimensional simulation of seawater temperature

In this research, the simulation of seawater temperature is for the period of April 1, 2015, to April 1, 2016, which was simultaneous to the seawater temperature measurements in Önundarfjörður. As shown in Figure 59, the result of the simulation has acceptable correlations at location A. The average simulated and measured seawater temperature at location A were 4.73°C and 4.17°C, respectively.

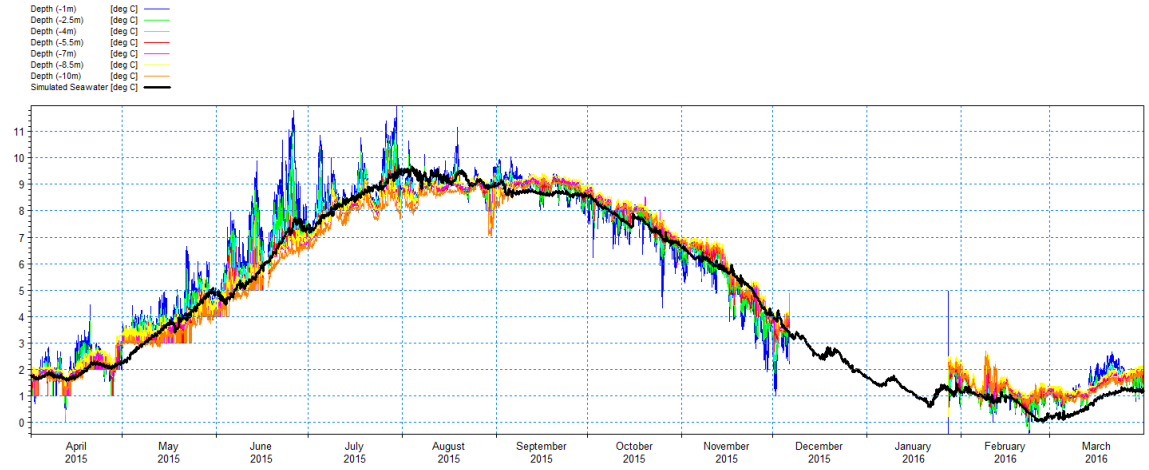

Figure 59. 2D simulated and measured seawater temperature at location A

The discrepancies between the simulated result and the measured data might be explained by the fact that the effects of ice coverage parameter in the model over the fjord was ignored. Also, the deepest sensor was placed at location A at -10 m, which is not at the bottom of the fjord. Moreover, it seems the instrument was not able to record the minimum temperatures during several periods, in particular in May and June. These defects which were due to technical problem of the instrument, were observed more often for the deeper sensors. The simulation showed that the seawater temperature was not only affected by ambient air temperature, but it was also strongly correlated with tidal currents throughout Önundarfjörður. The results of the simulation demonstrate that there is no considerable difference in seawater temperature throughout the fjord. However, in front of the port and along the northern shoreline of the fjord, higher depth average seawater temperatures were observed. Results of the comparisons show that the south and center of the fjord were dominated by colder seawater, especially in the second half of the year. Figure 60 depicts the variety of seawater temperatures over the area.

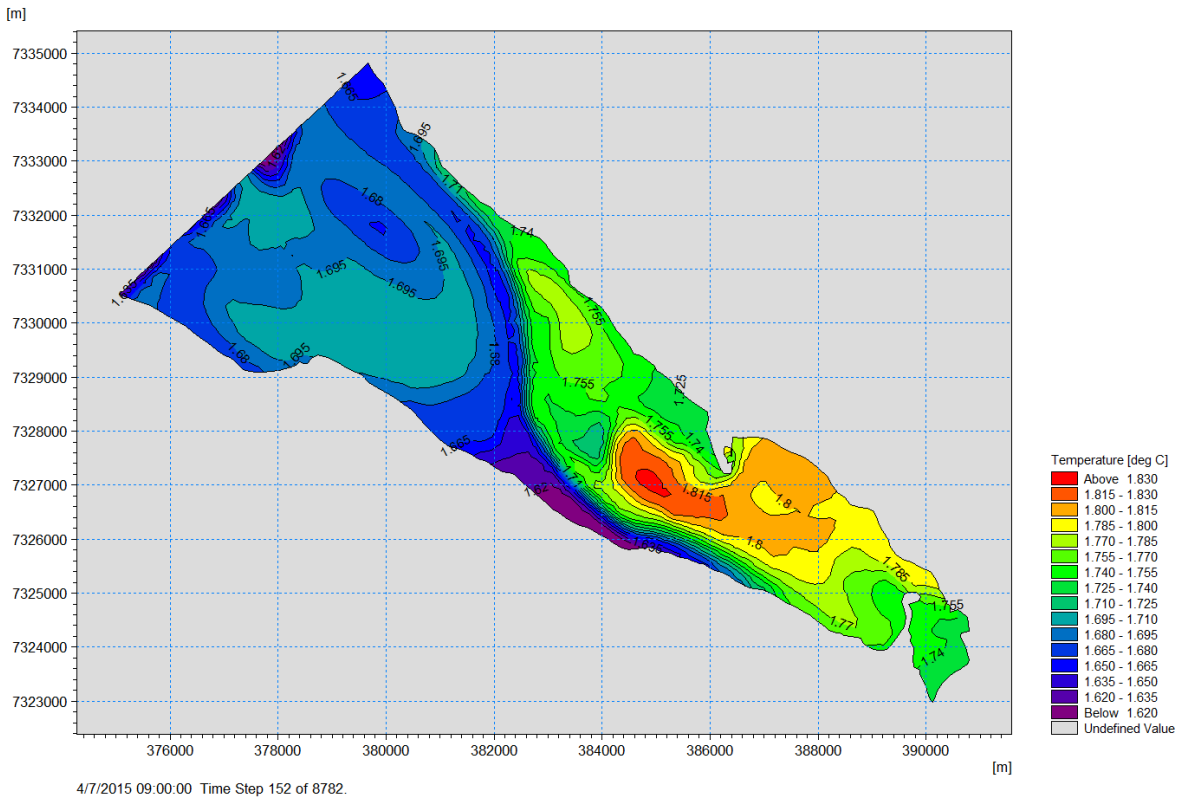

Figure 60. The variety of seawater temperatures in Önundarfjörður

6.3.3 3-Dimensional simulation of currents

In this research, information acquired from 2D simulations by MIKE21 were used to analyze seawater temperatures and currents in 3D simulations by MIKE 3. For 3D simulations, vertical parameters such as vertical mesh, vertical eddy viscosity, vertical dispersion, and 3D equations were taken into account. The results of the one-year simulation show that there is not a uniform pattern of currents from the surface to the bottom of Önundarfjörður. This variety is more distinct around obstacles, such as the head of the tip of the peninsula and beach cusps. The simulations indicate that during flood, the current mostly flows over the bottom layers to the fjord, as shown in Figure 61.

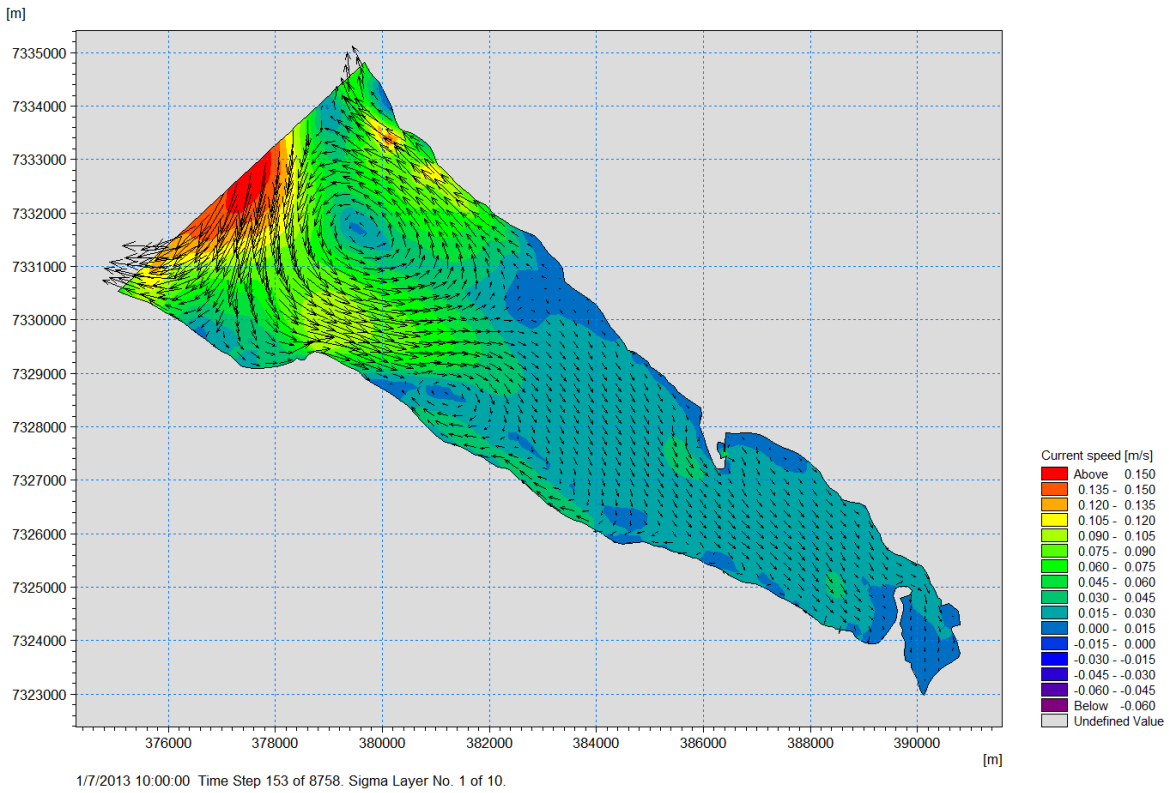

Figure 61. Prevailing current patterns over the bottom layer during flood

As illustrated in the figure, during flood, the higher velocity current is appears mostly near the mouth of the fjord, and the velocity decreases towards the inner side of the domain. However, during ebb the current predominantly flows at the surface layers with a higher longshore velocity component towards the mouth of the fjord, as delineated in Figure 62.

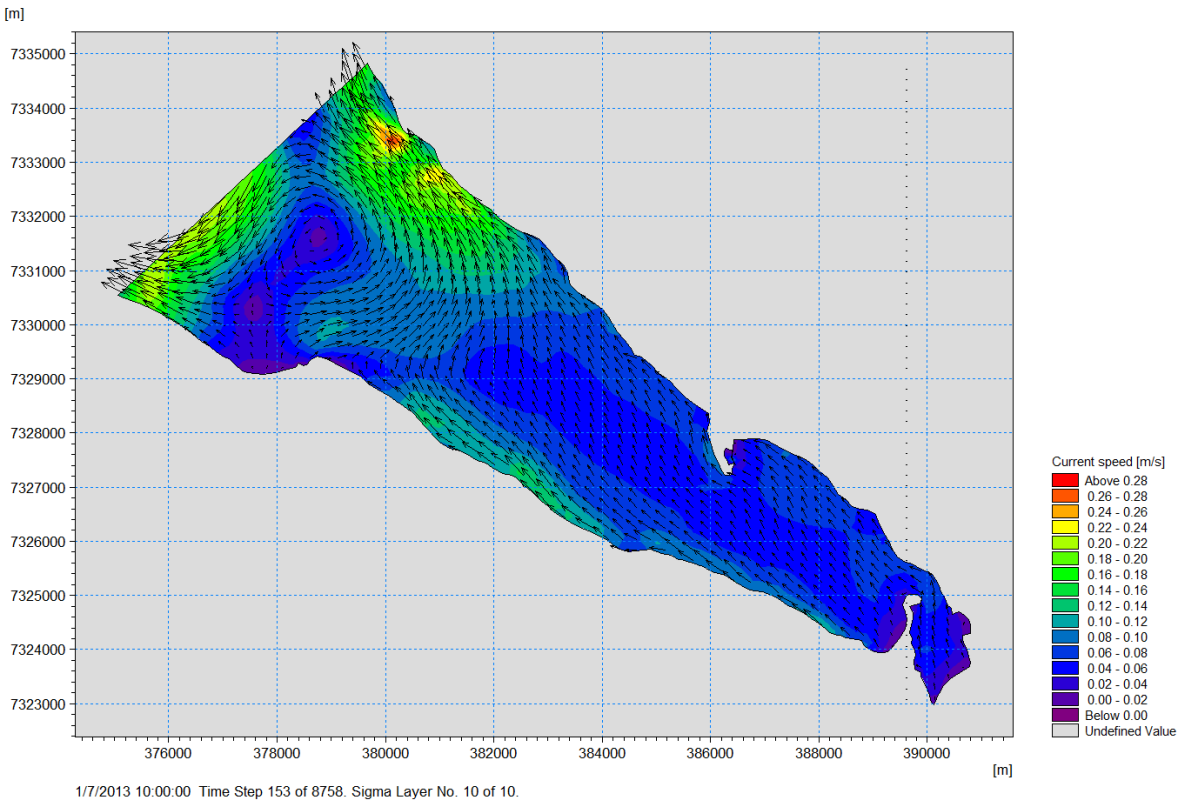

Figure 62. Current pattern at the surface layer during ebb

Also, wind-driven currents on the surface layer flows to the mouth of the fjord along with the prevailing east and southeast winds. The results demonstrate that a strong vortex flows from the surface layer to the bottom in front of the mouth of the fjord, as illustrated in Figure 63.

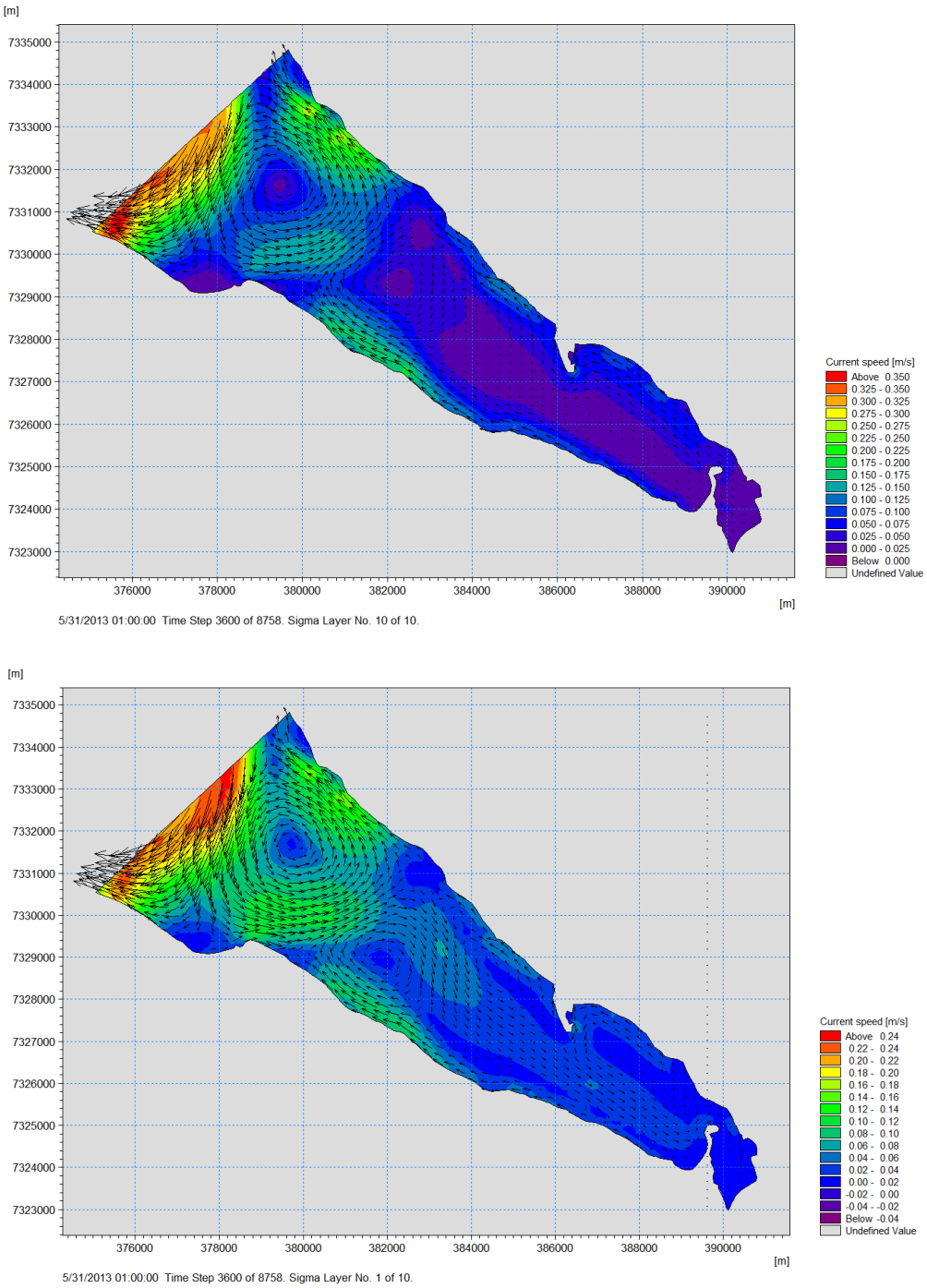

Figure 63. Surface and bottom current velocities at the up and down pictures, respectively

Figure 64 delineates the side view of the vortex. As shown in the figure, the formation of the vortex takes place from the surface to the bottom of the fjord. The formation is mainly due to the seabed features and the different directions of the currents in the area.

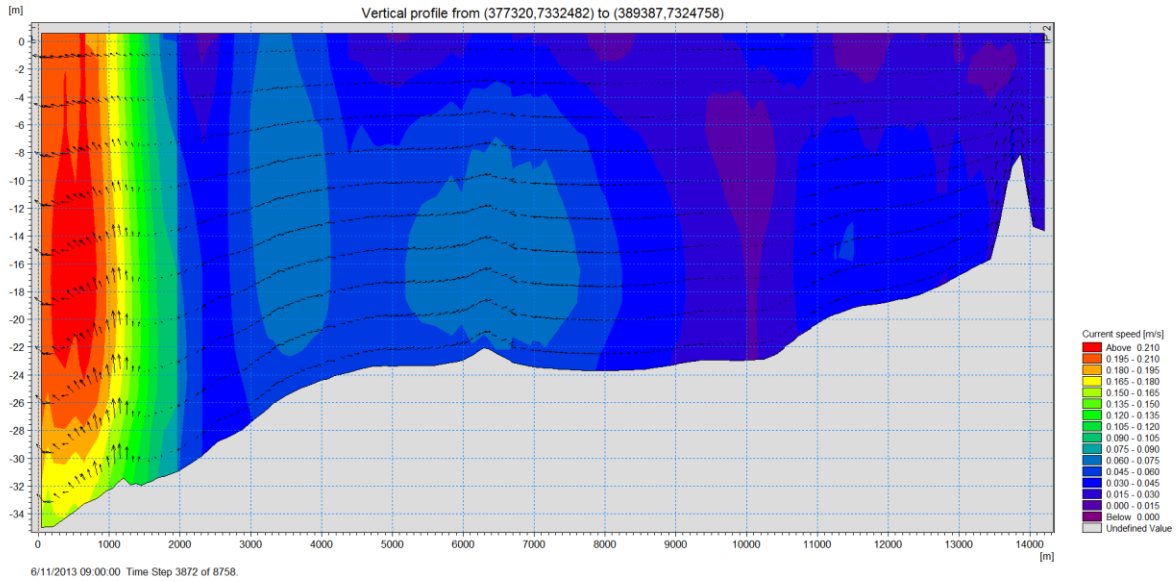

Figure 64. Strong vortex in front of the mouth of Önundarfjörður

Cross-shore currents and the formation of rings were constantly observed in the simulations. In general, the current components were mainly influenced by the tide and wind throughout the fjord. However, the effect of the wind was decreased at the deeper layers.

6.3.4 3-Dimensional simulation of seawater temperature

3D simulation of seawater temperature carried out from April 1, 2015 to April 1, 2016. The results of simulation show that surface seawater temperature is directly influenced by ambient air temperature. Generally, at the surface layers the maximum seawater temperature is observed along northern shoreline of the fjord, particularly in front of the port during one year of simulation. Also, over the bottom layers, the maximum seawater temperature is found along northern shoreline. However, in the center and along southern shoreline of Önundarfjörður seawater occasionally experiences high temperature in one year. In order to deliberate seawater temperature along the northern shoreline three areas will be investigated. The reasons of delibration of seawater along the northern shoreline are higher temperature and the vicinity to the town. In these areas, hereafter called T1, T2 and T3 (see Figure 65) seawater temperature is considered at the surface and bottom layers.

Figure 65. Selected areas along northern shoreline

The results of comparisons demonstrate that, from April to September there is no significant difference of seawater temperature between the areas. However, from September to the end of March bottom layers of area T1 and surface and bottom layers of T2 experience higher seawater temperature as delineated in Figure 66.

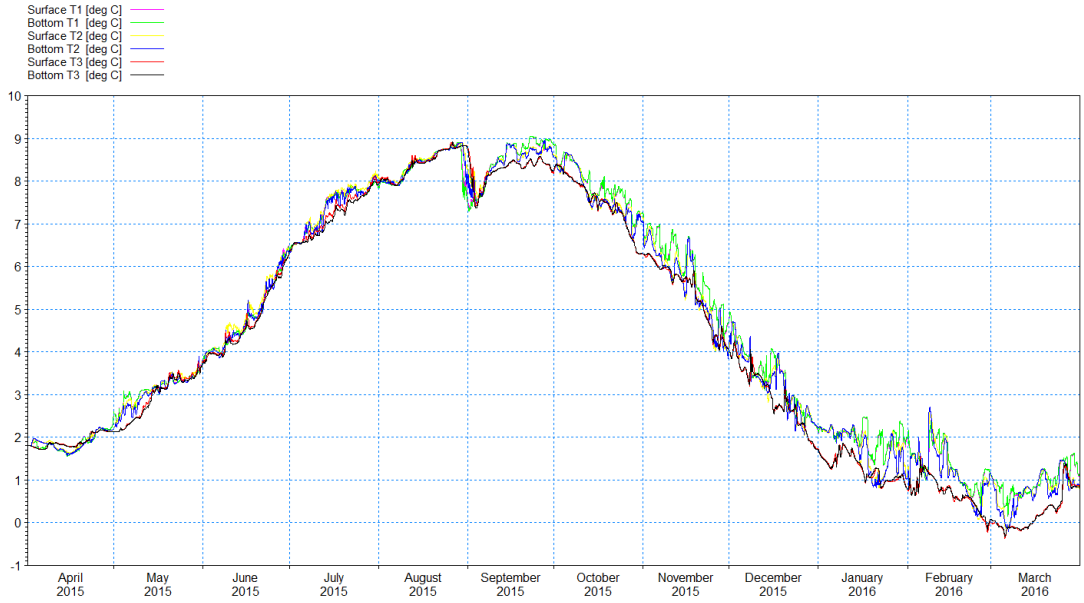

Figure 66. Comparisons of surface and bottom seawater temperature in the areas

Horizontal and vertical dispersion of seawater temperature throughout the fjord demonstrate that, in general, lower layers have more steady temperature with less variability in compare to the surface layers as depicted in Figure 67.

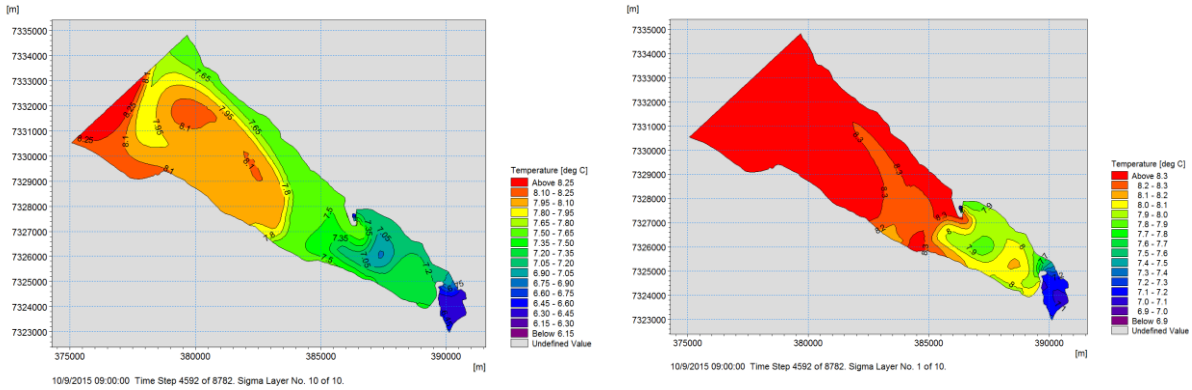

Figure 67. Surface bottom seawater temperature at the left and right side respectively

7 Discussion

7.1 Site selection based on the measurement results

Comparisons among the measurements over one year indicate almost uniform conformity, with similar seawater temperatures among the locations in Önundarfjörður. The comparison of recorded data among locations during the period of measurement is depicted in Figure 68.

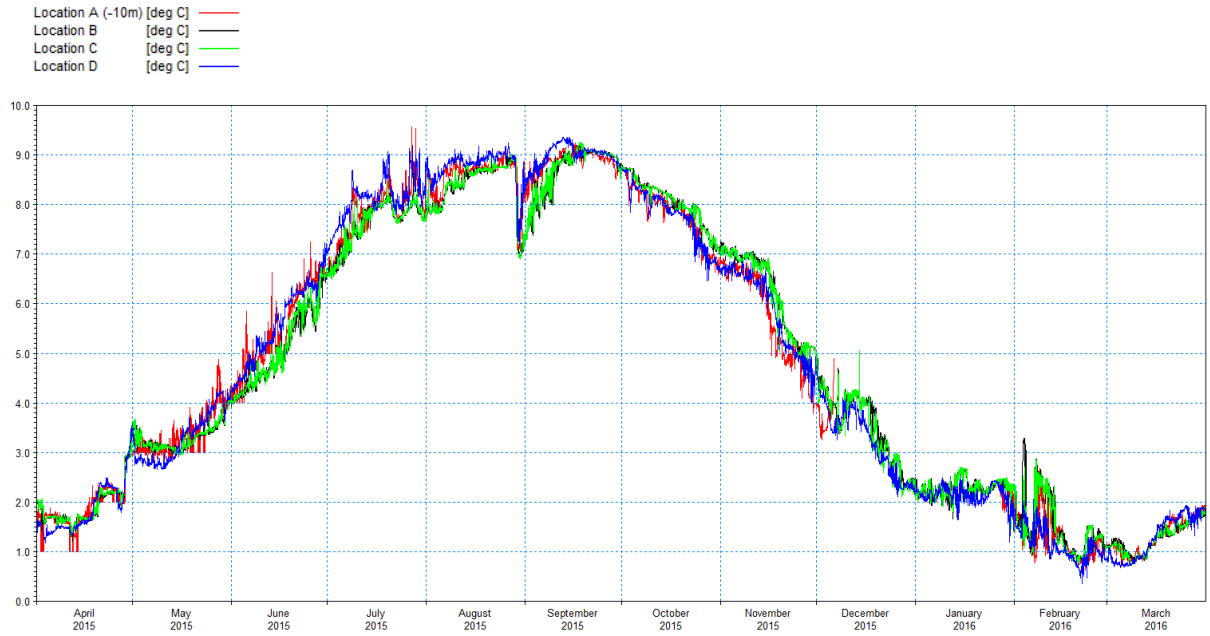

Figure 68. Comparison of seawater temperature among locations A(-10m), B, C, & D

The general agreement among locations, with slight changes in trends and anomalies occurring at all locations, indicate the coherent variation of seawater temperature throughout the fjord during the year. As shown in the figure, at the bottom layers the seawater temperatures rarely fall below 1 °C and never exceed 10 °C. The lowest monthly seawater temperatures recorded at all locations occurred in February, while the highest monthly temperatures were observed in

July and September. Figure 69 shows the drop in seawater temperatures at all locations in late August.

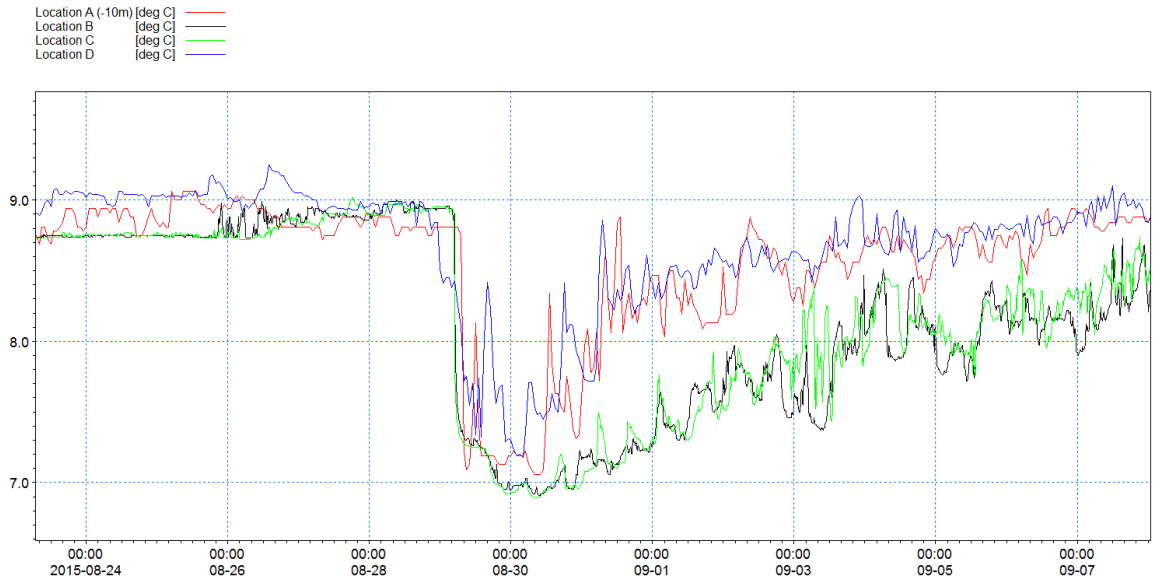

Figure 69. Seawater temperature falls at locations in Önundarfjörður in the late August

As can be seen from the figure, the drop in seawater temperatures started from location D. Thereafter, the seawater temperature dropped at locations C, B, and finally A. The result of the simulation reveals that flowing of a cold front current to the fjord is the main reason for the drop in temperature at the locations. The cold front, as depicted in Figure 70, flowed to Önundarfjörður from the south of the mouth of the fjord.

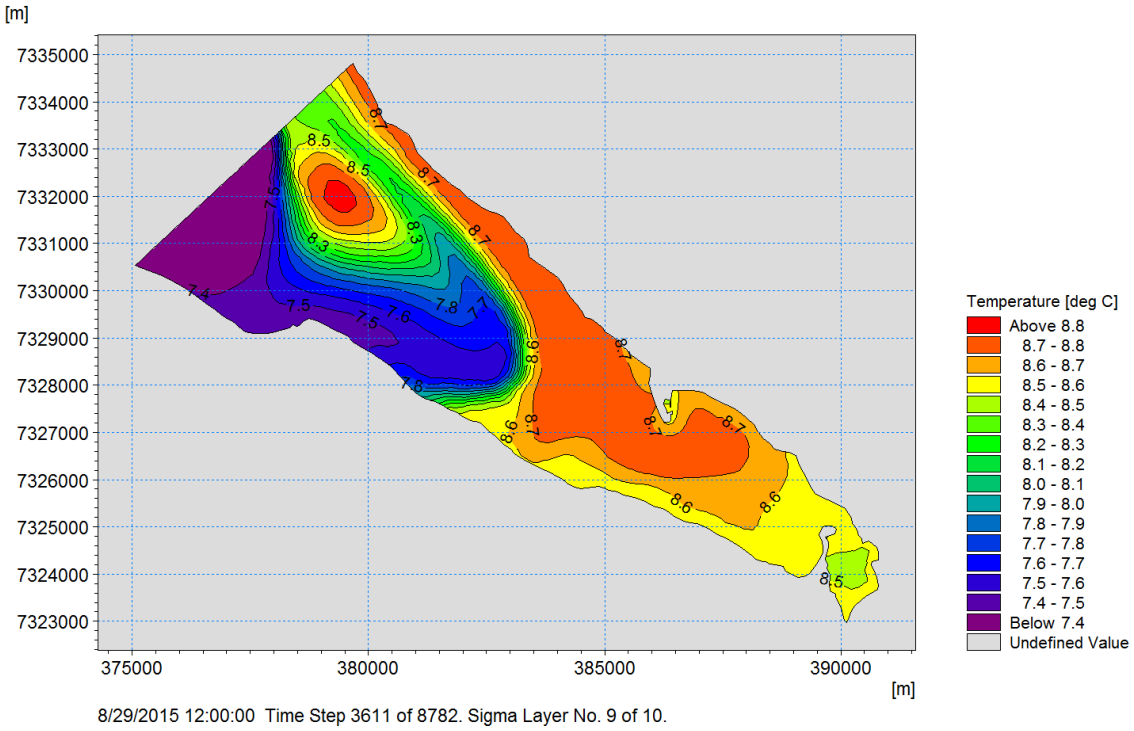

Figure 70. The flow of cold front current to Önundarfjörður

As illustrated in the last figure, the cold front flowed toward location D initially. Thereafter, the front came to locations C, B, and A, respectively. Figure 71 presents a comparison of the maximum, minimum, and average recorded seawater temperatures at the four locations.

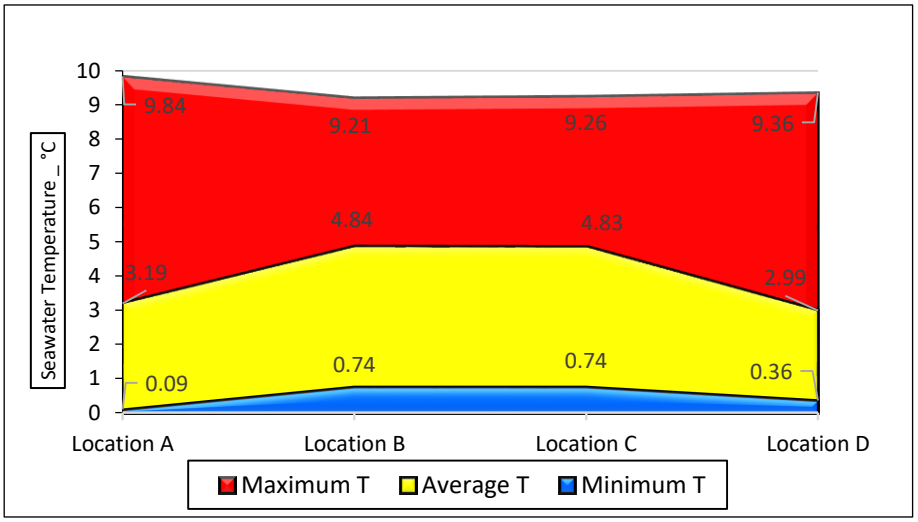

Figure 71. The maximum, average, and minimum seawater temperatures at the locations. At location A, the data are for a depth of -10 m.

As illustrated in the figure, location A had the highest maximum seawater temperature. However, locations B and C experienced higher average seawater temperatures during the year of measurement. In addition, the surface seawater temperature in Önundarfjörður was directly influenced by the ambient air temperature, as can be seen in Figure 72.

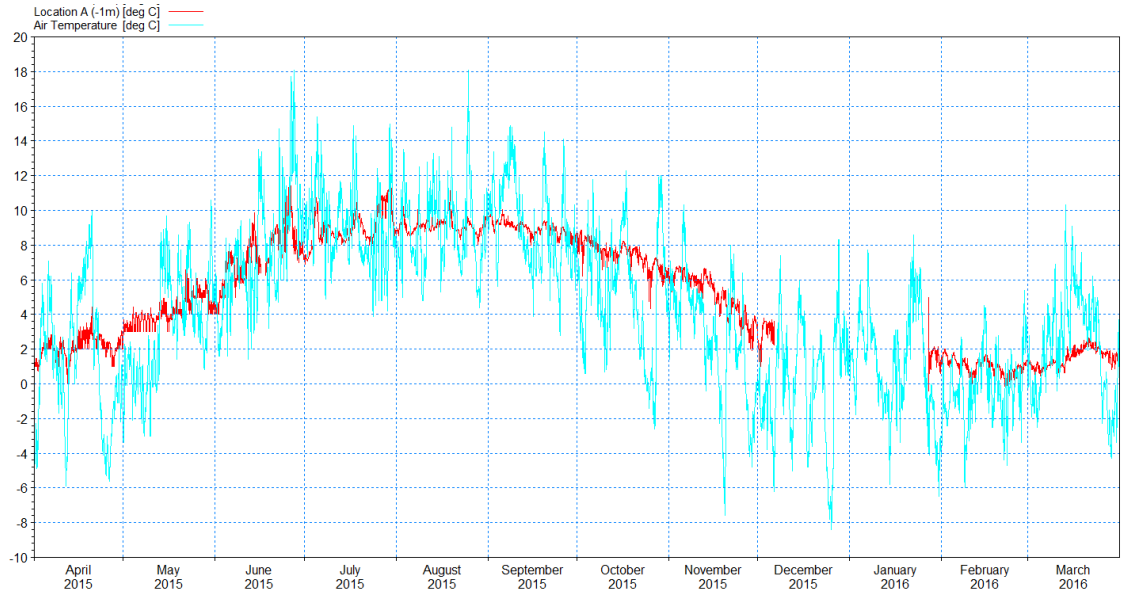

Figure 72. Ambient air and surface water temperatures in Önundarfjörður

As depicted in the above figure, from October to May the ambient air temperature fell below zero, and during this time the freezing of the surface water in Önundarfjörður was occasionally observed.

The following comparative diagrams show similarities between the two nearby locations.

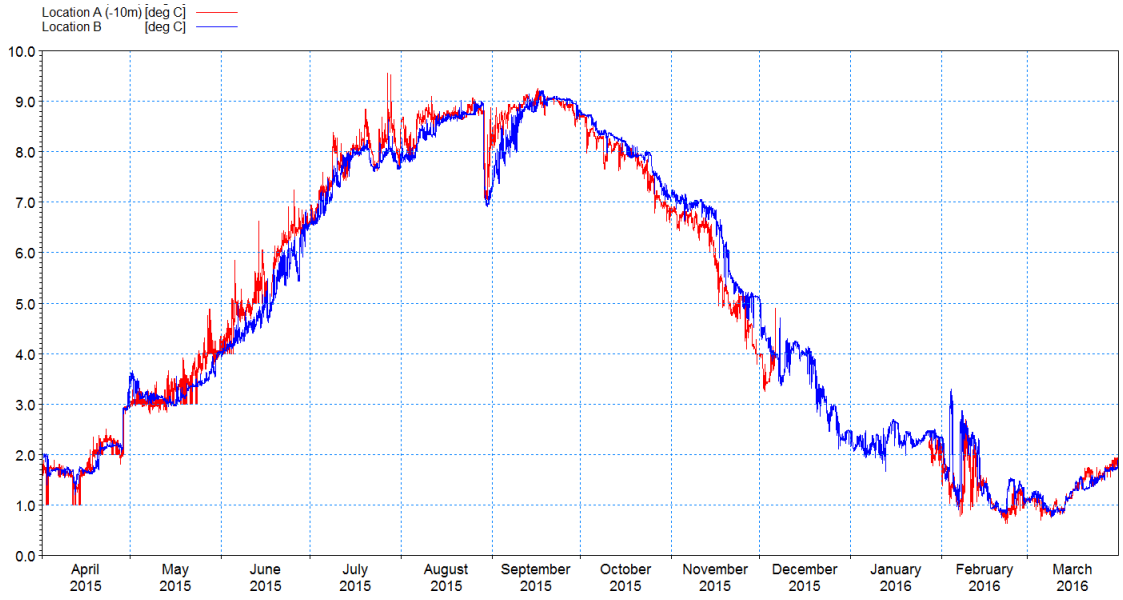

Figure 73. Comparison of seawater temperatures between locations A and B in Önundarfjörður

The graphed time series (Figure 73) reveals the same trend, with no considerable discrepancy between location A (at -10 m depth) and location B.

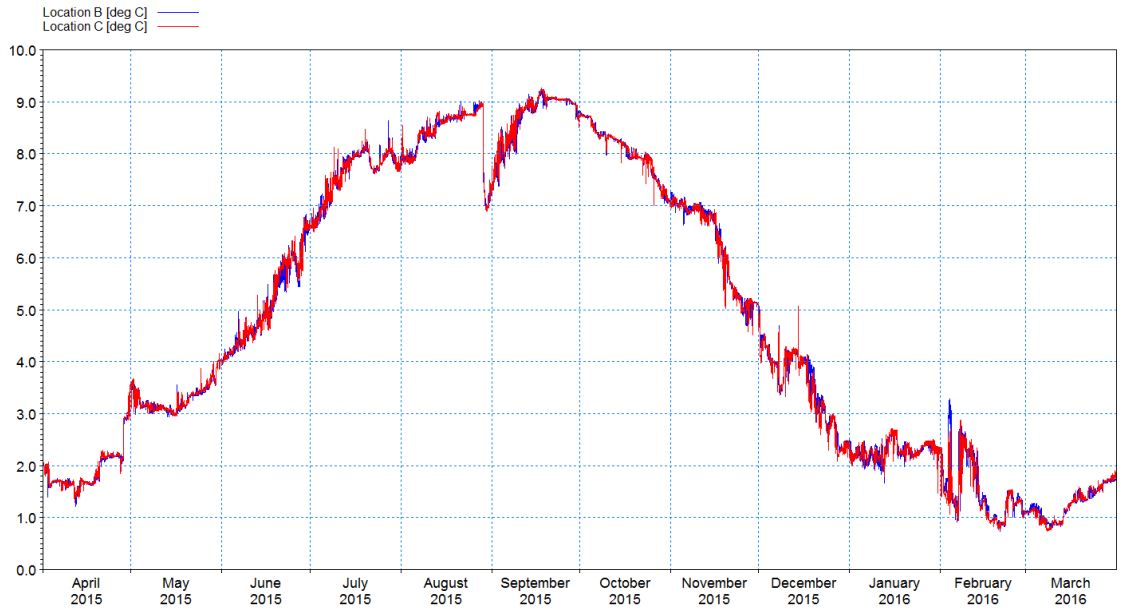

Figure 74. Comparison of seawater temperatures between locations B and C in Önundarfjörður

As shown from the Figure 74, the seawater at these locations had nearly identical temperatures. However, location C had a higher maximum seawater temperature during the measurement period.

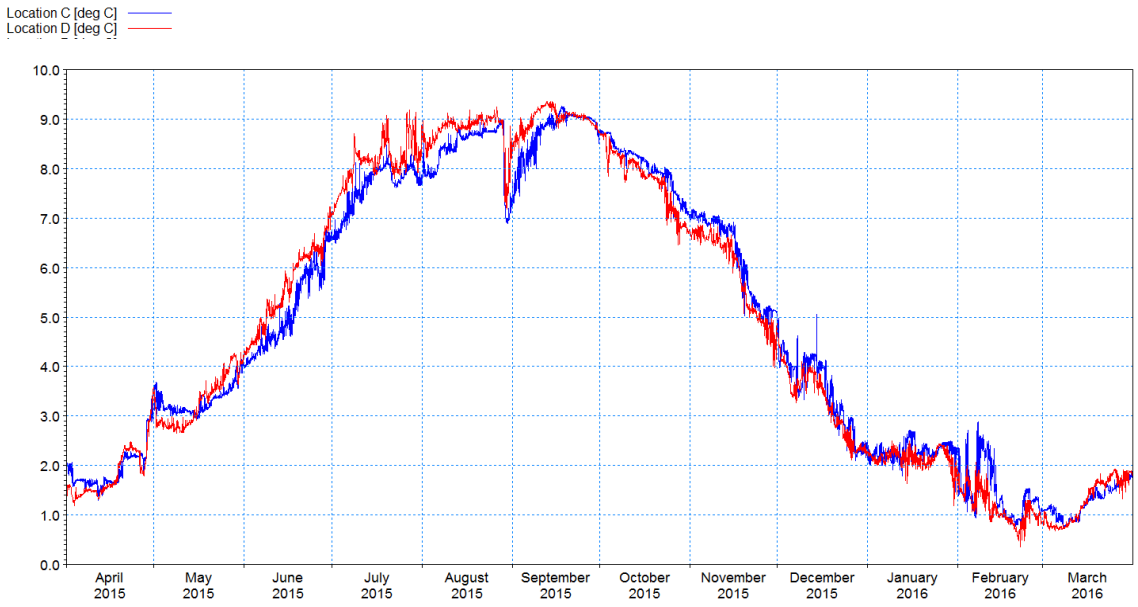

Figure 75. Comparison of seawater temperatures between locations C and D in Önundarfjörður

As can be seen from the Figure 75, the seawater at location D had a higher temperature from mid-May until late September. However, thereafter the seawater at location C mostly experienced higher temperatures.

A comparison of seawater temperatures recorded at nearly the same depth in locations A and D is shown in Figure 76.

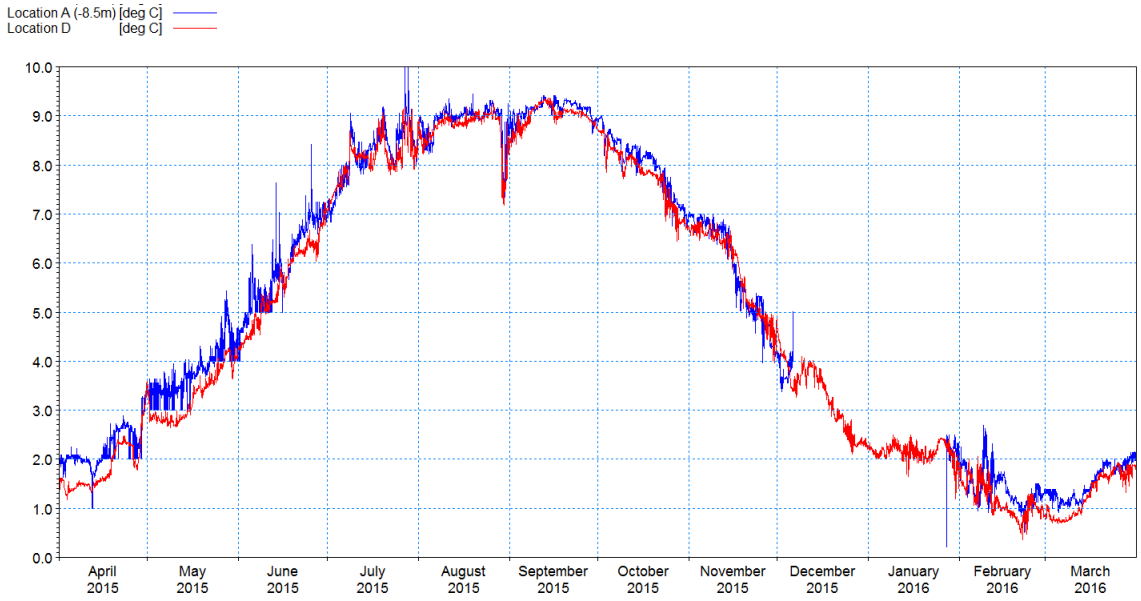

Figure 76. Comparison of seawater temperature between locations A and D in Önundarfjörður

The comparison between the innermost location in the fjord and the furthest location to the town (Figure 76) indicates that, in general, the latter location had lower seawater temperatures during the year.

Overall, there was a minor difference in the monthly seawater temperature between the locations. Analysis of the seawater temperature measurements over one year at four locations indicates that locations B and C seawater have higher bottom seawater temperatures in comparison to other locations, in particular during the wintertime. In this regard, the denouement of the measurements suggests that the locations west side of Flateyri and around the tip of the peninsula have higher potential with respect to installing heat exchanger in the fjord.

7.2 Site selection based on the simulation results

The collected measured data provide the modeler with insight for evaluating the areas of interest. Also, the outputs of the model serve as an informative source that aids in the investigation of the main oceanographic parameters over the area. As already mentioned in the previous chapter, the current predominantly flows with higher velocity along the shore of Önundarfjörður. On the other hand, the seawater along northern shorelines of the fjord generally yielded higher temperatures. So, those areas have priority for the purposes of this research. Over the entire research area, the results of the simulations indicate that there are four locations in which the seawater has relatively higher temperatures throughout the year and in particular in wintertime. These locations are hereafter called locations 1, 2, 3, and 4. Locations 1 , 2, and 3 are found along the northern shoreline, and location 4 is around the southern shoreline of the fjord. Locations 1 and 4 are at the bottom layer, while locations 2 and 3 are found at depths of 4-6 m. The locations are depicted in Figure 77.

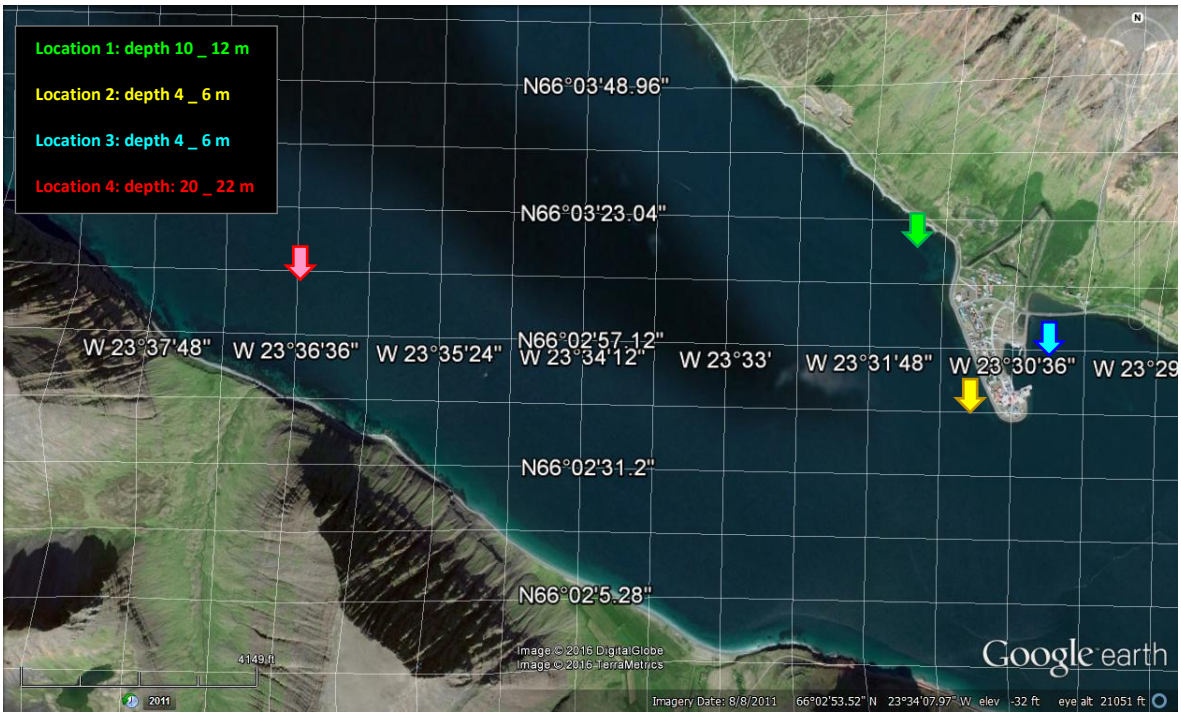

Figure 77. Selected locations with higher annual seawater temperatures in Önundarfjörður

Since locations 1, 2, and 3 are next to Flateyri, they are prioritized for considering the placement of heat exchanger, and the results of the seawater temperatures and current velocities recorded at these locations were compared together. A vertical profile of the simulation around the town is found in Figure 78.

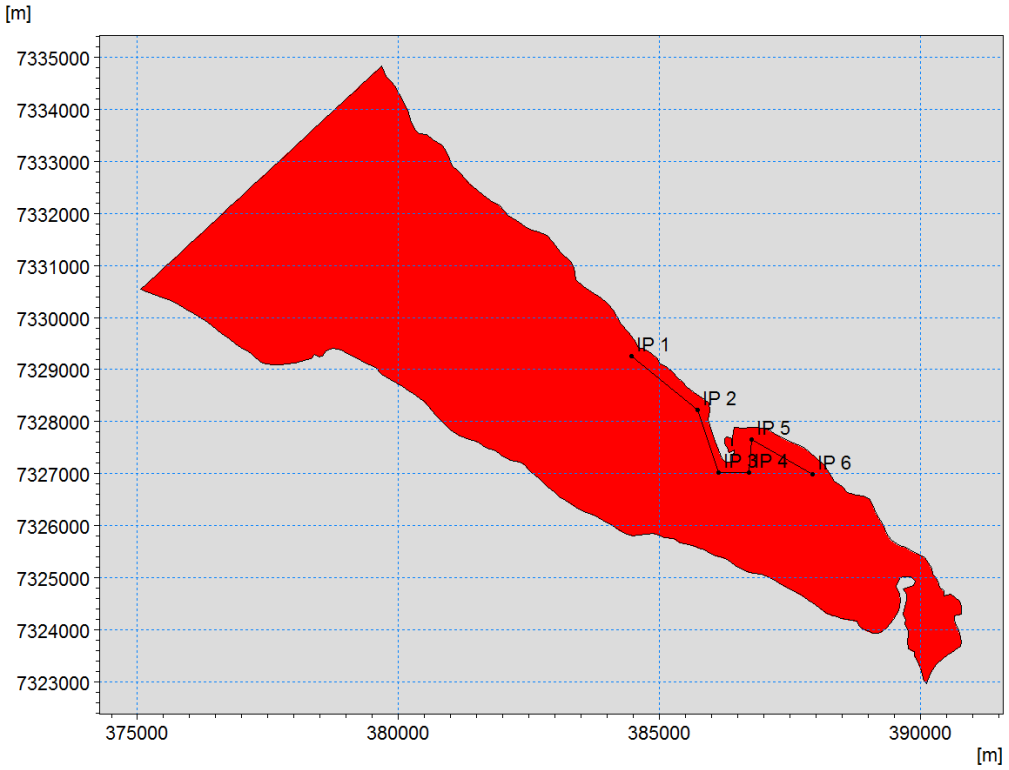

Figure 78. Vertical profile for simulating seawater temperature and current velocity from IP1 to IP6

Analysis of the profile reveals that at depths of 10-12 m before IP2, 4-6 m around IP3, and 4-6 m over IP5, Önundarfjörður mostly experienced higher temperatures during the year, as illustrated in Figure 79 and Figure 80.

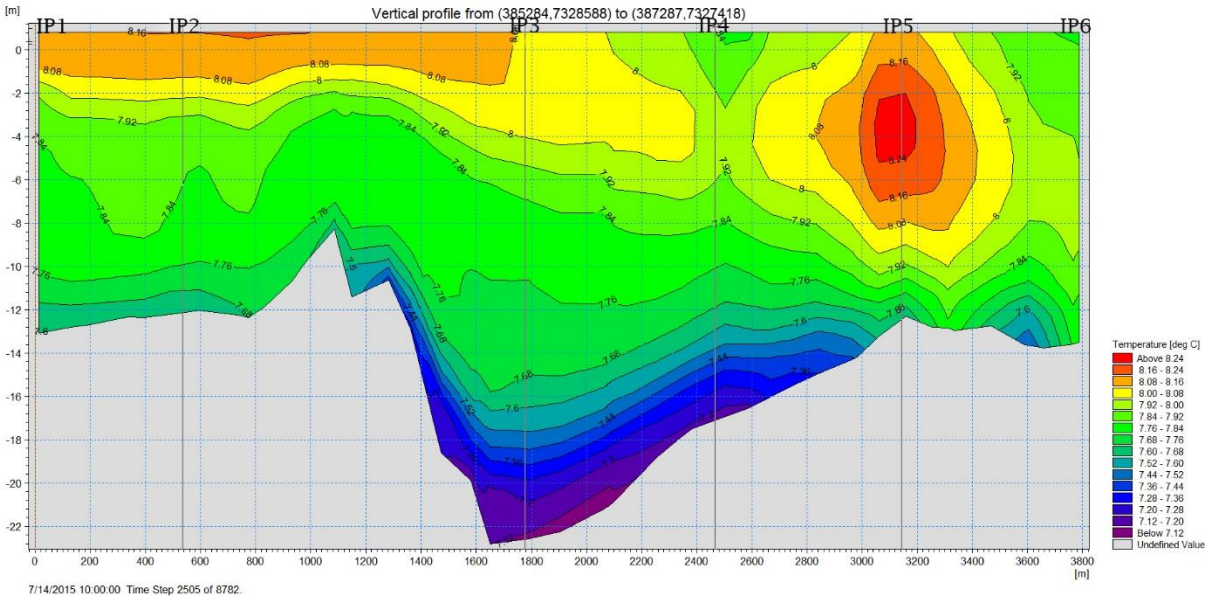

Figure 79. Vertical profile (see Figure 78) of simulated seawater temperatures in summertime

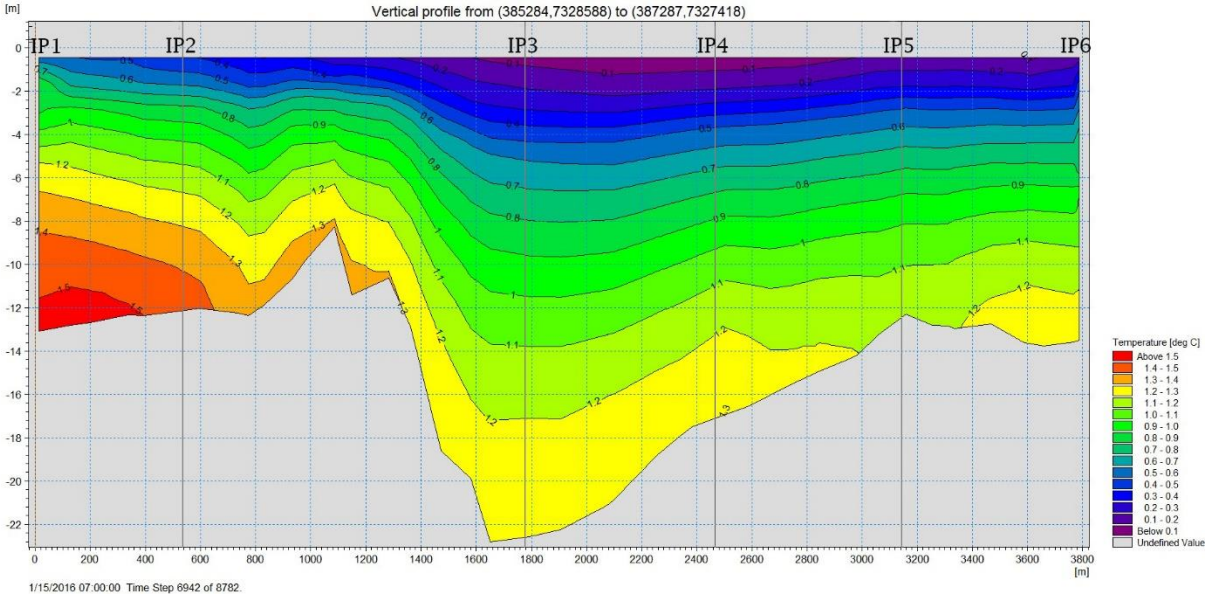

Figure 80. Vertical profile (see Figure 78) of simulated seawater temperatures in wintertime

The bottom features of the locations are marked in Figure 81.

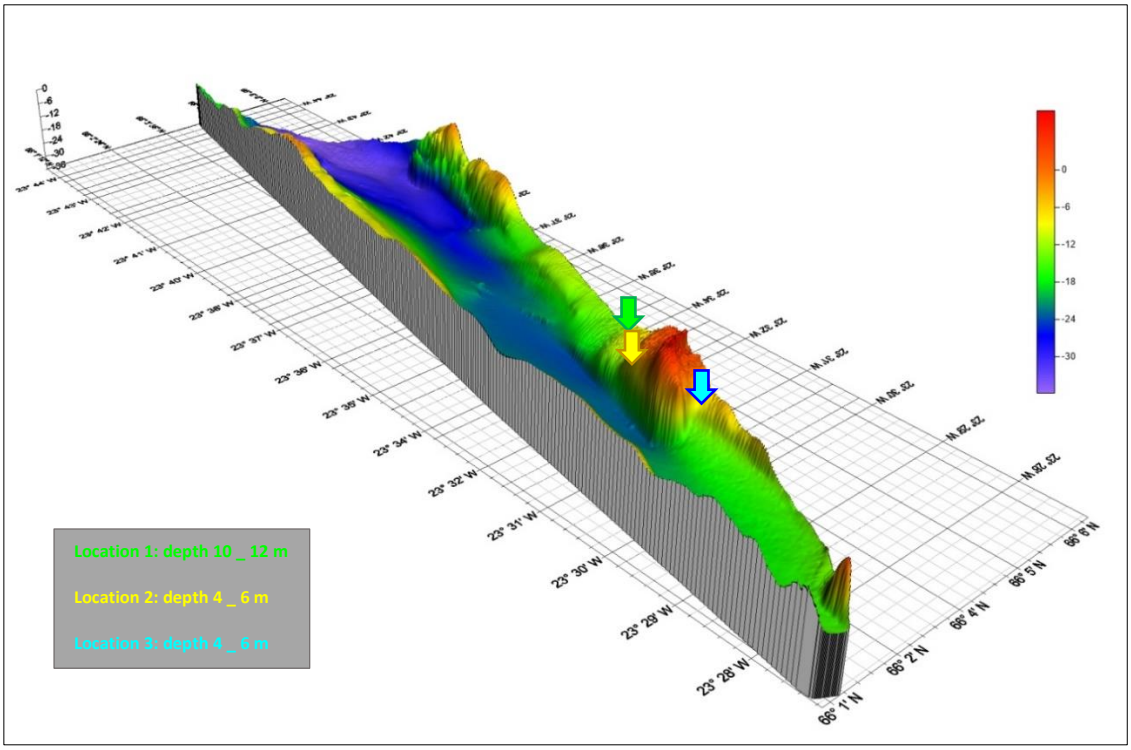

Figure 81. The bottom features of locations 1, 2, and 3

Comparison of the seawater temperatures recorded in three locations indicate that seawater had the highest temperature at location 1 in wintertime, as shown in Figure 82.

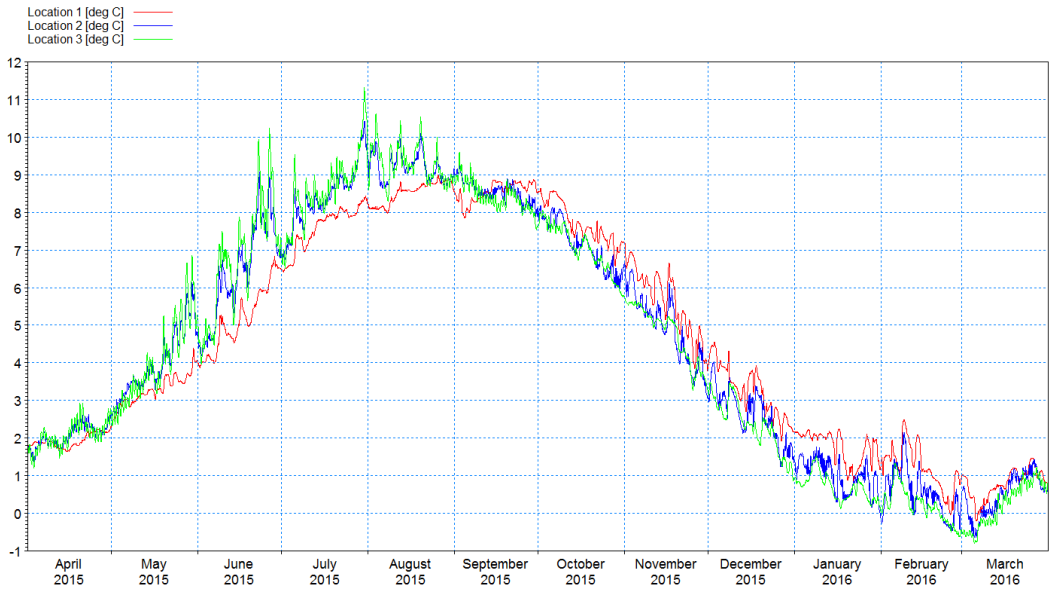

Figure 82. Comparison of simulated seawater temperatures at locations 1, 2, and 3

As depicted in the figure above, seawater at location 1 not only yielded the highest temperature in wintertime, but it also had the highest minimum temperature over the simulation period.

Technically, within the acceptable range of temperatures, heat exchanger(s) has the main rule to extracts heat from the heat source. However, in wintertime when the seawater temperature drops to a few degrees above the freezing point, a heat pump should be utilized in order to transfer required thermal energy from the seawater. Also, a higher current velocity is preferable for the system as it provides a greater volume of seawater as a heat source. The simulation shows that the northern shoreline was mostly dominated by longshore ebb currents flowing toward the mouth of the fjord. The higher current velocities at the surface layers were mostly observed in front of the port and at the tip of the Flateyri peninsula, as plotted in Figure 83.

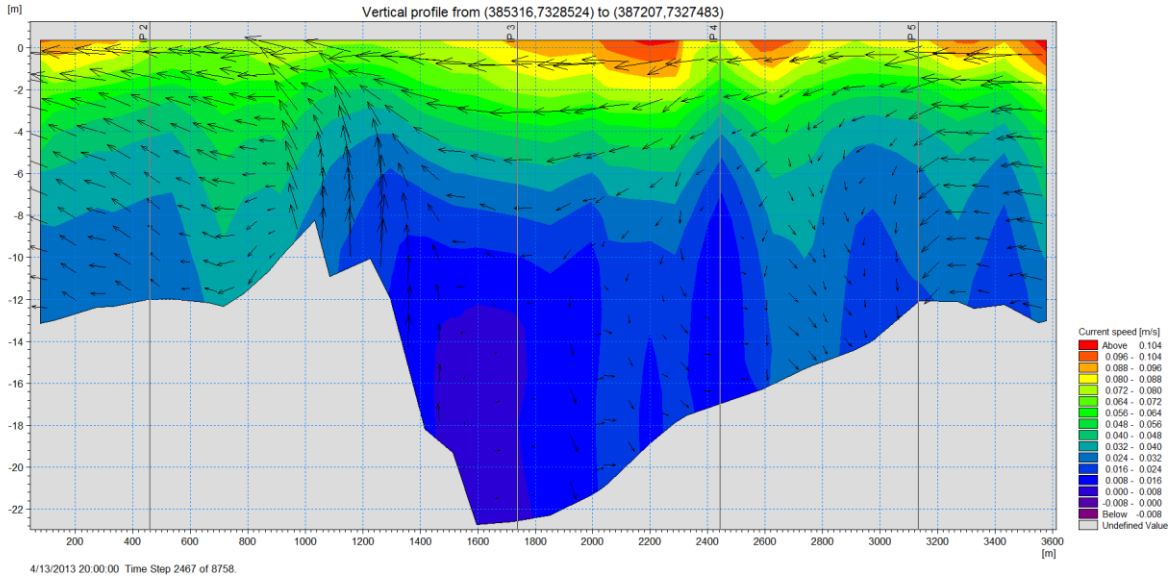

Figure 83. Ebb-dominated current pattern along the northern shoreline

The simulated current velocities throughout locations 1, 2, and 3 reveal that the highest maximum and the highest average current velocity are at locations 2 and 3, respectively. Figure 84 shows the current velocities at locations 1, 2, and 3.

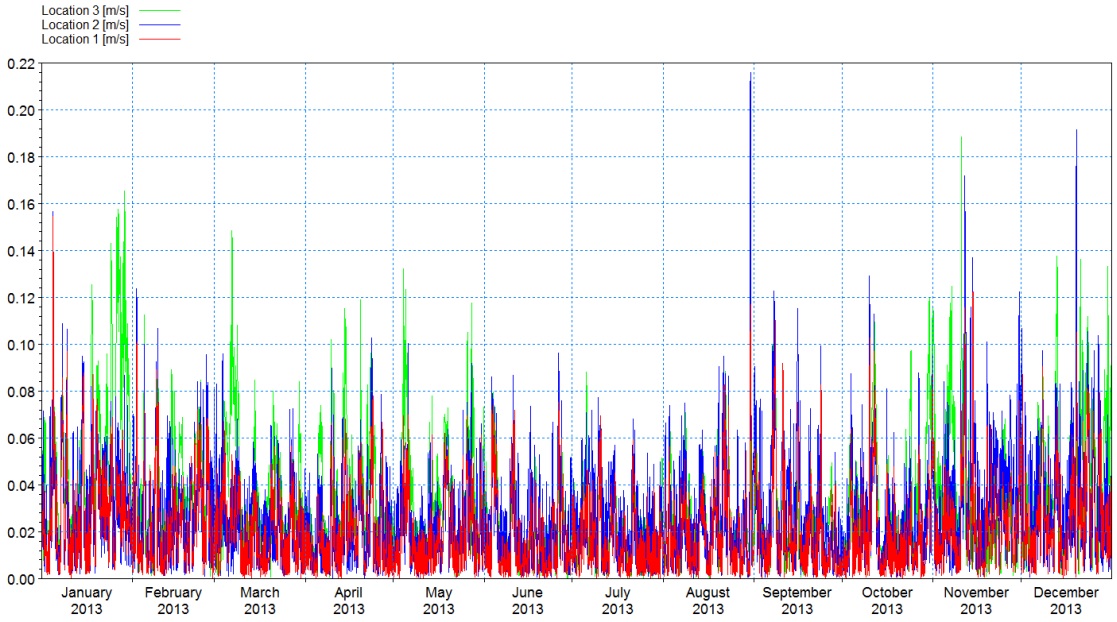

Figure 84. Comparison of current velocities at locations 1, 2, and 3

As can be seen from the last figure, there is conformance among the current velocities at the different locations. However, a distinct vertex was observed at location 2 and several maximums were observed at location 3.

As mentioned before, around the southern shoreline, location 4 experienced warmer conditions in comparison to other areas along the southern shore in Önundarfjörður. In this location, which is highlighted in Figure 85, the seawater had a higher average temperature during the year, particularly in wintertime.

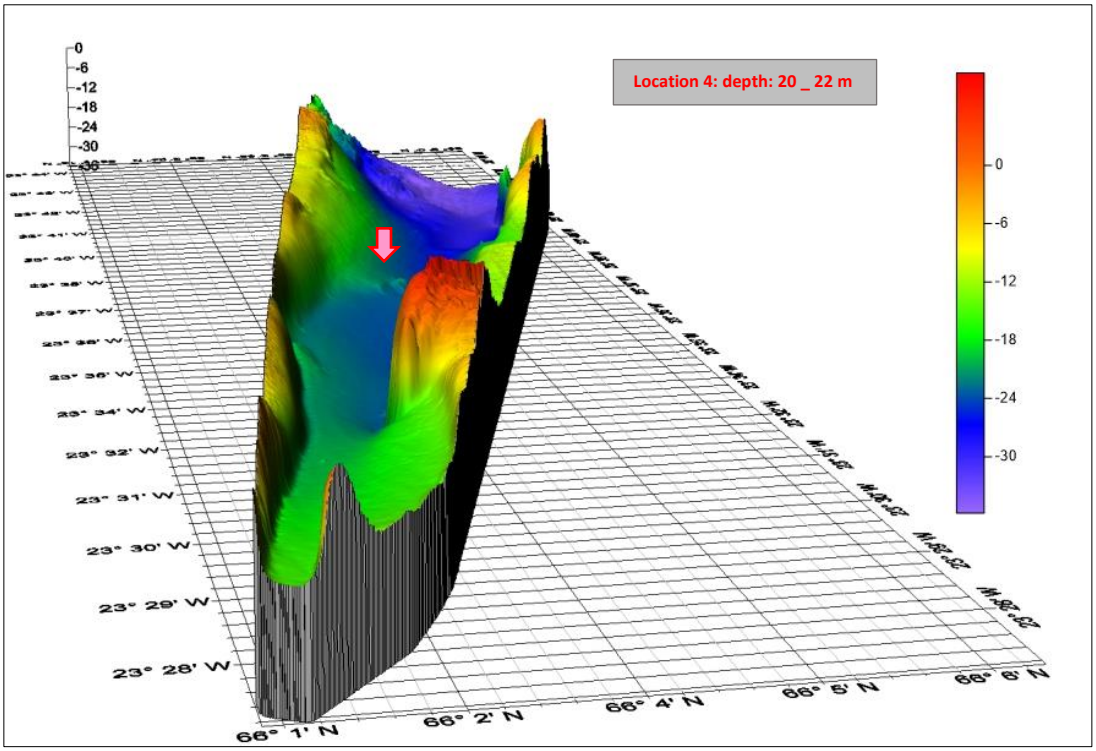

Figure 85. The bottom features of location 4

Figure 86 illustrates the vertical profile of the simulated seawater temperature along the southern shoreline.

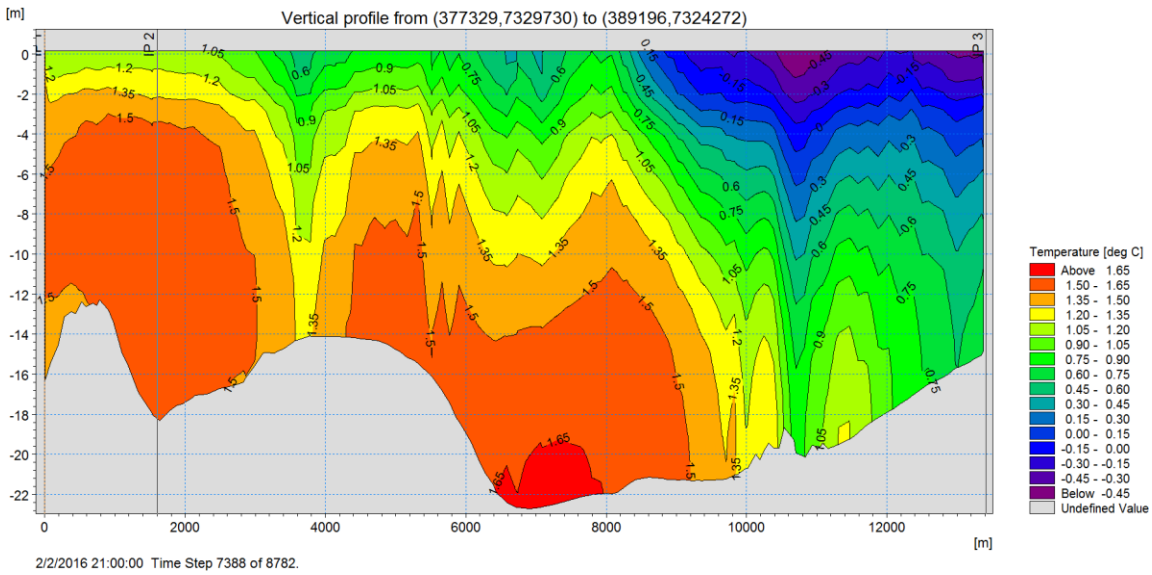

Figure 86. Vertical profile of simulated seawater temperatures in wintertime along the southern shoreline of Önundarfjörður

As can be seen in the Figure 86, the higher seawater temperatures were mostly restricted at location 4 during the wintertime. The monthly seawater temperature diagram at location 4 is shown in Figure 87.

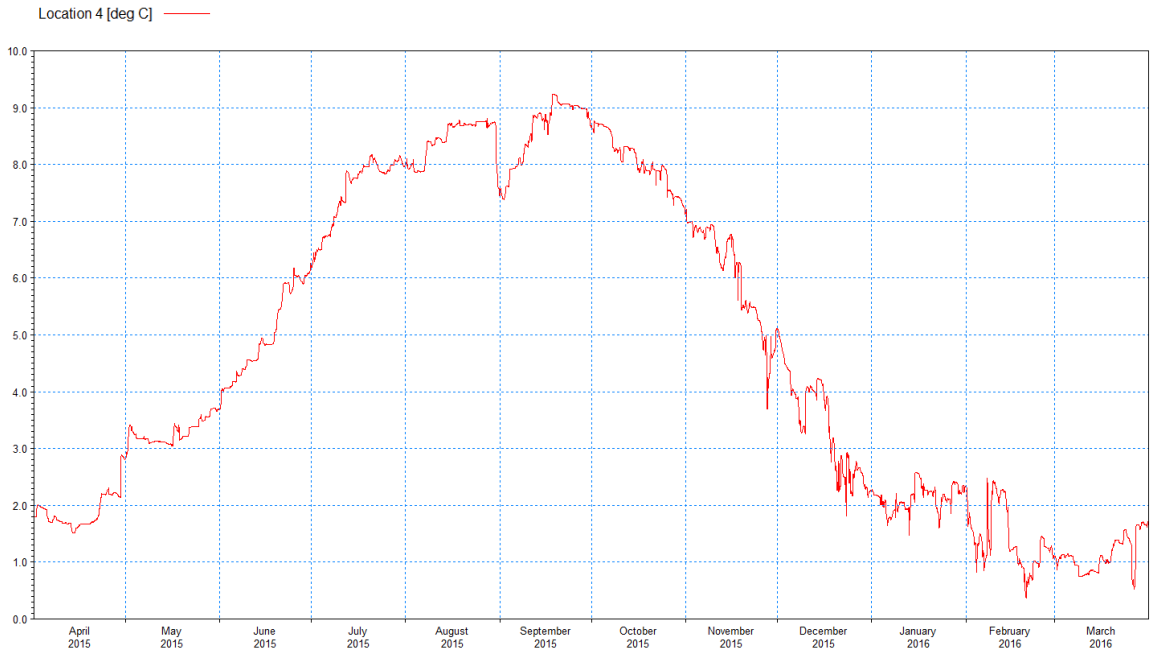

Figure 87. Simulated seawater temperature at location 4

As shown in the figure, the seawater temperatures were higher than 0°C during the simulation period. The results show that the location is influenced by mostly flood and also ebb. Figure 88 illustrates the monthly current velocity at location 4.

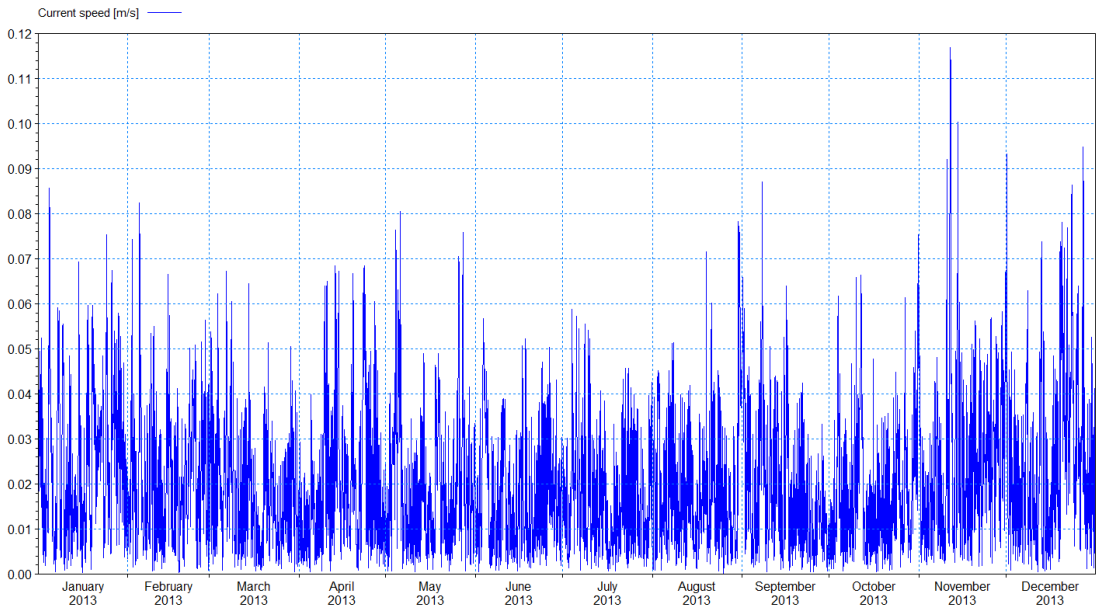

Figure 88. Simulated current velocity at location 4

As can be seen, the current velocity is mostly less than 0.05 m/s at this location during the course of the year. Table 6 presents the simulated seawater temperatures from April 1, 2015, to April 1, 2016.

Table 6. Seawater temperatures at locations 1, 2, 3, and 4

Seawater Temperature (°C)	Minimum	Maximum	Average	Standard Deviation
Location 1	-0.20	9.00	4.63	2.87
Location 2	-0.68	10.42	4.62	3.20
Location 3	-0.80	11.31	4.54	3.36
Location 4	0.36	9.23	4.75	2.82

The simulation showed that location 4 has the highest average seawater temperature during the year in comparison to the other three locations. The current velocities measured at the locations from April 1, 2015, to April 1, 2016 are provided in Table 7.

Table 7. Statistical information of current velocities at locations 1, 2, 3, and 4

Current velocity (m/s)	Minimum	Maximum	Average	Standard deviation
Location 1	0.00	0.15	0.02	0.01
Location 2	0.00	0.21	0.02	0.02
Location 3	0.00	0.18	0.03	0.02
Location 4	0.11	0.02	0.01	0.11

Although location 4 showed better conditions in the comparison, such as the highest minimum and average seawater temperatures, it is furthest from the town. Also, not only at location 4 the average current velocity is less than other selected locations, but location 4 is also at a greater depth, which would increase the cost of implementation. The analysis of the simulated results indicates that there are no considerable differences between the current velocities and seawater temperatures at locations 1, 2, and 3. However, location 1 has one advantage in that it has the highest seawater temperature during the winter time. Thereby, location 1 was determined to be the most appropriate location from which to extract heat from Önundarfjörður.

7.3 Fishing and aquaculture activities in Önundarfjörður

The existence of fragile marine ecosystems limits the implementation of MRE (Sotta, Niliot & Lefeuvre, 2012). Prior to any installation, implementation, and operation of MRE technology, the potential environmental impacts and environmental risks should be taken into account. Although WSHP systems have a few, if any, negative impacts on the direct environment, an investigation into the marine species, most likely to be affected, and the environment around the area of heat extraction are required. The development of MRE increases the potential for spatial

conflicts with other marine activities, such as commercial fishing (Reilly, O'Hagan & Dalton, 2015). Having a general overview about aquaculture activities in the area of interest should help reduce this potential for spatial conflict. In Iceland, regulations on fish farming are made under the authority of the Ministry of Industries and Innovation (Icelandic Ministry of Industries and Innovation, 2015). Furthermore, aquaculture activities and fish farming are mostly assessed by the Directorate of Fisheries. In order to implement seawater heat extraction with respect to the purpose of this research, the related regulations on aquaculture, published by Ministry of Industries and Innovation in Iceland, should be taken into consideration. In order to reduce and or prevent any spatial conflicts, the most relevant issues in the regulation are included; chapter II, article 4 about minimum distance between marine cage farms; chapter IV, Article 12 about Information on the total size of installations and precise location of farming stations; chapter V, article 21 about local audit of the locations of marine cage farms; chapter V, article 25 about demand for fish farming licenses in the area; chapter V, article 27 about profile description of marine cage farms and any future plans; chapter V, article 28 aboutduration of farm licenses; chapter V, article 32 about signs and markers on marine cage farms and also minimum distance from fishing and other maritime activities.

Jónsson (2014) presented the areas of interest for aquaculture and other utilizations in Önundarfjörður (see Figure 89). Furthermore, he pointed out that fishing activities have been limited in Önundarfjörður in the past few years.

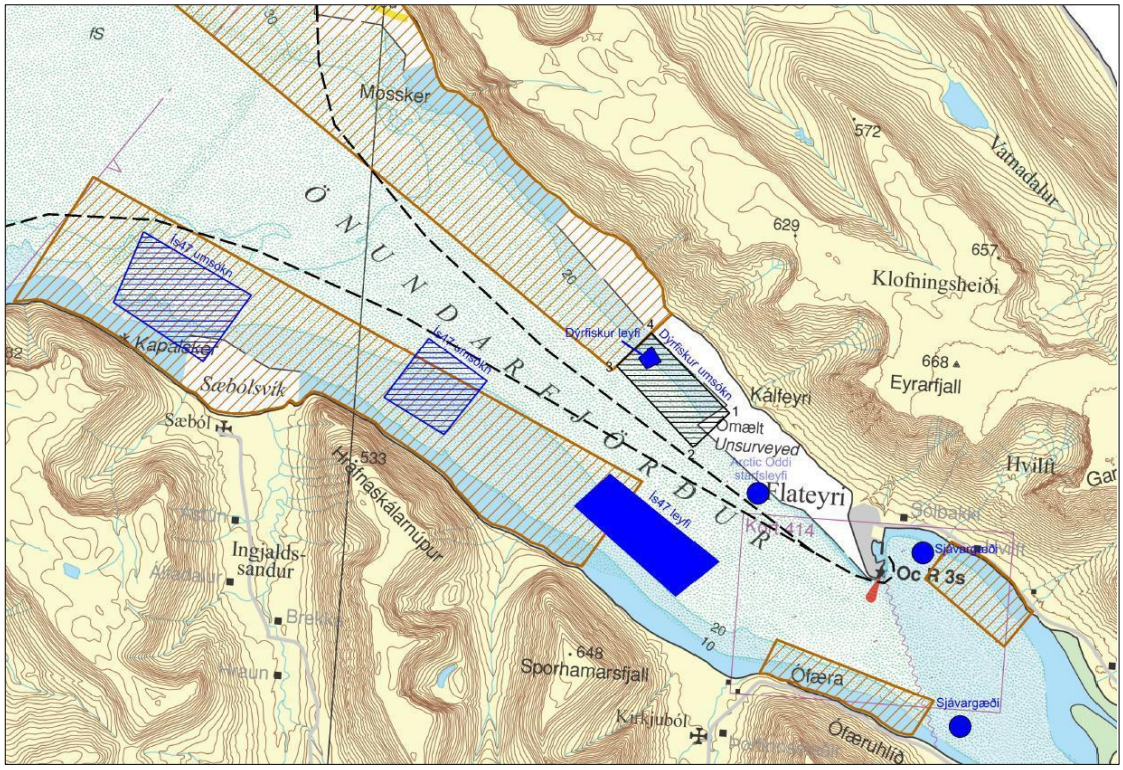

Figure 89. Interested area of aquaculture activity (blue areas), fishing ground (reddish-brown areas), lumpfish (oblique dark area), common navigation route (dashed line) in Önundarfjörður (Jónsson, 2014)

During the research period, field observations were also carried out in Önundarfjörður. Aquaculture activities are very common along the southern shore of Önundarfjörður. Also, according to the existing documents, the northern shore of the fjord is considered to be area of interest for aquaculture activities. So, in order to install a heat exchanger in Önundarfjörður, decision makers must first consider the potential impacts on the marine life in the fjord. However, in this research, locations 1 and 2 present fewer spatial conflicts with respect to fish farming areas and also to areas of interest for aquaculture activities.

7.4 Port activities in Önundarfjörður

Shipping routes are optimized in order to reduce navigational distances. The operation of MRE may increase the potential for spatial conflicts in the area with shipping activities (Cradden, Kalogeri, Barrios, Galanis, Ingram & Kallos, 2016). In Önundarfjörður, in order to install a heat exchanger in one of the areas of interest, potential conflicts with fishing boats and cruise ships should also be analyzed. In terms of port activities and navigation routes in the fjord, the implementation of a heat exchanger and the relevant facilities should not be placed in anchorage areas of the vessels. Furthermore, any activity taking place within the inner side of imaginary line from Valþjófsdalur to Ytribót (Figure 90) has to be considered and verified by the harbor committee (G. Kristjánsson, personal communication, April 7, 2016).

Figure 90. The red line is the imaginary line (Kortasjá, 2016)

It is important to allow sufficient space between the navigation routes of seaborne vessels and devices such as the heat exchanger, piping, and mooring facilities. Location 1 has the most promise in this regard because it allows the maximum spacing from marine activities and the minimum amount of spatial conflicts with the active navigation routes in Önundarfjörður.

8 Conclusion

Increasing energy demands among the public and private sectors, along with the scarcity of fossil fuels, have led policy makers and scientists to consider the use of renewable sources of energy. The heat stored in seawater is an immense source of renewable energy. Seawater source heat pump systems extract heat from seawater, even at low temperatures, to supply thermal energy. With the most efficient output, the system is being utilized as a renewable energy solution in countries with cold weather conditions. In the present study, the feasibility of heat extraction was investigated in Önundarfjörður in the northwest of Iceland. The research was conducted for one year, during which measurements of seawater temperatures were made at four locations in Önundarfjörður. Furthermore, in order to gain insights into the complex oceanographic conditions in the fjord, 2D and 3D simulations were carried out in the areas of interest. The measurements and simulations indicate that the seawater temperatures is higher than 0 °C and rarely exceed 10 °C in Önundarfjörður. In general, the seawater along the northern shoreline of the fjord has a higher temperature. The results of the simulations show that the fjord is tide-dominated. The high velocity currents prominently flank alongshores during ebb. The results reveal four preferable locations for heat extraction in Önundarfjörður. However, along the northern shoreline, bottom seawater in the west side of the town has superior conditions in comparison to the other locations in Önundarfjörður. Furthermore, various considerations, such as potential impacts on and conflicts with fishing, aquaculture, and port activities, were included in the analysis. Overall, regarding the results of the field measurements and outputs of the modeling as well as other relevant considerations, supplying heat for the target habitants by a seawater source heat pump system has been ascertained to be theoretically feasible. The feasibility suggests that similar research can be carried out in the west and south of the Iceland as well, as the seawater temperatures in those regions are relatively higher. Also, tide-dominated coastlines augment the potential utilization of the system in Iceland. High demand for space heating, cheap electricity prices as well as the concentration of inhabitants and industrial activities in coastal zones create exceptional opportunities for supplying thermal energy via seawater source heat pump systems in Iceland. Such a system could potentially provide social and economic advantages, diminish the demand for oil for heating, bring investment and

business opportunities, and enhance sustainable development without negative environmental impacts. With respect to the temperature of seawater in Önundarfjörður, the seawater source heat pump system, which is comprised of a district heating system, a heat pump, and heat exchangers for Flateyri, is presented schematically in Figure 91.

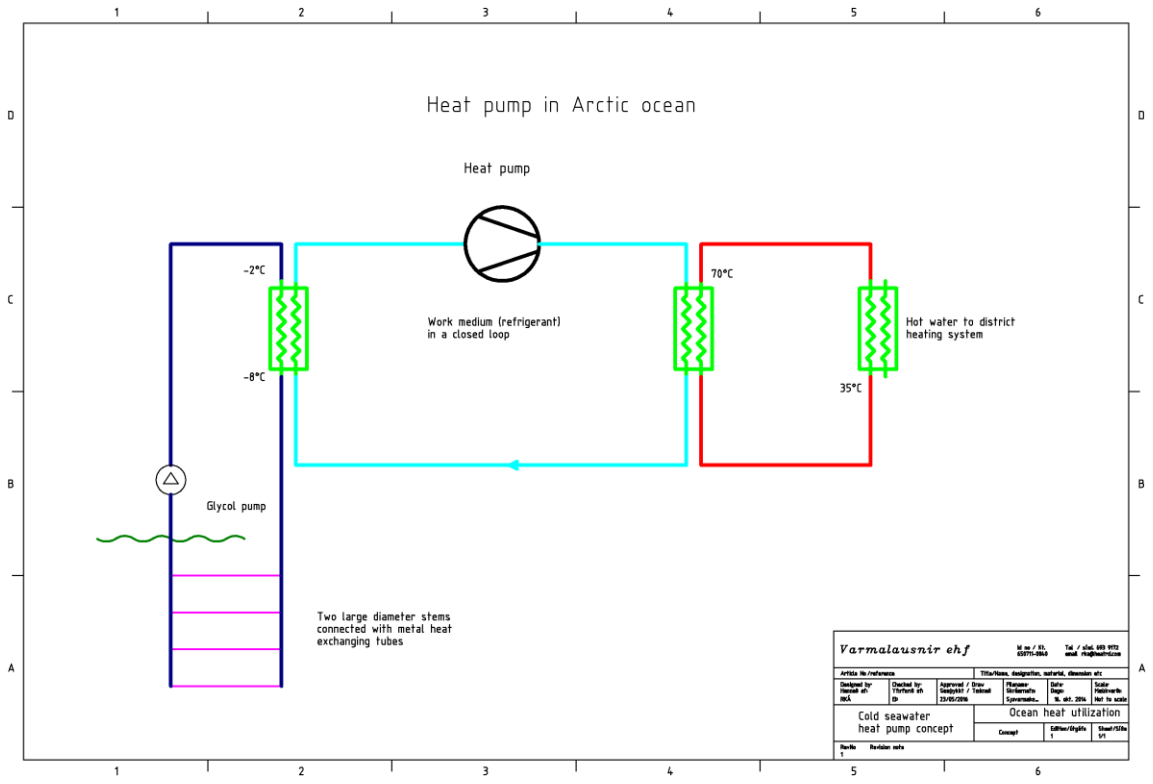

Figure 91. Schematic seawater source heat pump system for Flateyri, green boxes with zigzag line are heat exchanger (Varmalausnir - Heat RD Company, 2016)

Figure 91 illustrates a rough concept of a closed-loop system for the purpose of the present research. The system extracts thermal energy from the seawater via a Glycol pump. Then, a heat pump transfers the energy to the (retrofitted) district heating in Flateyri. In general, the system should be able to supply 70 °C hot water in district heating from Önundarfjörður.

Moreover, this work has contributed to the compilation of a comprehensive and informative database of oceanographic parameters throughout the area of interest.

9 Recommendations and further research

In this research, all attempts were made to demonstrate comprehensive and accurate outcomes. However, the author would like to mention the following recommendations for further research in this field of study.

- In order to obtain better data analysis, it is recommended that measurements of seawater temperature and currents be carried out across a wider spatial area.
- In order to acquire higher confidence of the feasibility in the region, a pilot installation included designing and implementing of one or more heat exchangers as well as a seawater source heat pump system is recommended.
- Since there are several maritime users in Önundarfjörður, in order to avoid any spatial conflicts, Marine Spatial Planning (MSP) and Integrated Coastal Zone Management (ICZM) should be addressed in further studies.
- Risk management analysis as well as Strategic Environmental Assessment (SEA) and Environmental Impact Assessment (EIA) are recommended in further research.
- The use of consistently measured data in the field as the input data of the model is suggested. Also, better calibration of the model increases the accuracy of the outputs.

10 References

Alaska Center for Energy and Power. (no date). *An Investigation of the Alaska SeaLife Center Seawater Heat Pump Demonstration.*

Anonymous. (2014). Þættir úr vistfræði sjávar 2013 (Environmental conditions in Icelandic waters 2013). Hafrannsoknir nr. 175, (in Icelandic, English summary), Reykjavík, Retrieved from: www.hafro.is/Bokasafn/Timarit/fjolrit-175.pdf

Arya, A., Dhanjibhai, D. (2015, December). Optimization of shell and tube heat exchanger. *International Journal of Advanced Technology for Science & Engineering Research, 1*(2), 27-35.

Ásmundsson, R. (2005). *Varmadælur Hagkvæmni á Íslandi.* Orkustofnun.

Ásmundsson, R. (2016). personal communication. (M. Eskafi, Interviewer)

Ásmundsson, R., Ólafsson, K., Þorsteinsson, E. (2015). *Arctic Ocean heat utilization.*

Astthorsson, O., Gislason, A., Jónsson, S. (2007, November). Climate variability and the Icelandic marine ecosystem. *Deep Sea Research Part II, 54*(23–26), 2456–2477.

Baker, A., Schaefermeyer, D. (2013, May 1). Sea water heat pump project. *ACEP Rural Energy Conference Forum.*

Baltic Sea Region Energy Cooperation [BASREC]. (2014). *District Heating and Cooling, Combined Heat and Power and Renewable Energy Sources.*

Björnsdóttir, J. (2014, January 30). *The Night We Never Forget*. Retrieved from Iceland on reviewline: http://icelandreview.com/stuff/reviews/2012/03/21/night-we-never-forget

Bollmann, M., Bosch, T., Colijn, F., Ebinghaus, R., Froese, R., Güssow, K., Khalilian, S., Krastel, S., Körtzinger, A., Langenbuch, M., Latif, M., Matthiessen, B., Melzner, F., Oschlies, A., Petersen, S., Proelß, A., Quaas, M., Reichenbach, J., Requate, T. , Reusch, T., Rosenstiel, P., O. Schmidt, J., Schrottke, K., Sichelschmidt, H., Siebert, U., Soltwedel, R., Sommer, U., Stattegger, K., Sterr, H., Sturm, R., Treude, T., Vafeidis, A., van Bernem, C., van Beusekom, J.,

Voss, J., Visbeck, M., Wahl, M., Wallmann, K., Weinberger, F. (2010). *world ocean review, Living with the oceans.* maribus.

Borre, A. (2011, August). Definition of heat pumps and their use of renewable energy sources. *REHVA*, 38-39.

Bowditch, N. (2002). *The American practical navigator : an epitome of navigation.* Bethesda Maryland: National Imagary and Mapping Agency.

Chua, K., Chou, S., Yang, W. (2010, December). Advances in heat pump systems: A review. *Applied Energy, 87*(12), 3611–3624. doi:10.1016/j.apenergy.2010.06.014

Cradden, L., Kalogeri, C., Barrios, I., Galanis, G., Ingram, D., Kallos, G. (2016, March). Multi-criteria site selection for offshore renewable energy platforms. *Renewable Energy, 87*, 791–806. doi:10.1016/j.renene.2015.10.035

Dallas Semiconductor Company. (n d). *DS18B20 Programmable Resolution 1-Wire Digital Thermometer.* Retrieved from www.maximintegrated.com: https://datasheets.maximintegrated.com/en/ds/DS18B20-PAR.pdf

Danish Hydraulic Institute. (2016). *MIKE 21 and MIKE 3 Flow Model FM Manual.* Danish Hydraulic Institute.

Denker, J. (2005). *Modern Thermodynamics.*

Edenhofer, O., Pichs-Madruga, R., Sokona, Y., Seyboth, K., Matschoss, P., Kadner, S., Zwickel, T., Eickemeier, P., Hansen, G., Schlömer, S., von Stechow, C. (2011). *Summary for Policymakers. In: IPCC Special Report on Renewable Energy Sources and Climate Change Mitigation.* Cambridge, United Kingdom and New York, NY, USA: Cambridge University Press.

Eisentraut, A., Brown, A. (2014). *Heating without global warming, Market Developments and Policy Considerations for Renewable Heat.* International energy agency.

Erlichson, H. (1998). Sadi Carnot, Founder of the Second Law of Thermodynamics.

EZGİ, C. (2014). Material selection for seawater cooled heat exchangers. *Naval Science and Engineering, 10*, 1-12.

Farhami, N., Bozorgian, A. (2011). Factors Affecting Selection of Tubes of Heat Exchanger. *International Conference on Chemistry and Chemical Process. 10.* Singapore: IACSIT Press.

Forsén, M. (2005). *Heat pumps technology and environmental impact.* Swedish Heat Pump Association.

Friotherm brochure. (no date). Värtan Ropsten – The largest sea water heat pump facility worldwide, with 6 Unitop 50FY and 180 MW total capacity. Retrieved from https://www.google.com/url?sa=t&rct=j&q=&esrc=s&source=web&cd=1&ved=0ahUKEwifwKCsw67JAhXInBoKHQkgCAkQFggdMAA&url=http%3A%2F%2Fwww.friotherm.com%2Fwebautor-data%2F41%2Fvaertan_e008_uk.pdf&usg=AFQjCNFz8QXPxyecdFfrij1AJbjXfbV1Ww&sig2=kRxZNaWGvJPtvFb59sz-MQ&c

Generalic, E. (2015, February 22). *Carnot cycle*. Retrieved from Chemistry Dictionary & Glossary: http://glossary.periodni.com/glossary.php?en=Carnot+cycle

Golden Software Company. (no date). *Surfer 13* . Retrieved from Golden Software.

Goyal, R., Rathod, P. (2011). Hydrodynamic Modelling for Salinity of Singapore Strait and Johor Strait using MIKE3 FM. *2nd International Conference on Environmental Science and Development. 4.* Singapore: IACSIT.

Haiwen, S., Lin, D., Jing, S., Xin, J., Zhiyong, R., Haiyang, Y. (2015, October 15). Field measurement and energy efficiency enhancement potential of a seawater source heat pump district heating system. *Energy and Buildings, 105,* 352–357. doi:10.1016/j.enbuild.2015.07.069

Haiwen, S., Lin, D., Xiangli, Li., Yingxin, Z. (2010, June). Energy-saving judgment of electric-driven seawater source heat pump district heating system over boiler house district heating system. *Energy and Buildings, 42*(6), 889–895. doi:10.1016/j.enbuild.2010.01.001

Hani, A., Koiv, T. (2012, August). The Preliminary Research of Sea Water District Heating and Cooling for Tallinn Coastal Area. *Smart Grid and Renewable Energy, 3*, 246-252.

Hanna, E., Jónsson, T., Ólafsson, J., Valdimarsson, H. (2006, February 14). Icelandic Coastal Sea Surface Temperature Records Constructed: Putting the Pulse on Air–Sea–Climate Interactions in the Northern North Atlantic. Part I: Comparison with HadISST1 Open-Ocean Surface Temperatures and Preliminary Analysis of Long-Term Pattern. *Journal of climate, 19.*

Heat Pump Center. (n.d.). Retrieved from http://www.heatpumpcentre.org/en/aboutheatpumps/howHPworks/Sidor/default.aspx

HeatPump-Reviews. (2009). *Heat Pump Refrigeration Cycle (II)*. Retrieved from heatpump-reviews.

Hossain, A. (2014, July 2). *Refrigeration*. Retrieved from slideshare: http://www.slideshare.net/ArafatHossain89/1refrigeration

Icelandic Marine Research Institute. (2016, March 9). *Horizontal distribution of properties*. Retrieved from Hydrography: http://www.hafro.is/Sjora/

Icelandic Ministry of Industeries and Innovation. (2009). *The Icelandic national renewable energy action plan for the promotion of the use of energy from renewable sources.*

Icelandic Ministry of Industries and Innovation. (2015, December 11). *Regulation of aquaculture.* Retrieved from Regulation collection: http://www.reglugerd.is/reglugerdir/eftir-raduneytum/sjavaroglandbunadar/nr/19913

Ingólfsson, Ö., Grimsdottir, H., Jónsson, M. (no date). Monitoring Snowpack Temperature Gradient Using Automatice Snow Depth Sensor.

International Renewable Energy Agency. (2013). *Heat Pumps, Technology Brief.*

Jackson, T. (2000). *Renewable Energy Sources.* United Kingdom: Centre for Environmental Strategy, University of Surrey .

Jónsson, A. (2014, February 10). Tilkynning um stækkun í 2.000 tonna ársframleiðslu á regnbogasilungi í Önundarfirði.

Jónsson, B. (2010). *Harnessing tidal energy in the Westfjords.* University Centre of the Westfjords, Faculty of Business and Science. Ísafjörður: University of Akureyri.

Jónsson, M., Grimsdottir, H., Breien, H., Kristensen, K., Zeinali, A. (2014). *SNAPS Northern Periphery programme; SNAPS Work Package 2: SM4 snow sensor.*

Jónsson, S. (1999). Temperature time series from Icelandic coastal stations. *Journal of Rit Fiskideildar*, 59-68.

Jónsson, S., Valdimarsson, H. (2012, June 8). Hydrography and circulation over the southern part of the Kolbeinsey Ridge. *ICES Journal of Marine Science*. doi:10.1093/icesjms/fss101

Ketilsson, J., Petursdottir, H., Thoroddsen, S., Oddsdottir, A., Bragadottir, E., Gudmundsdottir, M., Johannesson, G. (April 2015). Legal Framework and National Policy for Geothermal Development in Iceland. *Proceedings World Geothermal Congress*, (pp. 19-25). Melbourne, Australia.

Kristjánsson, G. (2016, April 7). Feasibility of Ocean Heat Extraction in Sub-arctic Ocean; Case Study Önundarfjörður in Iceland. (M. Eskafi, Interviewer)

Loftsdóttir, Á., Guðmundsson, B., Ketilsson, J., Georgsdóttir, L., Júlíusson, M., Hjaltason, S. (2015). *Energy statistics in Iceland 2014.* Icelandic National Energy Authority.

Loftsdóttir, Á., Guðmundsson, B., Ketilsson, J., Georgsdóttir, L., Júlíusson, M., Hjaltason, S. (2015). *Energy Statistics in Iceland 2014.* ORKUSTOFNUN, National Energy Authority.

Loftsdottir, A., Thorarinsdottir, R. (2006). *ENERGY IN ICELAND, Historical Perspective, Present Status, Future Outlook.* National Energy Authority and Ministries of Industry and Commerce.

Logemann, K., Harms, I. (2006, December 11). High resolution modelling of the North Icelandic Irminger Current (NIIC). 291–304.

Logemann, K., Ólafsson, J., Snorrason, Á., Valdimarsson, H., Marteinsdóttir, G. (2013, October 30). The circulation of Icelandic waters – a modelling study. *Ocean Science*, 931–955. doi:10.5194/os-9-931-2013

Lombardo, F. (2012, May–July). Improved extreme wind speed estimation for wind engineering applications. *Wind Engineering and Industrial Aerodynamics, 104–106,* 278–284. doi:10.1016/j.jweia.2012.02.025

Malmberg, S., Jónsson, S. (2002). Climatic/human impact on hydro - biological conditions in Icelandic waters. *Annual Science Conference, 19.*

Malmberg, S., Valdimarsson, H. (2003). Hydrographic conditions in Icelandic waters, 1990-1999. *ICES Marine Science Symposia*, 50-60.

MTS Systems Corporation. (2005). *Heat Exchanger Care and Water Quality Guide.* Minnesota, the U.S.A.

Mukherjee, R. (1998). Effectively Design Shell-and-Tube Heat Exchangers. *American Institute of Chemical Engineers*.

Murphy, J. (2007). Energy Saving Strategies for Water-Source Heat Pump Systems. *Trane Engineers Newsletter, 36–2*.

National Oceanic and Atmospheric Administration [NOAA]. (2014). Climate Change Indicators in the United States: Ocean Heat.

National Renewable Energy Laboratory. (2001, March). Renewable Energy: An Overview. *Energy efficiency and renewable energy*. USA: National laboratory of U.S. Department of Energy. doi:102001-1102FS175

Reilly, K., O'Hagan, A., Dalton, G. (2015, August). Attitudes and perceptions of fishermen on the island of Ireland towards the development of marine renewable energy projects. *Marine Policy, 58,* 88–97. doi:10.1016/j.marpol.2015.04.001

Reynolds, R., Smith, T., Liu, C., Chelton, D., Casey, K., Schlax, M. (2007, November 15). Daily High-Resolution-Blended Analyses for Sea Surface Temperature. *Journal of* climate, 20. doi:10.1175/2007JCLI1824.1

Sólbergsson, S. (2016, April 22). Feasibility of Ocean Heat Extraction in Sub-arctic Ocean; Case Study Önundarfjörður in Iceland. (M. Eskafi, Interviewer)

Sotta, C., Niliot, P., Lefeuvre, C. . (2012). *Documentary summary of the environmental impact of renewable marine energy.* Marine Energy in Far Peripheral Island Communities.

Star ODDI Company. (n.d.). *Starmon mini - underwater temperature recorder*. Retrieved from Star ODDI: http://www.star-oddi.com/products/34/subsea-temperature-recorder/default.aspx

Subbarao, P. (n d). Shell and tube heat exchangers.

Sustainable Energy Authority of Ireland. (no date). *Heat Pump Technologies, Best Practice Guide*. Dublin, Ireland.

The Directorate of Fisheries. (n. d). *Induvidual vessels*. Retrieved from Fiskistofa.

Þórðardóttir, Þ., Eydal, A. (1996). *Phytoplankton at the ocean Quahog harvesting areas off the northwest coast of Iceland 1994.* Reykjavík: Marine Research Institute.

Þórisson, B. (2013). Straummælingar út af Mosdal í Önundarfirði 2013.

Våge, K., Pickart, R., Spall, M., Valdimarsson, H., Jónsson, S., Torres, D., Østerhus, S., Eldevik, T. (2011, August 21). Significant role of the North Icelandic Jet in the formation of Denmark Strait overflow water. *Nature Geoscience*. doi:10.1038/NGEO1234

Valdimarsson, H., Malmberg, S. (1999). Near-surface circulation in Icelandic waters derived from satellite tracked drifters. 23-39.

Värme samägt. (2012). *Miljörapport för Värtaverket 2012*. Stockholm: Värme samägt med Stockholms stad.

Visit westfjords. (n d). *Flateyri*. Retrieved from Visit westfjords: http://www.westfjords.is/en/moya/toy/index/town/flateyri

Wandong, Z., Tianzhen, Y., Shijun, Y., Huan, Z. (2014, Novomber 26). The thermal performance of seawater-source heat pump systems in areas of severe cold during winter.

Energy Conversion and Management, 90, 166–174. doi:10.1016/j.enconman.2014.10.050

Willen, M., Atlason, A. (2009). Retrieved from http://focuswestfjords.com/towns/flateyri/

Xiang-li, L., Lin, D., Hai-wen, S. (2010, January). Optimal design of district heating and cooling pipe network of seawater-source heat pump. *Energy and Buildings, 42*(1), 100–104. doi:10.1016/j.enbuild.2009.07.016

Young, J., Minsung, K., Ki, C., Young, L., Ho, R. (2014, May). Potential to enhance performance of seawater-source heat pump by series operation. *Renewable Energy, 65* , 236-244. doi:10.1016/j.renene.2013.09.021

Zhena, L., Lin, D., Shu, H., Shuang, J., Zhub, Y. (2007, December). District cooling and heating with seawater as heat source and sink in Dalian, China. *Renewable Energy, 32*(15), 2603–2616. doi:10.1016/j.renene.2006.12.015

11 Appendices

Appendix A: Technical features of the Starmon mini

The information retrieved from the catalog of the device (Star ODDI Company, no date).

Sensors	Temperature
Size (diameter x length)	25mm x 130mm
Housing material	Plastic or Titanium
Weight (in air/in water)	Plastic housing: 80g , Titanium housing: 170g
Memory type	Non-volatile EEPROM
Memory capacity	262,000 measurements (standard)
Memory extension option	393,750 measurements or 524,250 measurements
Memory management	Custom programming
Temperature resolution	0.001°C (0.0018°F)
Temperature accuracy	+/-0.025°C (0.045°F)
Temperature range	-2°C to +40°C (28°F to 104°F) Outside ranges available upon request
Temperature response time	Plastic housing: Time constant (67% of full value) is 18 s. Option for fast response of 2 sec. Titanium housing: Time constant is 6 s.
Data retention	25 years
Clock	Real time clock, Accuracy +/-1 min/month
Sampling interval	From 1 second up to 90 hours
Communications	9 pin RS-232C serial cable w/USB serial converter
Attachment hole	2.8 mm in diameter
Battery life	10 years - For a sampling interval of 10 minutes. Battery is replaceable.

Appendix B: Technical features of the thermometer used in SM4

The information was retrieved from the catalog of the device (Dallas Semiconductor Company, no date):

- Unique 1-Wire® Interface Requires Only One Port Pin for Communication
- Each Device has a Unique 64-Bit Serial Code Stored in an On-Board ROM
- Multidrop Capability Simplifies Distributed Temperature-Sensing Applications
- Requires No External Components
- Can Be Powered from Data Line; Power Supply Range is 3.0V to 5.5V
- Measures Temperatures from -55°C to +125°C (-67°F to +257°F)
- ±0.5°C Accuracy from -10°C to +85°C
- Thermometer Resolution is User Selectable from 9 to 12 Bits
- Converts Temperature to 12-Bit Digital Word in 750ms (Max)
- User-Definable Nonvolatile Alarm Settings
- Alarm Search Command Identifies and Addresses Devices Whose Temperature is Outside Programmed Limits (Temperature Alarm Condition)
- Available in 8-Pin SO (150 mils), 8-Pin μSOP, and 3-Pin TO-92 Packages
- Software Compatible with the DS1822
- Applications include thermostatic Controls, Industrial Systems, Consumer Products, Thermometers, or Any Thermally Sensitive System

Appendix C: Information about the Flateyri weather station

The Information was retrieved from Iceland Meteorological Office (2016)

Type	Automated observational station
World Meteorological Organization number	4113
Location	66°02.99', 23°30.58' (66.05, 23.51)
Height above sea-level	3.0 m
Beginning of weather observations	1997


Háskólasetur
Vestfjarða
University Centre
of the Westfjords